All-optical communication system based on orthogonal frequency-division multiplexing (OFDM) and optical time-division multiplexing (OTDM)

Master Thesis, March 3rd 2014

Héctor Cañibano Núñez

DTU Fotonik
Department of Photonics Engineering

Héctor Cañibano Núñez

All-optical communication system based on orthogonal frequency-division multiplexing (OFDM) and optical time-division multiplexing (OTDM)

Master Thesis, March 3rd 2014

Supervisors:

Hans Christian Hansen Mulvad, Assistant professor

Pengyu Guan, Postdoc

DTU - Technical University of Denmark, Kgs. Lyngby - 2013

All-optical communication system based on orthogonal frequency-division multiplexing (OFDM) and optical time-division multiplexing (OTDM)

This report was prepared by:

Héctor Cañibano Núñez

Advisors:

Hans Christian Hansen Mulvad, Assistant professor

Pengyu Guan, Postdoc

DTU Fotonik

Technical University of Denmark

Oersteds Plads, Building 343

2800 Kgs. Lyngby

Denmark

Tel: +45 30 06 09 46

hector.canibano@gmail.com

Project period: September 2013 - March 2014

ECTS: 35

Education: MSc

Field: Photonics Engineering

Remarks: This report is submitted as partial fulfillment of the requirements for graduation in the above education at the Technical University of Denmark.

Table of contents

Table of contents 1
Abstract 3
Acknowledgements 4
Chapter 1 Introduction 5
Chapter 2 Theoretical background 7
2.1 OFDM 7
2.2 DWDM 9
2.3 OTDM 10
2.4 Fiber-based switching 11
2.4.1 Non-linear Optical Loop Mirror (NOLM) 11
2.4.2 Kerr-shutter 12
2.4.3 Four-Wave Mixing (FWM) 13
2.5 Raised Cosine 14
2.6 Modulation 17
2.7 Demodulation 18
Chapter 3 General principle 20
3.1 Setup description 21
Chapter 4 Simulations 23
4.1 Simulation setup 23
4.2 Simulation results 26
4.2.1 Parameters 26
4.2.2 Scenario 1 31
4.2.3 Scenario 2 46
Chapter 5 Experiment 58

5.1 Experiment setup 58
5.2 Laboratory Results 61
5.2.1 Setup without multiplexing/demultiplexing 61
5.2.2 Setup with multiplexing/demultiplexing 74
Chapter 6 Conclusions 79
6.1 Simulation conclusions 79
6.2 Experimental conclusions 80
6.2.1 Achievements in the non-multiplexing/demultiplexing experimental scheme 80
6.2.2 Achievements in the full experimental scheme 81
6.3 Future work 81
References 82

Abstract

We propose and demonstrate a novel principle that combines optical orthogonal frequency-division multiplexing (O-OFDM) and optical time-division multiplexing (OTDM). The principle is based on generating and time-multiplexing an OFDM symbol with a low duty-cycle, thus obtaining a higher aggregate bitrate. In principle the low duty-cycle OFDM symbol can be generated by pulse carving the symbol from a WDM source. In the receiver the obtained OTDM+OFDM signal is time-demultiplexed, which then allows frequency-demultiplexing the different subcarriers with an optical band-pass filter (OBPF). We have performed numerical simulations to identify the dependence of the performance on a number of parameters, for example to optimize the OBPF bandwidth. In an experimental demonstration, we achieve error-free performance for a 640 Gbits/s DPSK OFDM+OTDM signal based in a 50GHz spacing grid, yielding a spectral efficiency of 0,8 bit/Hz/s. Note that the OFDM symbol in the demonstration is achieved from a wavelength selective switch (WSS) based transmitter instead of by pulse carving a symbol from a WDM source.

Acknowledgements

I would like to express my gratitude towards every single person that has made this thesis possible. I will always be in debt with my supervisor Hans Christian Hansen Mulvad, as his help has been invaluable in a lot of different ways. I give him all the credit about the intellectual thinking behind the principle proposed in this thesis, so the fact that I am writing these lines now is just a consequence of him giving me the opportunity to develop his idea. He has also been a perfect guide in my learning process through the achievement of this thesis, giving me the appropriate tools to progressively increase my knowledge about the different fields of high-speed optical communications. He has always taken responsibility on the progress of my work and has been willing to help in any way he could until the very last minute. I also owe him all my field experience in the laboratory, which I completely lacked before arriving to Denmark. He provided me with some preliminary experience way before the experiment exposed in this thesis, and the experiment itself was a constant learning experience.

I would also like to thank my other supervisor, the postdoc Pengyu Guan, for his indispensable help with the setup in the laboratory and the unselfish effort he made when making the measurements, spending his time disinterestedly so I could have the results shown in this thesis.

I am also grateful to the MSc student Mads Lillieholm, who was my learning partner in my first laboratory experience. More important than that, he has been the only person to keep me company in the office through my stay in Denmark and he has always been a great support.

Overall, I really enjoyed the friendly atmosphere in the High-Speed Optical Communications group, where all I found was helpful people who were always glad to solve any doubts I had. I have to thank the group leader, Leif Katsuo Oxenløwe, for paying attention to my need of carrying out an experiment and reserving the laboratory for it.

I am also very grateful to the former group leader, Christophe Peucheret, who accepted my solicitude to develop my thesis in DTU even when the deadline had passed long before. He also provided the Matlab code that made my simultions possible.

Finally, I need to thank my Spanish tutor, Joan M. Gene Bernaus from UPC Barcelona. He was very helpful back when I was looking for a destination for my thesis development, and when everything suddenly was ruined he assumed a responsibility that wasn't his and quickly reacted to put me in contact with DTU, which probably saved my thesis. In addition, DTU has turned out to be a perfect environment to develop my work and my Danish stay has been a life-changing experience, for which I am doubly thankful to him.

Chapter 1

Introduction

We live in a world where Internet is penetrating more and more into all kind of societies and with very high data transmission requirements for all kind of applications, which translates into an increasing Internet traffic. An approach to this demand would be to improve the spectral efficiency and the dispersion tolerance of the transmitting format, which is achieved through orthogonal frequency-division multiplexing (OFDM) [1,2]. In the same way that we have seen for OTDM, the research towards all-optical OFDM has allowed to push OFDM super-channels up to Tbit/s capacity [3, 4]. OFDM demultiplexing has usually been performed with optical Fast Fourier transform (O-FFT) [3] to avoid intercarrier interference, but this method increases the complexity and power consumption of the demultiplexer. An alternative demultiplexing method is the use of time-lenses to perform a spectral magnification of the OFDM super-channels, reducing the inter-carrier interference at detection and allowing demultiplexing by means of a simple optical filter. A different approach to high capacity is time-division multiplexing. Classical electrical time-division multiplexing (ETDM) systems find their bottle neck at a rate ≈100Gbit/s [5, 6], which is not enough to cover the rate demand. On the other hand, optical time-division multiplexing (OTDM) systems allow single-channel bit rates over 1 Tb/s [7, 8]. Data processing at such high rates is not possible by means of electrical processes; instead, optical signal processing (OSP) allows to transparently process data regardless of the bit rate, as it is based on non-linear optical effects with femtosecond response times. OSP makes it possible to achieve high-speed OTDM, where high transmission rates are obtained by time-interleaving low duty-cycle data tributaries of e.g. 10Gbit/s [7]. OTDM is another possible approach to follow when looking for higher capacity and energy efficiency operation, as it focuses on increasing the single-channel bit rates to achieve simpler systems by means of fewer frequency channels.

It seems clear that both OTDM and OFDM schemes allow us to increase the data rate, but each of them reaches the desired capacity in a different way. In this thesis we propose a novel principle that combines both OTDM and OFDM. OTDM allows us to time-interleave low duty-cycle and low rate data tributaries, which simplifies the speed requirements of the transmitter equipment. OFDM allows us to increase the spectral efficiency and at the same time to perform the frequency-demultiplexing in a very simple way when combined with OTDM (because the other tributaries are removed, hence avoiding intertributary interference). More precisely, the principle we propose consists of low duty-cycle OFDM

symbols (cut in time with a pulse carver) that are OTDM multiplexed. In the receiver's part, they are time-demultiplexed and finally frequency-demultiplexed with an optical band-pass filter (OBPF). A very interesting aspect of this principle is that the OFDM signal can be achieved from standard WDM transmitters. The challenging points in this principle are the time-demultiplexer, which relies on the femtosecond response of OSP, and the OFDM generation, which relies on the compatibility with existing DWDM equipment, and has very strict orthogonality requirements. Another challenging point will be the pulse carver that will allow us to reach low duty-cycle OFDM symbols.

The main objective of this thesis is to demonstrate the principle. In a first approach through simulations, we will try to identify the dependence of the performance on a number of parameters. We will also optimize those parameters in order to minimize the interference, which can have different sources. In a second approach through an experimental demonstration, we achieve error-free performance using our principle, for a 640Gbit/s DPSK OTDM+OFDM signal, based on a a 50GHz channel spacing, and yielding a a 0,8 bit/Hz/s spectral efficiency.

The thesis structure will be the following:

- In Chapter 2 we find a theoretical chapter that will introduce the basis of the principle, namely the OFDM and OTDM schemes, and other useful background regarding different aspects that appear on the thesis: modulation, pulse shape (raised-cosine), non-linear processes and fiber-based switching methods, and compatibility with DWDM.
- In Chapter 3 we will explore in detail the principle of this thesis, following a setup description that will help us understand the most important details of its operation.
- After that, in Chapter 4 we will focus on the numerical simulations and their results. Mainly, we will consider some of the possible parameters in the system, we will try to optimize them and obtain conclusions about their influence in the performance of the system.
- Then in Chapter 5 we will proceed to present the experimental results. It will be important to describe the laboratory setup, as it will be different from the one presented in the general principle (it will neither start with a WDM source nor use a pulse carver). We use a different setup because our department collaborated with CUDOS visiting researchers, and they provided an alternative transmitter based on a wavelength selective switch (WSS) [4]. We will focus on optimizing the system for its different parameters, having the simulations background to compare. As we have said, we reach error-free performance.
- Finally, we will explain the conclusions obtained through the thesis, and name some possible future research on this direction.

Chapter 2

Theoretical background

The goal in this chapter is to provide an overview of the theoretical basis behind the principle proposed in this thesis. We will not overextend on the theory, but we will focus on explaining the operation mechanism of the different schemes that we will use.

These schemes include OFDM and OTDM as the multiplexing methods, DWDM as the reference for the carrier spacings, fiber-based switching methods for time-demultiplexing, raised-cosine as the pulse shape and DPSK modulator and demodulator as our way to encode data.

2.1 OFDM

Orthogonal frequency-division multiplexing (OFDM) is a well-known multiplexing technique in the world of wireless telecommunications. Optical OFDM is a more recent approach, but is widely considered one of the most promising technologies for future high-speed optical communications [9]. An OFDM system multiplexes several subcarriers in the frequency domain, with one special feature: the subcarriers are orthogonal. The most obvious consequence of this fact can be observed when looking at an OFDM spectrum Figure 1 the modulated subcarriers spectra overlap, which allows a very tight packing and improves the spectral efficiency. In addition, the encoding of the information in a large number of subcarriers makes OFDM robust against dispersion (both chromatic and polarization mode).

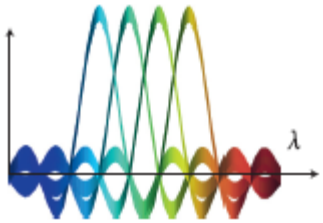

Figure 1 - OFDM spectrum with 4 orthogonal subcarriers

In Figure 2 we can see the transmitter and receiver schemes of an electrical OFDM. The main innovation that this multiplexing method brought was the use of the *inverse fast*

Fourier transform (IFFT) in order to achieve orthogonality between subcarriers, and the opposite operation (FFT) for demultiplexing [2, 3].

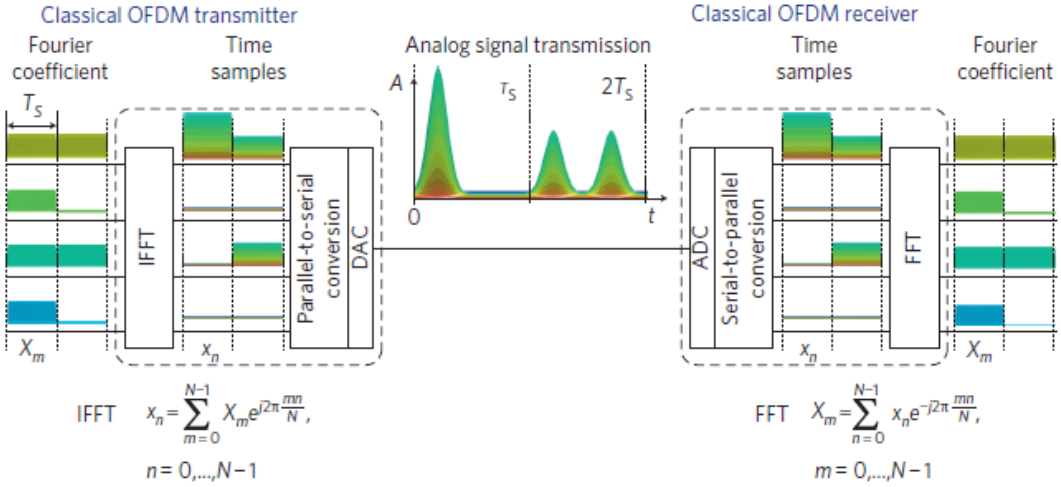

Figure 2 - OFDM processing. Classical implementation: N=4 parallel data streams are interpreted as complex Fourier coefficients in the frequency domain. The IFFT yields time-domain samples x_n of a signal. Parallel-to-serial and digital-to-analog conversion provides an analog OFDM signal A(t) with the spectrum at Figure 11. After transmission, the information is retrieved through the inverse process: an analog-to-digital conversion and a serial-to-parallel conversion followed by an FFT return the Fourier coefficients representing the data streams.

The scheme above would be also applicable to an electro-optical OFDM system. The data would be electrically processed, and the digital-to-analog converter (DAC) would create the optical subcarriers. However, this kind of system has a bottleneck in the electrical processing part, which cannot adapt to the high-speed data transmission rate required nowadays. This is why an all-optical OFDM system is really interesting.

As we can see in Figure 3, the all-optical OFDM transmission scheme becomes really simple. A group of lasers produce equally-spaced emission frequencies (known as a *comb* source) which become the subcarriers, which are then *IQ* modulated with the information to be transmitted and coupled together, forming an OFDM signal. The receiver scheme, on the other hand, becomes complex when trying to achieve interference-free demultiplexing; the spectra overlap of the subcarriers prevents the use of OBPF for carrier demultiplexing (which is possible in DWDM), hence needing further optical processing based on Fourier transform. Optical Fourier transform (OFT) is achieved with *time-lenses*, based on parabolic phase modulation and dispersion [10, 11]. As we will discuss later, several options are considered to improve the reception of the OFDM signal, always based on combinations of OFT and IOFT (*inverse optical Fourier transform*) [12].

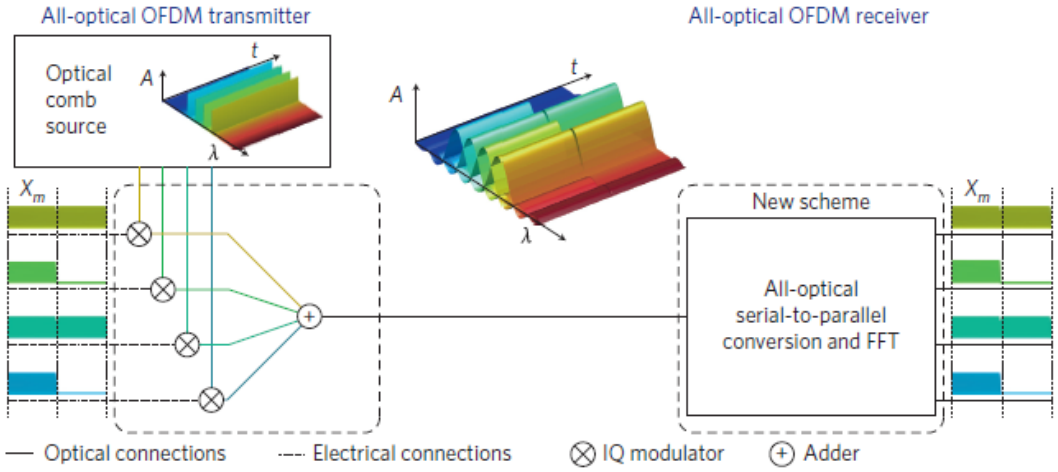

Figure 3 - OFDM processing. All-optical implementation: data streams are IQ-modulated on equidistant, frequency-locked subcarriers. After summation, an OFDM signal is obtained as with the classical method.

2.2 DWDM

Dense Wavelength Division Multiplexing (DWDM) is a technology that multiplexes a number of optical carrier signals with different wavelengths into the same optical fiber, always within the C-band (1530nm – 1565nm). It differs from normal WDM in that the number of optical channels within the band is higher, which has been achieved with the development of higher-quality lasers, low-dispersion fibers, dispersion-compensation modules and erbium-doped fiber amplifiers (EDFAs). A basic requirement in WDM systems is that each carrier or channel is separated from the others by a guard band, which allows the use of optical band-pass filters (OBPFs) to demultiplex them (see figure 4)

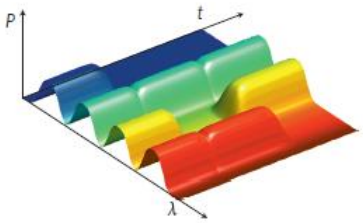

Figure 4– DWDM spectrum with 4 channels

DWDM is the most common multiplexing scheme in optical communications and so a vast majority of optical equipment works under its specifications. In this thesis we are only interested in the channel spacing aspect in DWDM, as we want our system to be compatible with existing equipment. The different channel spacings that we will consider are (ITU-T G.694.1):

Channel spacing (GHz)	Channel spacing (nm)
25	0.2
50	0.4
100	0.8
200	1.6

2.3 OTDM

In the world of traditional telecommunications, time-division multiplexing (TDM) is commonly used in the electrical domain to obtain digital hierarchies of aggregated tributary signals. The limitations imposed by high-speed electronics led to the creation of the optical TDM (OTDM), where different optical signals (called tributaries) are multiplexed in the time-domain (interference-free), while sharing the same wavelength [13]. In order to take full advantage of the optical multiplexing, all-optical multiplexing and demultiplexing systems are required.

The multiplexing process is carried out through the use of delay lines, which allow the different modulated tributaries to be orthogonal in the time domain. The other requirement is that the pulse width must be N times smaller (where N is the number of tributaries) than the distance between two consecutive pulses (low duty-cycle), so pulses from other tributaries can be interleaved in between. This way, the resulting aggregate rate will be N times the base rate. Figure 5 shows the basic multiplexing setup:

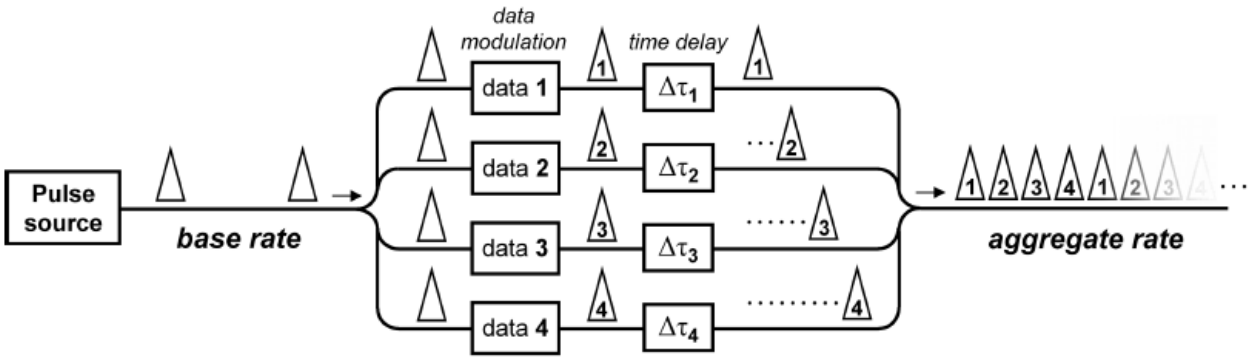

Figure 5 - Design of an OTDM transmitter based on optical delay lines. N=4 tributaries in this case [22]

The demultiplexing process always involves the presence of a control pulse, which will be non-orthogonal (in the time-domain) to one of the tributaries, hence affecting it. We can take advantage of this dependence in several ways, so we can isolate (demultiplex) the desired tributary. These different demultiplexing techniques include the use of a *non-linear optical loop mirror* (NOLM), a *Kerr shutter*, or a *four-wave mixing* (FWM) process. It is also

necessary to have a clock recovery module to synchronize the demultiplexer to the OTDM base data rate. Figure 6 shows the basic demultiplexing setup:

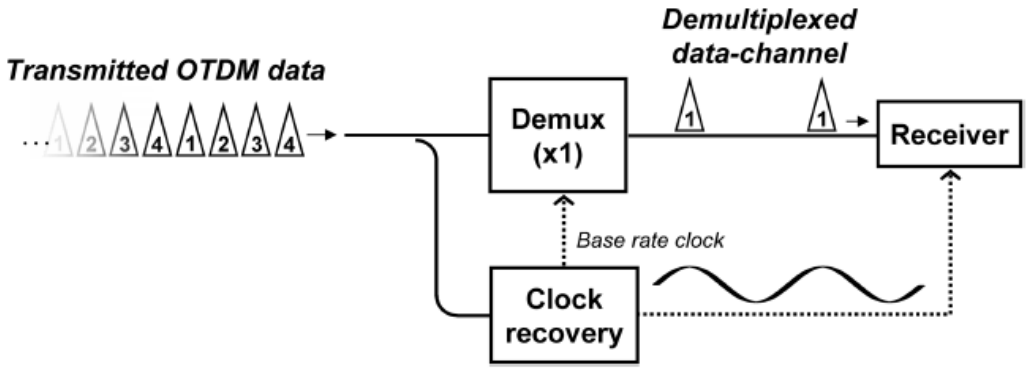

Figure 6 – Design of an OTDM receiver [22]

2.4 Fiber-based switching

As stated above, there are some different techniques to achieve all-optical demultiplexing in an OTDM system. These techniques are not only interesting for demultiplexing but also for pulse carving, as they allow a reduction of the pulse width of a given tributary. The different techniques we consider are based on the non-linear optical effects that happen inside an optical fiber when two optical fields are coupled together in it.

- Self-phase modulation (SPM): The refractive index of a fiber depends on the intensity of the fields propagating through it. If there is only one field in the fiber, it will affect itself by introducing a non-linear phase shift on itself, depending on its pulse shape and intensity.
- Cross-phase modulation (XPM): When more than one field propagates simultaneously through the fiber, those fields will affect each other in terms of a non-linear phase shift. The difference between SPM and XPM is that the phase-shift introduced by the latter is 2 times larger than the one introduced by SPM. If we want to take advantage of that phase-shift, using XPM will be more effective.
- Four-wave mixing (FWM): The presence of three optical fields copropagating simultaneously in the same direction inside a fiber originates a fourth field, whose frequency (ω_4) is related to the frequencies (ω_1, ω_2, ω_3) of the three former fields.

2.4.1 Non-linear Optical Loop Mirror (NOLM)

The non-linear optical loop mirror is based on an interferometer structure, where the OTDM signal is divided into two paths with the same length. The addition of a control pulse in one of the propagation directions (e.g. clockwise), synchronized in time with one of the

OTDM tributaries, will introduce a cross-phase modulation (XPM) on that tributary when going through the non-linear fiber. That non-linearity will introduce a different phase-shift in each propagation direction, which will result in a change on the transmittivity and reflectivity coefficients in the coupler, when the two paths encounter each other again. The system is designed so that the absence of a control pulse causes a total reflection, whereas the presence of the control pulse causes a total transmission. If the control pulse is synchronized with one tributary, that tributary will be transmitted and the rest will be reflected, hence achieving demultiplexing. The XPM-based operation of the NOLM that can be used for demultiplexing was proposed in [14], and used for the first demonstration of 640Gbit/s demultiplexing in [15]. In Figure 7 we can see the NOLM principle of operation:

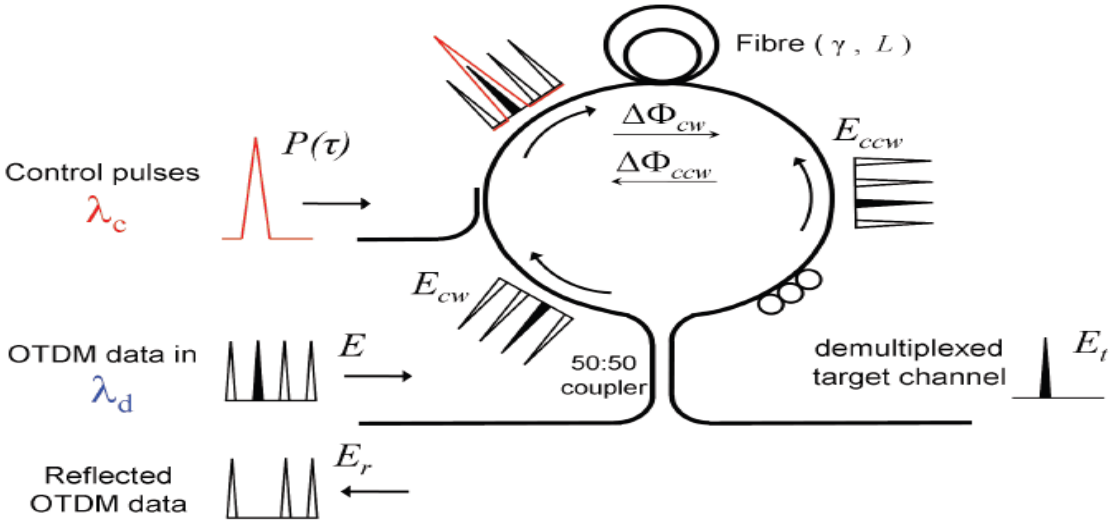

Figure 7 – Model of the NOLM for time-demultiplexing

The main drawback of this system is the possible leakage from the neighbour channels that can induce inter-channel interferometric cross-talk (IXT) on the demultiplexed channel. This leakage can be the result of counter-propagating XPM, or also due to the limited extinction ratio in the coupler in the non-ideal setup.

2.4.2 Kerr-shutter

The Kerr-shutter is a demultiplexing technique based on the polarisation-dependence of XPM, and its operation mechanism was explored in [16]. Using a high-power control pulse, synchronized in time with one target channel, a XPM-based polarisation-rotating effect of 90º is induced in said channel, which is then demultiplexed using a polarisation beam splitter (PBS). In order to achieve the desired polarization rotation, it is necessary to accomplish a 45º difference between the linear polarization of the OTDM signal and the polarization of the control signal (which is achieved using *polarisation controllers, PC)*. When this happens, and when propagating through a highly non-linear fiber, the parallel

component ($E_{//}$) and the perpendicular component ($E_{\perp}$) of the OTDM signal are affected differently by the XPM effect, which means that they are induced different phase shifts. When the difference between these two different phase shifts is π (as shown in the *state-of-polarisation* diagrams in figure 8), the polarization of the desired channel is rotated 90º. The Kerr shutter has been used for demultiplexing of OTDM bit rates up to 640 Gbit/s [17].

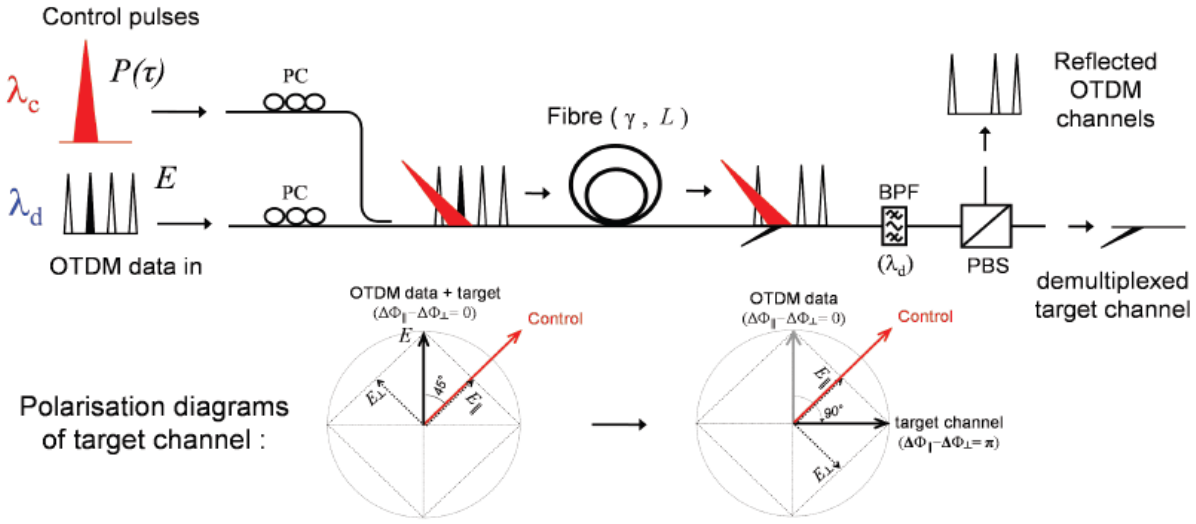

Figure 8 – Model of the Kerr shutter for time-demultiplexing

The main drawback when using this demultiplexing technique can be the high power necessary for the control pulse, which is not always feasible. However, as this method doesn't require a loop structure, the problems derived from the counter-propagating field that happened in the NOLM are avoided.

2.4.3 Four-Wave Mixing (FWM)

We have seen two demultiplexing methods that take advantage of the non-linear process of XPM. The last demultiplexing technique that we consider will take advantage of FWM. In that non-linear process, three optical fields generate a fourth one with frequency $\omega_4 = \omega_1 \pm \omega_2 \pm \omega_3$. If we consider the degenerate FWM case where $\omega_1 = \omega_2$, the resulting frequency for the fourth field is $\omega_4 = 2^* \omega_1 - \omega_3$, provided that certain phase-matching requirements are fulfilled.

The demultiplexing scheme includes again the presence of a control pulse (pump), with frequency $\omega_1 = \omega_2 = \omega_{Pump}$. The OTDM signal will be allocated in frequency $\omega_3 = \omega_{Signal}$. If we follow the frequency relation established above, we see that the resulting fourth field (called *idler*) will appear at frequency $\omega_4 = \omega_{Idler}$, as we can see in Figure 9:

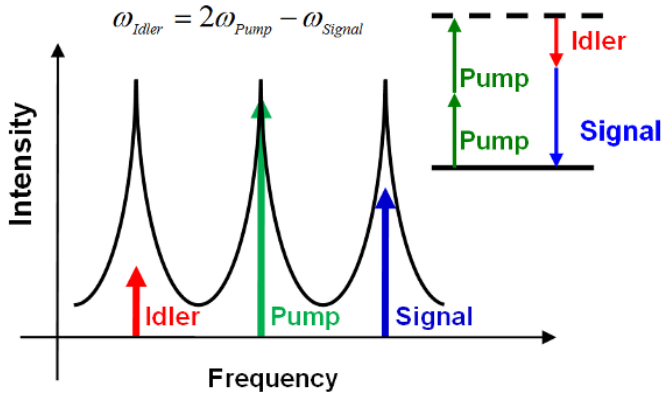

Figure 9 – Four-wave mixing process

The field relationship is:

$$E_i \propto E_p^2 E_s^*$$

The phase-matching requirement is that the pump is located at the zero-dispersion wavelength of the fiber. In that case, the equation $\omega_{Idler}=2*\ \omega_{Pump} - \omega_{Signal}$ will be valid for both $\omega_{Signal} > \omega_{Pump}$ and $\omega_{Signal} < \omega_{Pump}$, which means that the idler will be always symmetric about the signal, leaving the pump in the middle of them. FWM is useful for demultiplexing because the idler field can only exist if the pump and the signal fields copropagate simultaneously. If we synchronize the pump with one of the OTDM tributaries, the idler field will become a replica of that tributary at a new wavelength. In addition, the idler can be amplified up by means of parametric gain [18].

The main drawback when using FWM is that the wavelength of the signal changes, which can be troublesome depending on where the zero-dispersion wavelength of the fiber is. The idler frequency could happen to be at the limits of the C-band, which could worsen the performance of the system depending on the bandwidth of the amplifiers and receiver. It can also be a problem if the application specifically requires maintaining the same wavelength.

2.5 Raised Cosine

Regarding the shape of the pulses after the pulse carver, we need to remember that the idea explored in this thesis will be, at some point, put into practice in a laboratory. If we tried to simulate our system within ideal conditions, the pulses would be always perfectly rectangular, but that would not be a realistic approach. As we want our simulations to be as close as possible to the laboratory results, we will lower our aspirations and expect a non-perfect, to some extent, rectangular pulse. This kind of shape is provided by a raised-cosine pulse, which has been used to achieve ultrahigh-speed TDM before [19], and follows the next definition [20]:

$$r(t) = \begin{cases} 1, & 0 \le |t| \le \frac{1-\alpha}{2T} \\ \frac{1}{2}\left\{1 - \sin\left[\frac{\pi}{2\alpha}(2T|t| - 1)\right]\right\}, & \frac{1-\alpha}{2T} \le |t| \le \frac{1+\alpha}{2T} \\ 0, & \frac{1+\alpha}{2T} \le |t| \le 0 \end{cases}$$

$$R(f) = \frac{\sin(\pi f/T)}{\pi f/T} \frac{\cos(\alpha\pi f/T)}{1-(\alpha\pi f/T)^2}$$

Where T is the pulse width, and 0 < α < 1. This α is precisely the parameter that determines how close the pulse shape is to a rectangular pulse. In Figure 10 we can see how the shape looks for different values of α:

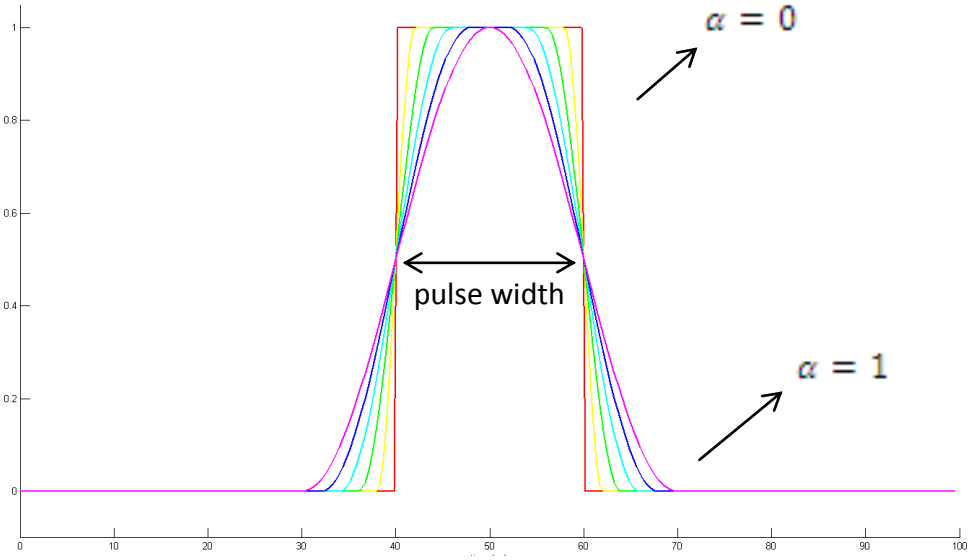

Figure 10 – Raised cosine pulse for variable roll-off factor

As we can see, the defined parameter T or pulse width is the same regardless of the value of α, as it represents the width of the pulse at the half of its maximum amplitude (FWHM). However, the total width of the base of the pulse is two times larger when α=1, compared to when α=0. As these pulses will be one next to another, conforming an OTDM signal, the α factor will condition the minimum distance between pulses in order to have zero interference between them. In the following figures we can see what would happen in our scenario; with α=0 the pulses don't interfere with each other (Figure 12), while with α=1 there is some interference (Figure 11). In this latter case the interference is not significant, because at the sampling instant (in the center of the pulse) there is no interference; however, we need to be aware of this phenomenon if we want to increase the number of tributaries. If we wanted absolutely interference-free pulses, the capacity of the system would be reduced to the half (as seen in figure 13).

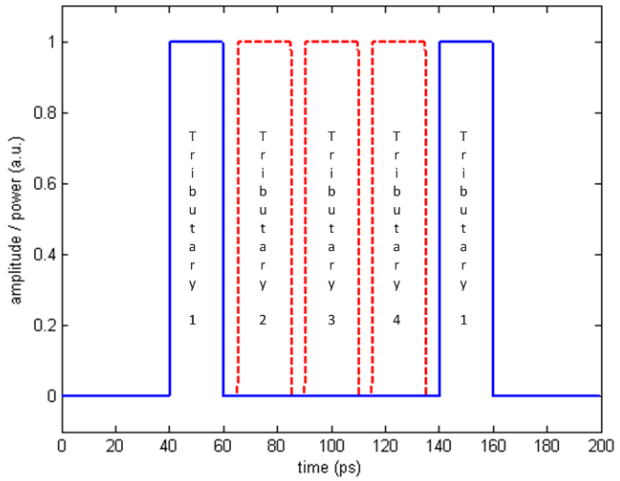

Figure 12 – OTDM with roll-off factor = 0 and 4 tributaries

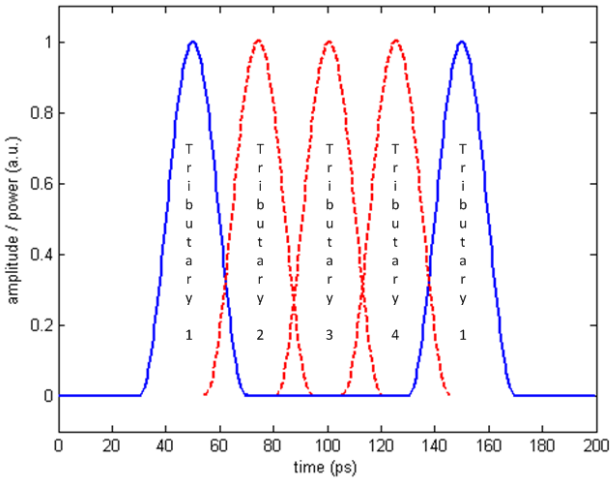

Figure 11 – OTDM with roll-off factor = 1 and 4 tributaries (interference)

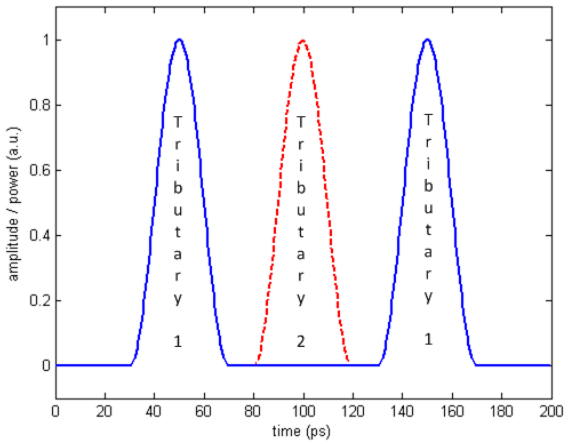

Figure 13 – OTDM with roll-off factor = 1, 2 tributaries (interference-free)

Another important issue regarding the raised-cosine is the form of its spectrum, which also depends on the value of α. The amplitude and width of the main lobe is always the same, which guarantees that the signal will match an OFDM scheme. However, the amplitude of the secondary lobes is smaller for higher values of α, as can be appreciated in figure 14. This becomes relevant when having an OFDM signal, as those secondary lobes introduce interference on the neighbour carriers.

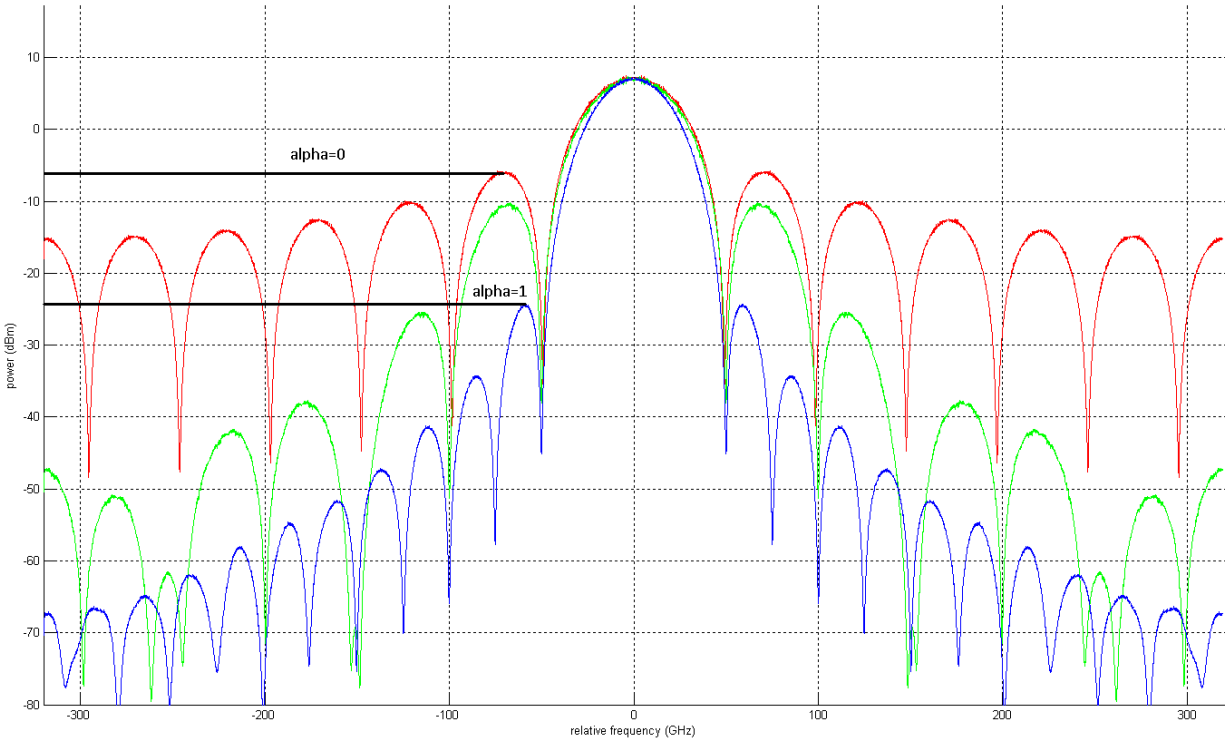

Figure 14 – Raised cosine spectrum for variable roll-off factor

In the simulation results chapter we will see how the roll-off factor affects the performance of the system. It will be important to remember the previous statements about the pulse shape and the spectrum when trying to understand those results.

2.6 Modulation

The kind of digital modulation that we will use in this thesis will be a phase-shift modulation, specifically *differential phase-shift keying* (DPSK) [21]. DPSK is similar to BPSK in that the information is encoded into two possible fixed symbols with a π phase shift between them; however, BPSK highly depends on the channel, which could rotate the constellation and cause an ambiguity of phase. DPSK, on the other hand, encodes each bit depending on the bit before that one, i.e. adding a π phase shift or not to the phase of the previous symbol. This different encoding system from normal PSK modulations will require a special demodulator scheme.

The advantage of DPSK over an amplitude modulation like *on-off keying* (OOK) is that, in any particular scenario, DPSK will provide a similar *bit error rate* (BER) for a power 3dB smaller at the receiver's input. In addition, DPSK offers the possibility to be updated to higher-order modulations like DQPSK (*differential quadrature PSK*). We can see the constellation diagrams for these three modulations in Figure 15:

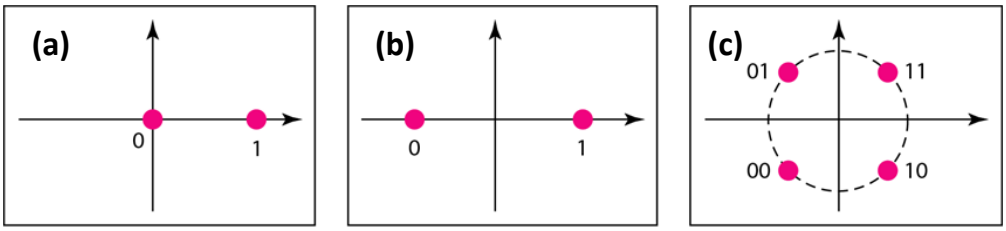

Figure 15– Constellation diagrams for different modulations. (a) OOK. (b) DPSK. (c) DQPSK with Grey coding

2.7 Demodulation

In amplitude modulations like OOK, demodulation is achieved with a simple direct non-coherent detection process, i.e. making the optical signal going through a photodiode, whose output is an electrical signal with intensity proportional to the optical power at the input. On the other hand, phase modulated signals (with PSK or similar) have a constant amplitude envelope, so direct detection is no longer useful: a coherent detection is needed. This is usually achieved with an interferometric structure, such as a Mach-Zehnder interferometer (MZI). In this kind of structure the optical beam with the modulated signal is splitted into two paths (*arms*) with the same length, and later coupled again together. In this coupling there may be a constructive or destructive interference, which will result in the presence or absence of amplitude envelope in the output, hence converting a phase difference into an amplitude difference.

This would be the traditional PSK demodulating scheme, but we will work with DPSK, which needs a small variation on the scheme: the addition of a delay line in one of the arms. This line introduces a time delay equal to the time duration of one symbol (this can be observed in figure 17). This way the interference in the coupler is produced between two consecutive symbols, hence obtaining an amplitude difference according to the phase difference between those symbols. This is the exact inverse process to the modulation, so demodulation is accomplished. In Figure 16we can see this DPSK demodulator, called *delay line interferometer* (DLI).

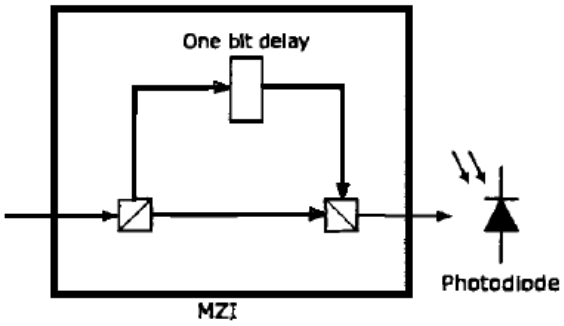

Figure 16 – Delay line interferometer (DPSK demodulator)

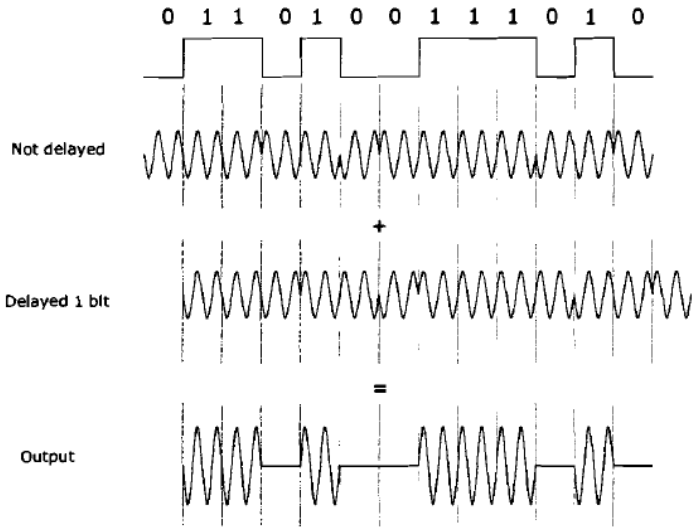

Figure 17 – Working principle of DPSK demodulator.

Chapter 3

General principle

The novel communications idea that we want to explore in this thesis combines the two multiplexing techniques explained in the theoretical introduction: OTDM and OFDM. OTDM offers the advantage of using low symbol rate tributaries, with low duty-cycle, to form a signal with a much higher aggregate symbol rate. Separately, OFDM offers the advantage of high spectral efficiency and robustness against dispersion. The resulting scheme when combining these two techniques could have the advantages of both of them, mentioned above. Another advantage is that we can build an OFDM signal with a WDM source (like the one in Figure 18), which guarantees the compatibility of this principle with commercial WDM equipment. However, as we are multiplexing in both time and frequency domain, the interference when demultiplexing can have multiple sources (intertributary, intersymbol or intercarrier) which can worsen the performance of the system. It is our task to determine if that interference will allow this idea to be feasible, and to evaluate the influence that the different parameters in the setup have on the performance.

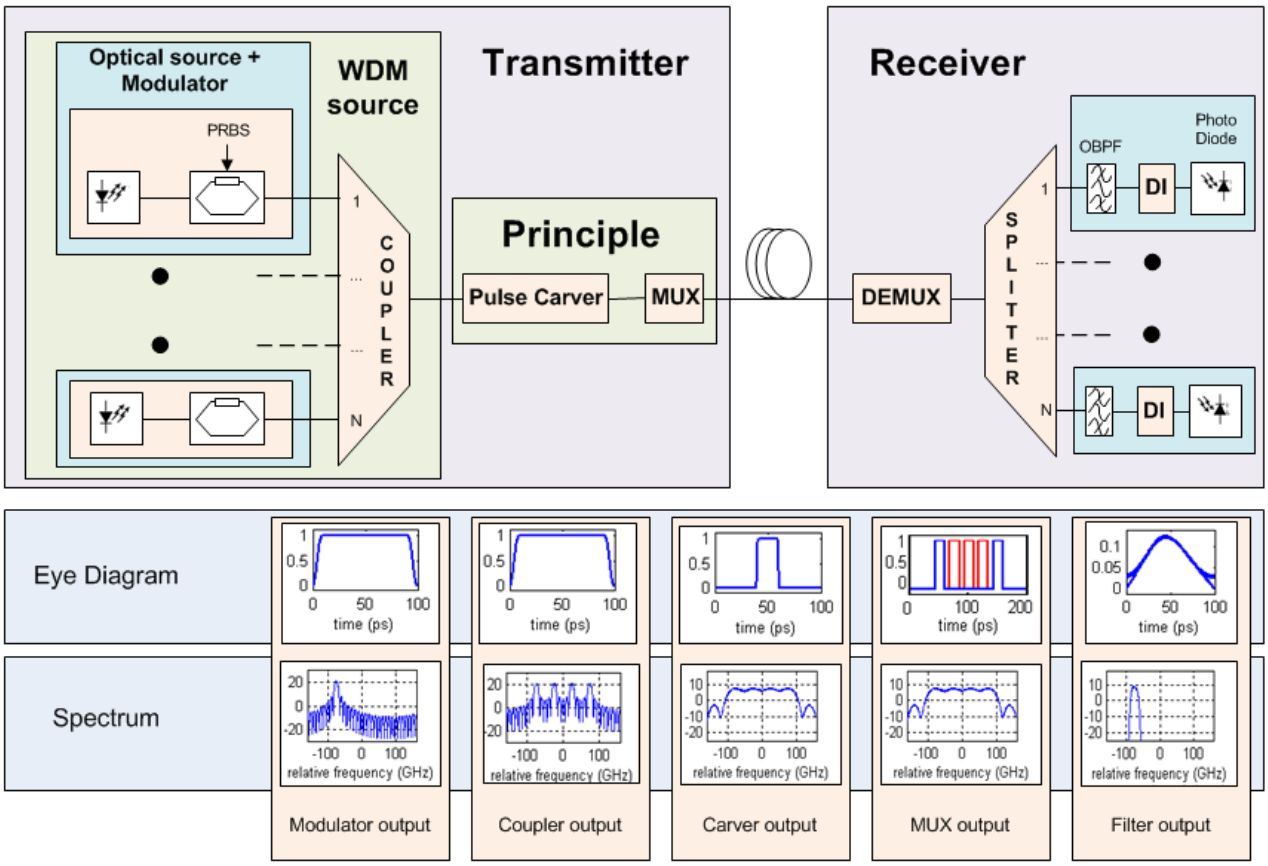

Figure 18 - General principle setup

In Figure 18 we can see the general setup of the idea explored in this thesis (top) and how the eye diagram and spectrum of the signal will evolve through the setup, in an example where there are 4 carriers at a distance of 50GHz from each other, and 4 tributaries involved (bottom).

In the following setup description, we will reference Figure 18 in order to translate the principle to numbers and make the explanation clearer. However, the principle is the same for other values of carrier spacing, number of carriers and number of tributaries.

3.1 Setup description

Transmitter

In the transmitter, we can observe the OFDM generation part (optical source + modulator + coupler + pulse carver) and the OTDM generation part (multiplexer). As we saw in the theoretical introduction, an optical OFDM signal can be achieved by simply locating the emission frequency of a group of lasers at the same distance one to each other (a frequency comb generator would be another option). The difference in the emission frequency (called *carrier* spacing) of the lasers will follow the DWDM specifications (ITU-T G.694.1), i.e. 25 GHz, 50 GHz, 100 GHz or 200 GHz (in Figure 18 we can see the 50 GHz case). Those signals are individually modulated with MZI modulators, which encode data into a certain phase modulation format (e.g. DPSK or DQPSK). The data comes from a *pseudo-random binary sequence* (PRBS) generator with a rate of 10 Gbit/s. The distance between the emission frequency and the first *zero* (where the main lobe ends) is 10 GHz, and the bit slot in the time domain is $1/(10\ GHz) = 100\ ps$, as can be observed in the eye diagram at the modulator's output. Note that the pulses observed in the Eye Diagrams in Figure 18 are just schematic; in reality, when using standard modulators, the pulse transitions would be slower.

The carrier spacing is still 50 GHz, and that should also be the distance between the emission frequency and the first *zero* in each carrier, in order to accomplish the orthogonality required for an OFDM signal. Broadening the spectrum by a factor of 5 (from 10 GHz to 50 GHz) is equivalent to narrowing the pulse width by a factor of 5 (from 100 ps to 20 ps). This is achieved with the pulse carver in the setup: we can see that at the carver's output the pulse width is 20 ps, and the spectrum is a near-flat pulse with a total bandwidth around 4*50GHz = 200 GHz; this is our OFDM signal. As the pulse width is 20 ps, but the pulses are separated 100 ps from each other, a low duty-cycle is achieved. The last step in the transmitter is an OTDM multiplexer. At the multiplexer's output, the spectrum of the signal is the same as at the input (the OFDM spectrum), but in the time domain we can see, in red, the new tributaries multiplexed with the first one. In conclusion, we have an OTDM signal made with OFDM symbols. We should also observe that if the pulse shapes are not close to being rectangular, we may have intertributary interference in the system after

performing OTDM demultiplexing. In order to explore this issue, a raised-cosine shape with variable roll-off factor will be used.

Receiver

The receiver will basically perform the reverse process compared to the transmitter. The first step is an OTDM demultiplexer, which can be implemented by any of the fiber-based switching methods explained in the theoretical introduction. The demultiplexer ideally extracts one of the tributaries without distortion. We are going to implement the OFDM demultiplexer as a tunable filter centered in the carrier wavelength. In this thesis we have considered that some intercarrier interference can be permitted without worsening the system performance too significantly, i.e. still reaching the error-free rate condition. As long as the filter's bandwidth is smaller than the carrier spacing (50 GHz in the example), the time-domain pulse will broaden, as observed in the filter's output in Figure 18. If it broadens too much, it will interfere with the neighbour pulses, hence causing intersymbol interference. Also, if the filter's bandwidth is too large, the intercarrier interference will increase. Those two different types of interference will represent the upper and lower limitations for the filter's bandwidth. They are theoretically explained in the raised-cosine chapter in the introduction and analysed in the results chapter.

After that, the last step will consist of DPSK demodulation and optical-electrical conversion of the signal.

Chapter 4

Simulations

4.1 Simulation setup

The general principle we have already described can be implemented in a number of ways; we know what kind of signals we want in each step, but the way to get those signals may change from paper to reality. In the laboratory, for example, the implementation will be done accordingly to the disposable equipment. In a simulation, each module of the setup can be programmed accordingly to its function, but may not be an exact replica of the real equipment, hence having a different behaviour.

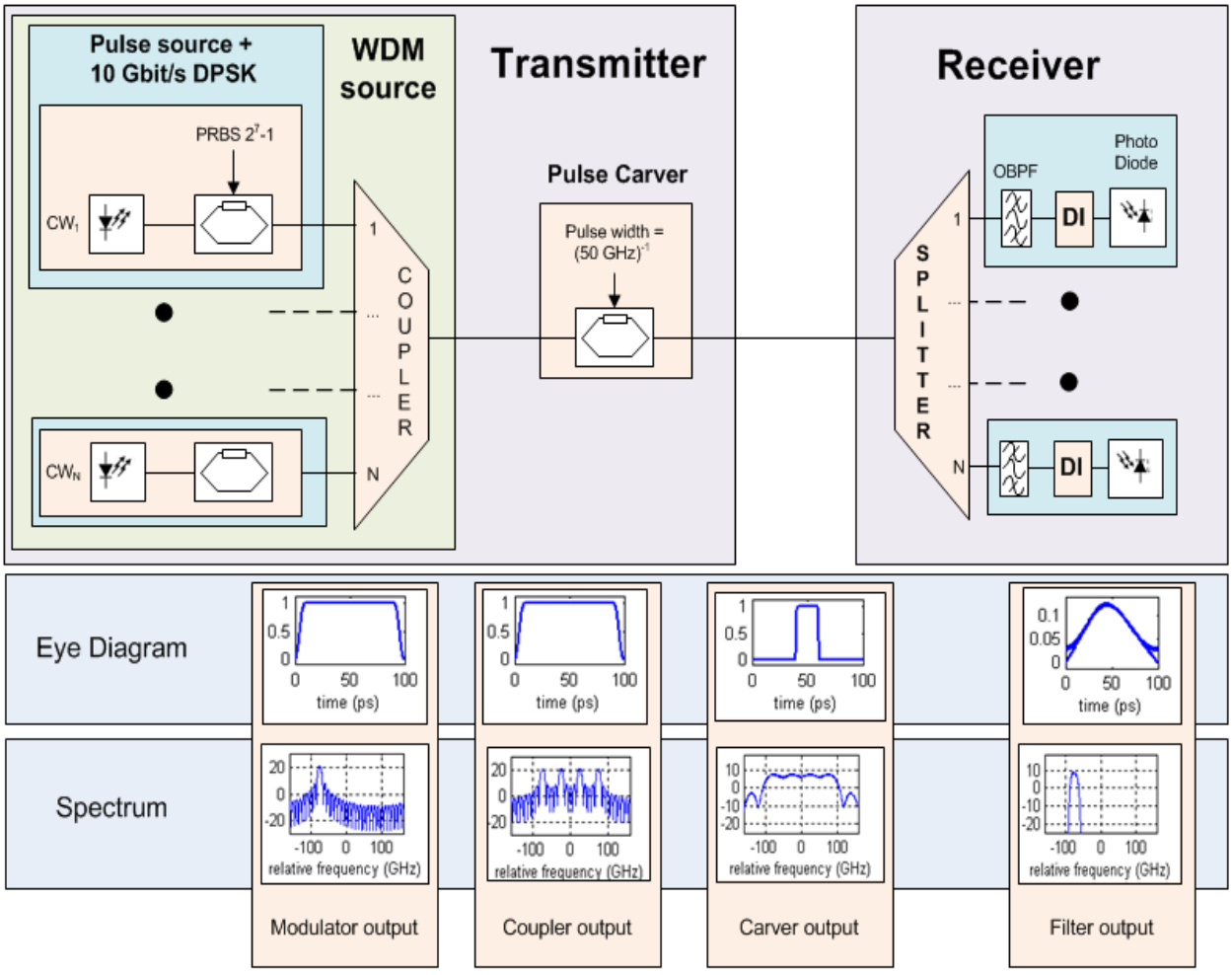

Figure 19 - Simulation setup

In Figure 19 we can see the system implemented in our simulations. It is almost identical, in form, to the general setup described previously. The main difference is that now we are assuming ideal OTDM multiplexing and demultiplexing processes; this is why we cannot see a *mux* or *demux* module in the scheme. To be consistent with that assumption, we will need to simulate almost rectangular pulses, to avoid the possibility of intertributary interference. We will also need to have these assumptions in mind when trying to understand the simulation results. Other ideal assumptions and implementation details in the simulation setup are:

In the **transmitter**:

- The optical sources will be implemented as *continuous wave* (CW) lasers. The assumption on these lasers is that they have an ideal spectral linewidth: they only emit power in a given wavelength.
- The PRBS generator is implemented as a shift register with a given generating polynomial and seed. The seed is obtained as a random number with the *rand()* command in Matlab. Using a PRBS we try to emulate the random data to be transmitted in a real transmission. The bit rate provided by the PRBS generator will be 10 Gbit/s. Also, the PRBS length will be set to 127 (2^7-1).
- The signal from the CW lasers will be modulated by a MZI module. The electrical signal that will drive the MZI is generated following the data pattern provided by the PRBS generator, so it will consist of 100 ps pulses, as we stated. In this case, the electrical signal will have a rectangular shape, but it can actually be any shape as long as it is flat-top in the middle, because then we can carve any shape that we want with the pulse carver.
- The coupler will be implemented as a simple addition of signals with no loss.
- The pulse carver will be implemented as another MZI module. This time the pulse width will be the inverse of the carrier spacing (20 ps in the case of 50 GHz spacing). The electrical drive signal will have a raised-cosine form in the time domain, for the reasons stated in the theoretical chapter.
- The output of the pulse carver will be connected to the input of the receiver, assuming ideal transmission through the fiber, with no loss or dispersion.

In the **receiver**:

- The splitter will be implemented as having an exact copy of the input signal in each of its outputs, with no loss.
- The OBPF will be perfectly centered at the carrier wavelength, and will have a given *full-width at half maximum* (FWHM). In the center of the filter bandwidth there will be only the desired carrier, while in the edge of the filter bandwidth there will also

be part of the neighbour carriers. This is why the frequency response of the filter will have a Gaussian shape instead of a rectangular one.

- In the demodulator, the time delay in the DLI will be perfectly adjusted to 1 bit slot.
- The optical-electrical conversion in the photodiode will have a 100% efficiency.

In general:

- The measures taken in the simulations will be 100% accurate.
- All the shapes applied to the signals (rectangular, raised-cosine or Gaussian) follow a mathematical definition. The consistency between the ideal definition and the final shape will depend on the number of samples per symbol in the simulation.

4.2 Simulation results

Once the setup and the system operation have been explained, it is time to look unto the system performance through numerical simulations. These simulations will be done under ideal assumptions regarding the behaviour of the optical components involved. In consequence, the following results represent a first approach to a real system implementation; the numerical values obtained are indicative of the viability of the idea. If we assume that our system is somewhat similar to a real one, i.e. the ideal assumptions don't distort too heavily the results, then the conclusions taken at the end of this chapter will be close to being credible. The final evidence of the feasibility of this scheme depends completely on a real implementation in an experiment.

Concerning the results themselves, they have been taken in order to evaluate the system under different conditions. The setup includes several parameters that can affect the final value of a simulation, hence they need to be considered, tuned, and optimized when possible. This doesn´t imply an absolute liberty when choosing the values for these factors, as we should always stay close to the limitations set by commercial equipment. However, we find appropriate to move a bit outside those limits, because this will give us further and more concrete information about the dependence of the system on each of its parameters.

When analyzing the results and trying to get conclusions from them it is important to have in mind all the results obtained before those, as the comparison between them will give us further information and a deeper knowledge of the system. That is where the strength of the results will be, as we will be able to see what the best and the worst case scenarios are, and to obtain the appropriate parameters through optimization processes.

4.2.1 Parameters

Investigated system parameters

These are the parameters that we will find in a physical setup. The parameters will either be chosen following an appropriate criteria or optimized numerically.

- **OBPF BW: Optical band-pass Gaussian filter bandwidth**

As we can see in Figure 18 there is an optical filter in the receiver to separate one carrier from the others. This process is not trivial, as in the pulse carving carried out in the transmitter the spectrum of all the carriers has been broadened and mixed. Hence, the bandwidth of this filter will determine how much power from the neighbour carriers will distort the power of one carrier in particular, and so affecting its Eye Opening Penalty.

- **Laser relative phase**

In order to create an OFDM signal, it is necessary to have one optical source for each carrier. These optical sources can be tuned to create a beam at a certain frequency, but the phase of the field they generate can or cannot be controlled. As all the lasers transmit simultaneously, the difference in the phase between lasers is a parameter to be considered, as it can cause intercarrier crosstalk at detection. This is why it is necessary to test which phase differences between carriers can have a more critical effect.

- **Carrier spacing**

The frequency distance between carriers is a fixed parameter that depends on the commercial DWDM scheme that we are applying. The different commercial values for this spacing are 25, 50, 100 and 200 GHz. We will get results for all these cases.

- **Number of carriers**

The performance of our system can be negatively affected by every new carrier added to it, as it introduces more interference to the other carriers. The available equipment in the laboratory consists of a 16 carriers DWDM source, with a frequency spacing between carriers of 50 GHz. In order to be able to validate the results in this thesis with a real experiment, we will also use 16 carriers as a starting point in our simulations. As we will also want to know how more or less carriers can affect the performance of the system, we will also get results (in the form of Eye Opening Penalty) for 4, 8 and 32 carriers. Doing this we will try to find a general trend that characterizes the addition of carriers.

- **Roll-off factor of raised cosine**

The pulse carver gives a raised cosine shape to the pulses in the setup. The Eye Opening Penalty and hence the quality of the scheme depends directly on the quality of these pulses. This is why it is necessary to find out what kind of shape is more beneficial to the performance of the system. When sweeping this parameter it will be important to remember the theoretical section regarding the raised cosine, and the positive and negative consequences (in terms of crosstalk) that the variation in the roll-off factor implies.

Simulation parameters

These are the parameters that will determine the quality and reliability of our simulations. They need to be fixed at the proper value in order to be able to carry out the main parameters sweep.

- **Number of symbols**

The quality of the received signal (in a certain carrier) depends on the phase difference between that carrier and the other ones. Since we are using a DPSK modulation (which is a phase modulation), one of the parameters that affect this phase difference is the data pattern that is transmitting each carrier. The ideal situation is an infinite length of this data pattern, where all the possible combinations in the phases of the carriers can happen, and so the worst case would be included for sure. However, we need a more feasible approach, for which it is necessary to choose a number of symbols (i.e. length of the data pattern) for our simulations. In this case we will sweep the number of symbols and try to find a minimum value that both requires a reasonable execution time and makes our results reliable (close to how the results would be with infinite symbols simulated).

- **Length of PRBS**

The bit pattern for every carrier is created in a PRBS generator module, which uses a generating polynomial and a seed that we define. The order of that polynomial will determine the length of the output sequence, and the seed will determine its period. Considering that the same PRBS length is used for all carriers, if the number of symbols is larger than the length of the sequence, the sequence is repeated, hence not offering any further information regarding phase combinations (even though it is not harmful, apart from a larger execution time). And if the length of the sequence is larger than the number of symbols, the autocorrelation between the data sequences of the carriers is no longer zero, which is harmful. This is why the PRBS length needs to be at least the same as the number of symbols used.

- **Number of simulations**

It is impossible to carry out an infinite number of simulations (changing the data pattern of each carrier from simulation to simulation) for the results to converge to a certain value. We will choose to make 15 simulations for all the upcoming results. This value will be discussed and justified.

Tools

- **Eye diagram**

The eye diagram is the superposition of all the pulses that form one particular carrier. In addition, and as the filtering process doesn´t perfectly separate the carriers spectrums, there will be remains from undesired carriers in the eye diagram, hence worsening its appearance. The visual inspection of the eye diagram, even when it is not a quantitative result, can give us an idea of what the quality of system is in a certain situation.

- **Spectrum diagram**

The frequency spectrum of the signal in the different key points of the system will also be a good reference when trying to establish if the simulations are working properly. Some interesting diagrams could be the way one carrier looks in the frequency domain when generated with rectangular pulses, the way the spectrum looks when all the carriers are put together, or how it changes when the signal goes through the pulse carver. It is also interesting to see what is the frequency shape of a raised cosine for different values of α, and if that shape corresponds with the one after the carver.

- **Eye Opening Penalty**

The Eye Opening Penalty (EOP) is the quantitative parameter chosen to evaluate the performance of this scheme. It is calculated using the following formula:

$$EOP \quad dB \quad = 10 * \log_{10} \frac{EyeReference}{EyeNorm}$$

Where *EyeNorm* is:

$$EyeNorm = \frac{Maximum\ Eye\ Opening}{NormPower}$$

Where *NormPower* is the average optical power of the signal, and *Maximum Eye Opening* is the difference between the lowest value of a 1 and the highest value of a 0 in the eye diagram. *EyeReference* is calculated in the same way that *EyeNorm*, but in this case the eye diagram where all the parameters are calculated corresponds to a reference situation with only one carrier. Hence, the function of the EOP is to illustrate how much the situation has been worsened because of the use of several carriers. It is important to remember that the EOP is indeed a penalty, so the best case will always be the lowest value.

Scenarios

There are several parameters to be simulated and optimized, and so we need some structure to obtain the results and present them. Following this idea we have divided the simulations in two possible scenarios with different conditions; the results for both of them combined will give us a broad panorama of the performance of the scheme.

- **Scenario 1)**

Starting point: fixed carrier spacing.

We want to test the different options for OBPF BW, relative laser phase and roll-off factor, always as a function of the number of carriers.

- **Scenario 2)**

Starting point: fixed total spectral width.

We want to test the different options for OBPF BW, relative laser phase and roll-off factor, always as a function of the carrier spacing.

What kind of results are we looking for?

As stated above, the results will be obtained after groups of 15 simulations, which will allow us to be partially independent of the data sequences used. As it is known that a critical point in any system is the worst performance than it can guarantee, all the results will be focused on finding the necessary conditions for that case to happen. In some cases we will be also interested in finding the best possible performance, so we can specify an interval of acceptable values for certain parameters. All of these results will be given in terms of EOP, and sometimes an eye diagram or spectrum diagram will be provided to enhance them.

4.2.2 Scenario 1

In this first scenario we have our starting point in the standard DWDM scheme with 16 carriers separated 50GHz one to another (50G DWDM). We will leave that spacing as a constant and ask ourselves what happens with the performance of the system when we sweep all the other main parameters of the setup.

In the parameters definition we stated that the different options for the number of carriers were 4, 8, 16 and 32. As the spacing between carriers remains the same, what we are valuing in this case is how the addition of distant neighbours affects one target carrier.

The simulations are based on the Eye Opening Penalty calculated for each carrier. Eye Diagrams will be provided in order to graphically understand the EOP values. We will see the results for sweeping the optical band-pass filter bandwidth, the initial relative phase between carriers, and the raised cosine roll-off factor.

Simulation parameters

As said in the definition of the parameters at the beginning of this chapter, the final results don't only depend on the system parameters, but also on the simulation parameters. If these parameters are not properly chosen, the results could not be acceptable.

We have chosen the reference situation of 50 GHz DWDM with 16 carriers to perform the parameter sweeps.

Number of simulations

All the results that we are going to see in this chapter consist of an average of 15 iterations. This is because the data pattern changes from simulation to simulation, and as the EOP for each carrier is very sensitive to that pattern, it is necessary to explore many different pattern combinations. However, the number of iterations chosen may or may not be enough to make our results reliable. That is why it seems necessary to evaluate how the EOP evolves when increasing the number of simulations. In concrete, we will evaluate how the highest EOP evolves (calculated with the proper OBPF BW and relative phase between carriers, which can be checked later in this section).

We are using a 50 GHz DWDM scheme with 16 carriers. This test has also been performed with 4, 8 and 32 carriers with similar results. The trend line that can be observed in Figure 20 follows the following logarithmic expression:

$$EOP = -0{,}014 * \ln(x) + 1{,}1988$$

Where x is the number of simulations. The trend line is automatically generated by the graphics software (Microsoft Excel).

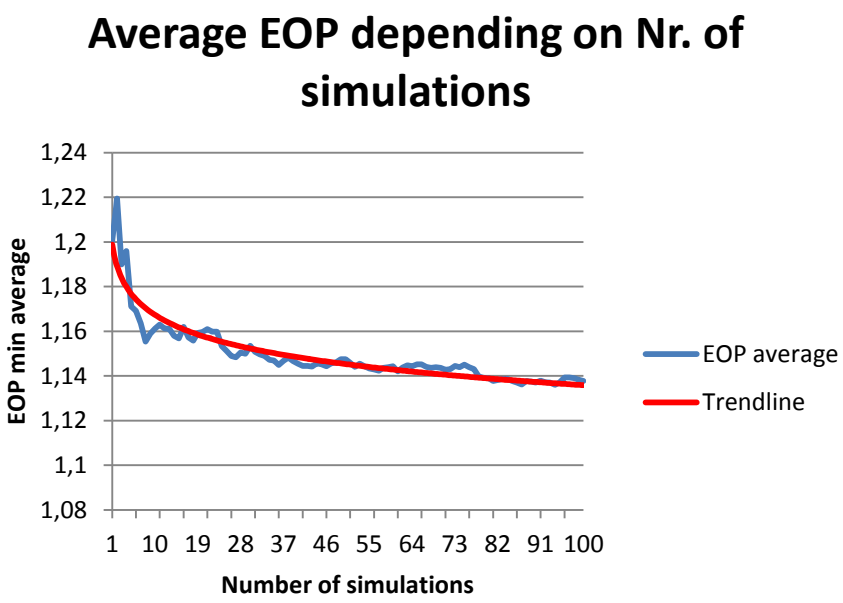

Figure 20 - Average EOP depending on Nr. of simulations.
Conditions: 16x50G DWDM; OBPF BW = 20 Ghz; Laser relative phase = π;
Number of symbols = 128; PRBS order = 7; Roll-off factor = 0,1; Data pattern = random

In this chart we can see a very clear tendency in the average highest value of EOP in this scenario. It is clear that the average is heavily influenced by the early variations in the data pattern, demonstrated by the different peaks found between 1 and 10 simulations. However, after a certain number of simulations, the average EOP value get closer to an asymptotic value, which seems to be around 1,14 dB.

It can be useful to calculate the error that we are making when doing 15 simulations instead of a higher number. For example, we can compare the average EOP value at 15 simulations (EOP_{15}) with the average EOP value at 100 simulations (EOP_{100}):

$$Error = \frac{|EOP_{15} - EOP_{100}|}{EOP_{100}} = 1{,}78\%$$

We can also compare the average EOP value at simulations (EOP_{15}) with the average EOP value in the trend line at 100 simulations $(EOP_{100}{}^{Trend})$

$$Error = \frac{|EOP_{15} - EOP_{100}{}^{Trend}|}{EOP_{100}{}^{Trend}} = 2{,}09\%$$

This shows us that even when doing a small number of simulations we are presumably a 2% far from the real value, at most, which gives us confidence about all the upcoming results.

Number of symbols

The upcoming results obtained in this chapter are all based on the EOP value. This number strongly depends on the appearance of all the pulses of the sequence. In the case where all the pulses are equal but one of them has a smaller eye aperture, the EOP will be severely affected. Then, it seems logical to think that if more symbols are involved in the simulations, the probability of worsening the EOP raises.

As we said in the introduction of this chapter, the number of symbols should be increased alongside with the PRBS length. In Figure 21 we can see the result of increasing only the number of symbols:

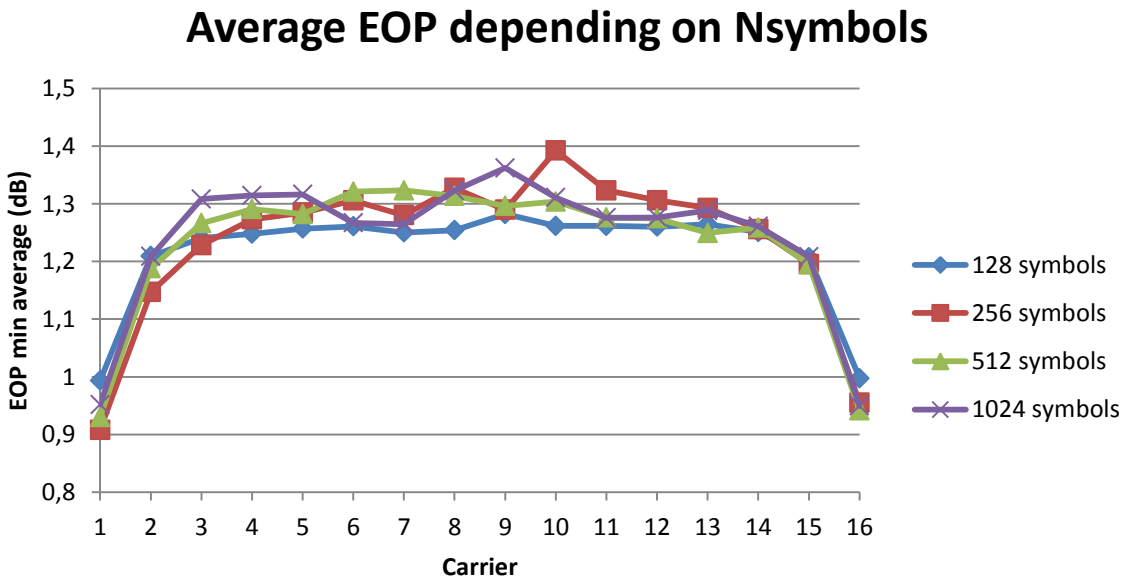

Figure 21 – Average EOP depending on Nsymbols
Conditions: 16x50G DWDM; OBPF BW = 19 Ghz; Laser relative phase = π; PRBS order = 7; Roll-off factor = 0,1; Data pattern = random; Number of simulations for the average = 15

As expected, the number of symbols by itself does not really affect the result. This is because even after raising the number of symbols of the simulation, the basic data sequence has the same length, so it is basically repeating itself. The only way the EOP could worsen would be if new combination of ones and zeros appeared comparing to the basic case (128 symbols), and that is not happening. In order to let that happen, it is necessary to increase the length of the PRBS .

PRBS order

To increase the length of the data sequence, we need to increase the order of the PRBS generating polynomial. We need to choose an appropriate polynomial, so the PRBS has the largest possible period. We also need to match the PRBS length with the number of symbols. By fulfilling these two requirements we will make sure that the autocorrelation of the data sequences will be perfect (zero) and that new combinations of ones and zeros will appear.

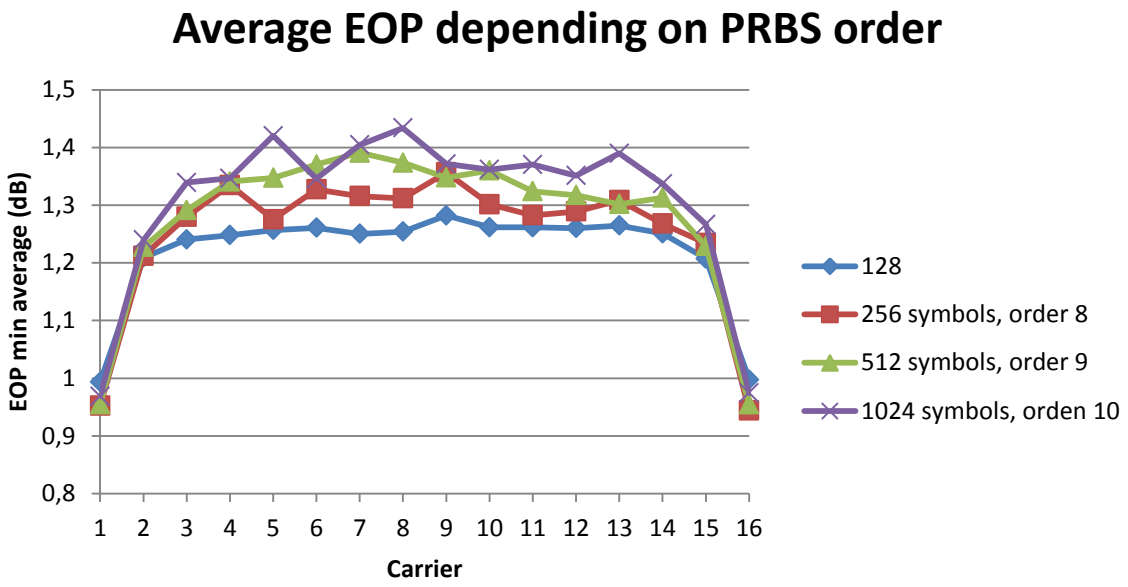

Figure 22 – Average EOP depending on PRBS order
Conditions: 16x50G DWDM; OBPF BW = 19 Ghz; Laser relative phase = π; Roll-off factor = 0,1; Data pattern = random; Number of simulations for the average = 15

As expected, we can see now in Figure 22 the influence of the number of symbols on the EOP value. Each time we double the number of symbols and the period of the sequence, the EOP gets a bit higher. However, the growth in terms of EOP is not linearly related to the increase in the number of symbols; note that this parameter doubles its value, while the EOP rises around 0,05 dB each time. This leads to think that the change between our results and a realistic symbol sequence could be around 0,2 dB in EOP. Again it is proportionally significant (it's the 15% of the average EOP value), but the EOP still remains low.

The explanation to this phenomenon is related to the dependence of the EOP on the relative phases of the carriers that form our OFDM signal. Those phases also depend on the data patterns used in each carrier. The longer the data patterns, the more different combinations of ones and zeros in the field (as long as they are correctly generated with a PRBS source). And if this happens, there are more different phase combinations, which make the probability of worsening the EOP higher.

System parameters sweep

OBPF BW

The first thing to notice when trying to sweep the OBPF BW is that the EOP depends on it, in a way that we can see in Figure 23. The shapes of these lines show that for low values of OBPF BW, the width of the pulses is wide enough to cause intersymbol crosstalk, so the penalty is high. For high OBPF BW values, there is more energy from the neighbour carriers interfering with our signal, worsening the EOP. It is possible to find an OBPF bandwidth for each carrier where they have their lowest EOP. In Figure 23 we show the lowest EOP among all the carriers, which happens at one of the edge ones (carrier number 4).

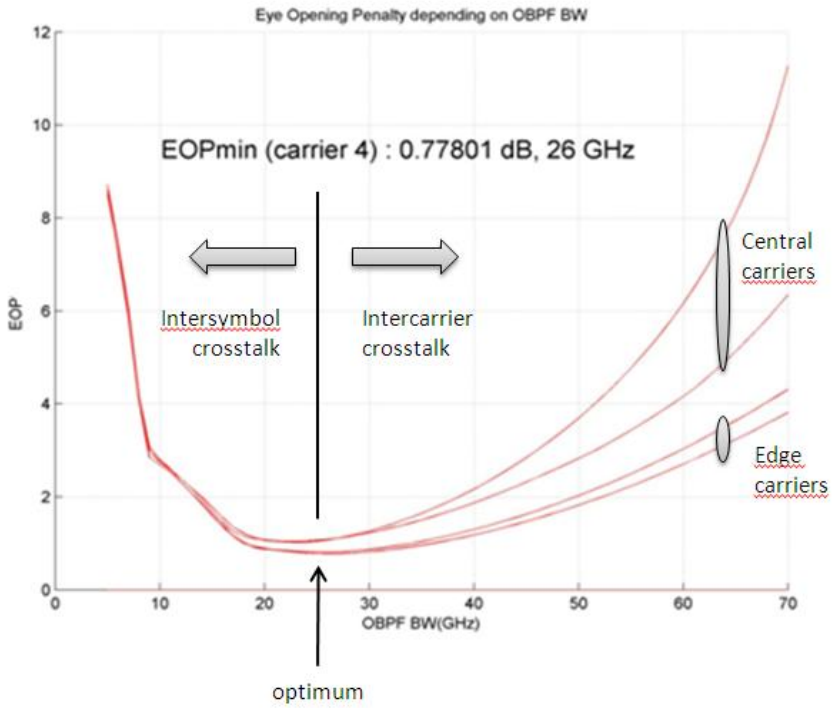

Figure 23 – EOP depending on OBPF BW
Conditions: 16x50G DWDM; Laser relative phase = π; Roll-off factor = 0,1; Data pattern = random; Number of simulations = 1 (NO AVERAGE); Number of symbols = 128. PRBS order = 7

This makes us notice that the symmetric carriers (in this case 1 and 4, 2 and 3) behave in a similar way, and that the penalty in the central carriers is higher than in the edge ones, which is easy to expect, as the former ones have more close-neighbours than the latter ones. For low values of OBPF BW the main crosstalk is the intersymbol one, and that is the reason why we observe a similar performance in all the carriers. For high values of OBPF BW the main crosstalk is the intercarrier one, and as it depends on the number of neighbour carriers and their data patterns, the performance changes from carrier to carrier.

As we were saying, it is possible to find an optimal OBPF BW (and its related minimum EOP) for each carrier. If we do this while sweeping the number of carriers we obtain the results in Figure 24 and Figure 25.

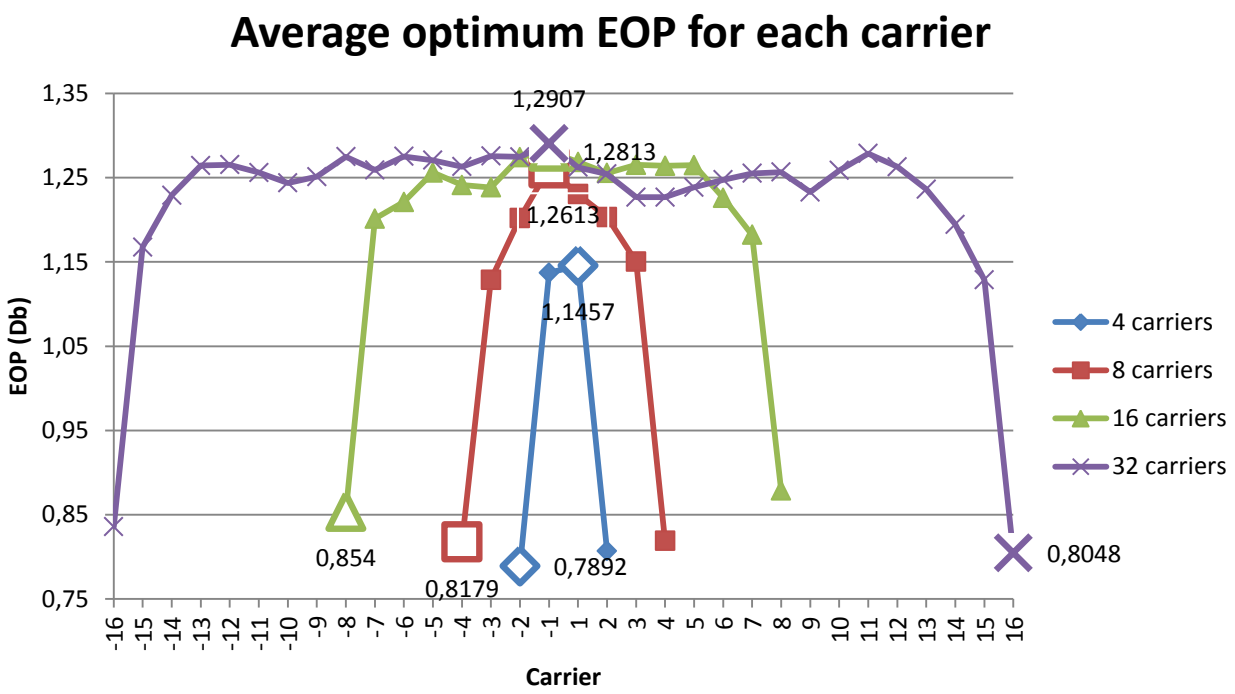

Figure 24 – Average optimum EOP for each carrier
Conditions: 50G DWDM; Laser relative phase = π; Roll-off factor = 0,1; Number of symbols = 128; PRBS order = 7;Data pattern = random; Number of simulations for the average = 15

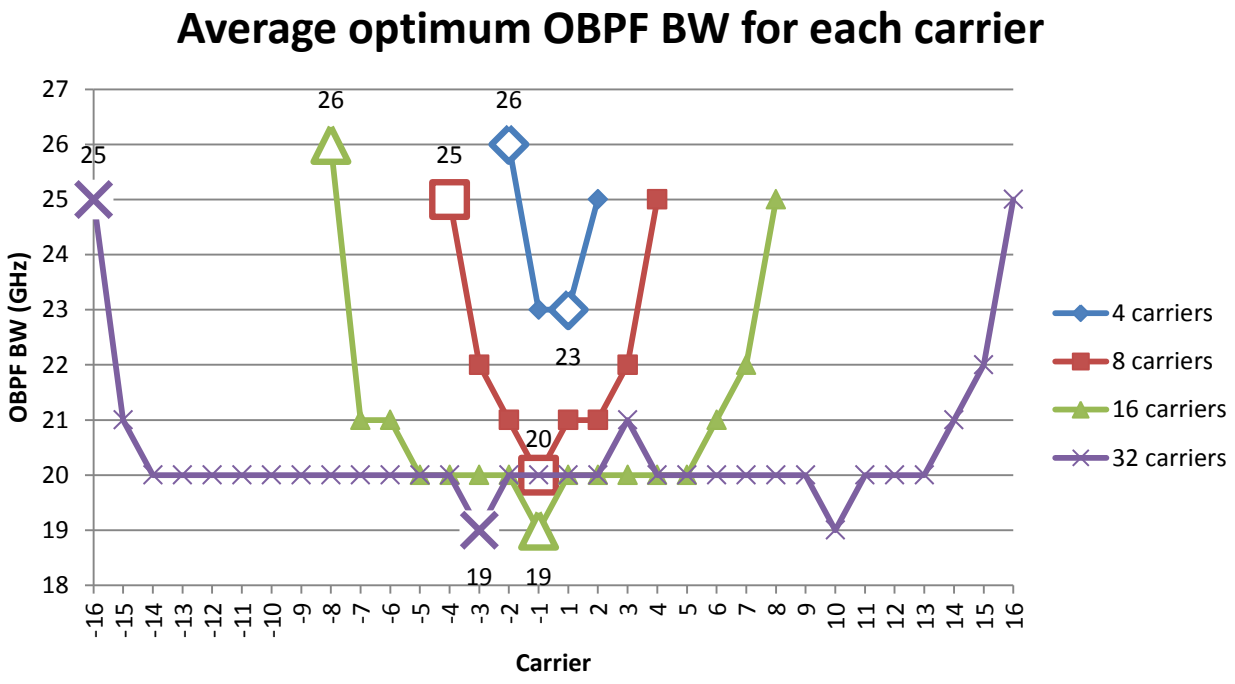

Figure 25 – Average optimum OBPF BW for each carrier
Conditions: 50G DWDM; Laser relative phase = π; Roll-off factor = 0,1; Number of symbols = 128; PRBS order = 7;Data pattern = random; Number of simulations for the average = 15

An ideal situation would allow us to use a different OBPF BW for each carrier, hence getting the optimal EOP for each of them. However, a real filter (AWG) has a fixed bandwidth, so it is necessary to choose a fixed value for the OBPF BW parameter. Regarding this decision, we suggest two different criteria:

- Worst case criteria: to choose the lowest OBPF BW from Figure 25. This worst case always happens in one of the central carriers, and it guarantees to have the highest EOP value among all the carriers. The concrete carrier where this worst case happens is not relevant, as the EOP value depends on the data pattern of the neighbour carriers, which changes randomly. The worst case criteria will lead us to the worst possible scenario for this scheme, which is interesting when we want to know the minimum specifications of the system.
- Best case criteria: to choose the highest OBPF BW from Figure 25. This best case always happens in one of the two edge carriers, and it guarantees to have the lowest EOP value among all the carriers. The best case criteria will lead us to the best possible scenario for this scheme, which is interesting when we want to know the best possible service that the system can provide.

Note that Figure 25 shows the optimum OBPF BW for each carrier. The two different criteria stated above (worst and best) still refer to this optimum values; the only difference is that the worst case chooses the *worst* optimum value, while the best case chooses the *best* optimum value. This is possible since we are working with several carriers.

In order to be able to identify both criteria cases we provide Figure 26 and Figure 27, where we can observe the highest and the lowest EOP and OBPF BW values for each number of carriers (this information can be extracted from Figure 24 and Figure 25).

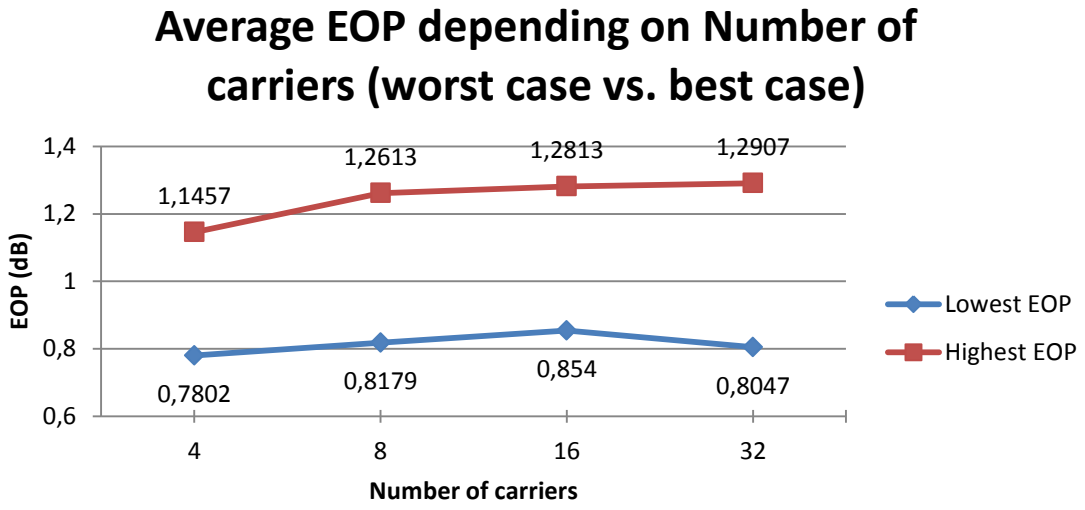

Figure 26 – Average EOP depending on Number of carriers (worst case vs. best case) Conditions: 50G DWDM; Laser relative phase = π; Roll-off factor = 0,1; Number of symbols = 128; PRBS order = 7;Data pattern = random; Number of simulations for the average = 15

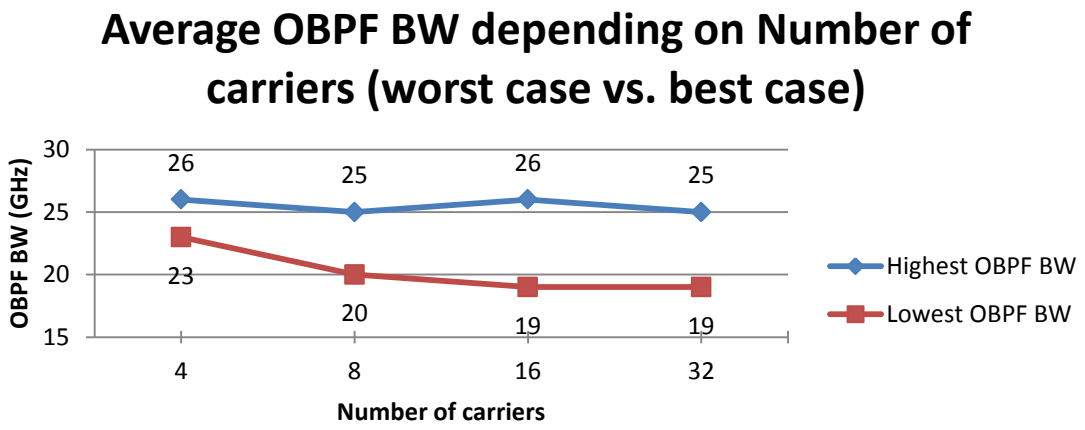

Figure 27 – Average OBPF BW depending on Number of carriers (worst case vs. best case) Conditions: 50G DWDM; Laser relative phase = π; Roll-off factor = 0,1; Number of symbols = 128; PRBS order = 7;

It is easy to see that the number of carriers doesn't really affect the optimal values of the EOP or the OBPF BW. If we look at Figure 26 and Figure 27 we can see that the most different case is when we work with 4 carriers; for a higher number of carriers (8, 16 or 32), we can see similar values for both the OBPF BW and the EOP, and for both the worst case and best case. From these results we can conclude that once we reach a certain number of carriers, any further addition of carriers will not worsen the EOP or change the optimal OBPF BW. This certain number of carriers is 8 in the current situation, where the carriers are spaced 50 GHz from each other.

Regarding the EOP values, we can see that the difference between the best and worst case when they stabilize is around 0,5 dB. This is a factor 1,12 in lineal scale, which can be graphically observed in the eye diagrams in Figure 29 and Figure 28. In Figure 29 (worst case), the higher interference from the neighbour carriers can be noticed especially in the edges of the diagram.

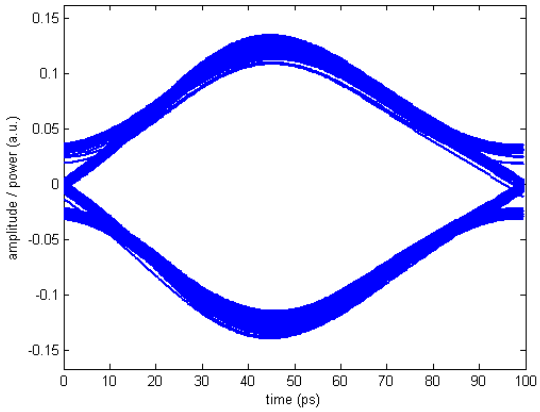

Figure 29 – Eye diagram for highest EOP Conditions: 8x50G DWDM; Laser relative phase = π; Roll-off factor = 0,1; Number of symbols = 128; PRBS order = 7; Data pattern = random; EOP = 0,81 dB

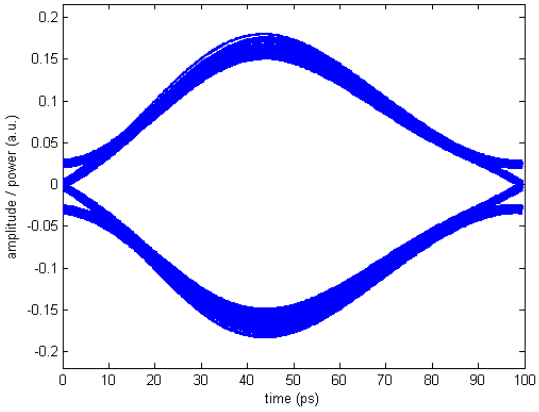

Figure 28 – Eye diagram for lowest EOP Conditions: 8x50G DWDM; Laser relative phase = π; Roll-off factor = 0,1; Number of symbols = 128; PRBS order = 7; Data pattern = random; EOP = 1,26 dB

Once we have an OBPF BW value that will guarantee us a worst case scenario (among all the optimal OBPF BW values), we can start sweeping the other parameters.

LASER RELATIVE PHASE

The purpose now is to find a laser relative phase that can lead us to an even more well-defined worst case scenario. As we are working with a DPSK modulation, our symbols will be optically transmitted with a 0 relative phase (logical 1) or a pi relative phase (logical 0); however, as there are several lasers involved and the spectrum of the carriers gets mixed, the relative phase difference between the lasers can affect the crosstalk between them, hence changing their EOP.

In this part we have considered two options: to be able to control the lasers initial phase or not. If we cannot control them, then the phases can take any random value between 0 and 2π. If we can control them, then we can fix them to whatever values we desire; however, we are working in scenarios with up to 32 different lasers, and so we should sweep all of those phases through all possible values. Instead, we can consider the extreme case where a carrier has a given phase (e.g. 0) and sweep the phase of its two immediate neighbours, which will be the ones affecting its performance the most. We have done this preliminary simulation, and we have seen that the highest interference happens when both neighbours have a relative phase to the target carrier of 0 or π . This leads us to take into account, apart from the random phase difference, the π and the 0 phase difference between carriers.

Regarding the random phase difference, it will be simulated with the following conditions: in every iteration a different random phase and a different data pattern will be assigned to every optical source. Also in every iteration the EOP will be calculated for each carrier. After doing 15 iterations, the average EOP for each carrier is calculated and shown in Figure 30 and Figure 31.

Again, we are sweeping the number of carriers between 4 and 32 with a fixed spacing of 50 GHz. In the following two images we can see the comparison between the three cases stated above (random phase, pi difference phase, same phase) for 8 carriers and 32 carriers. We want to see if the EOP converges (for the central carriers) when the number of carriers is equal to 8 or more, which is what happened in the previous section (when sweeping the OBPF BW).

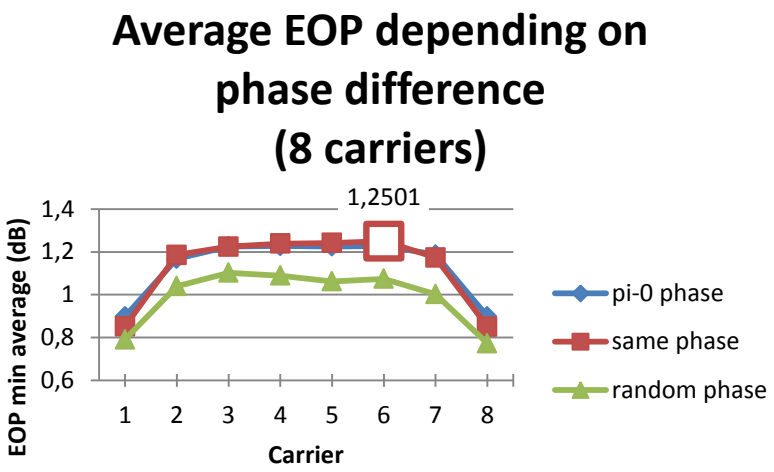

Figure 30 – Average EOP depending on phase difference (8 carriers)
Conditions: 8x50G DWDM; OBPF BW = 21 GHz; Roll-off factor = 0,1;
Number of symbols = 128; PRBS order = 7; Data pattern = random;
Number of simulations for the average = 15

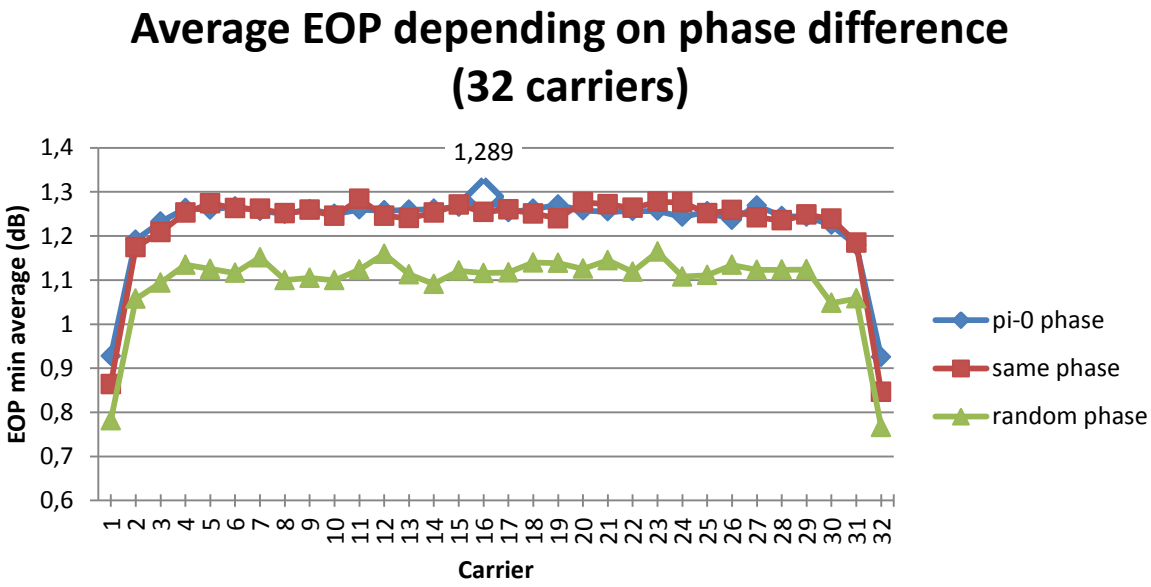

Figure 31– Average EOP depending on phase difference (32 carriers)
Conditions: 32x50G DWDM; OBPF BW = 20 GHz; Roll-off factor = 0,1; Number of symbols = 128; PRBS order = 7;
Data pattern = random; Number of simulations for the average = 15

We obtain two conclusions from the figures above. Giving an answer to what we were asking ourselves before, we can say that the tendency remains: there is barely a difference of 0,03 dB between the worst EOP value in the 8 carriers case and the 32 carriers one. As we are working with random parameters, this value could perfectly fluctuate from simulation to simulation. Again, the addition of carriers to the system (as long as there are at least 8 carriers) will have no effect on its performance, neither in terms of the laser's initial phase.

The second conclusion that we can extract is that the worst case is always when the carriers have the same phase or a π difference; in fact, since we are using a DPSK modulation, using a π phase difference will just invert the sign of the symbols of the neighbour carriers, while a 0 phase difference (same phase) will leave them as they were; anyway, as the data patterns are long enough to contain all kind of 0 and 1 combinations, it doesn't matter if the sign of the symbols is inverted with a π phase difference, because in the end it will have the same effect as not introducing a phase difference at all. In summary, both cases (π difference and same phase) are identical, and we will use this phase relationship in all simulations from now on to complement our worst case scenario.

We can also observe that the random phase case has always a lower EOP value compared to the other two cases. The difference is around 0,2 dB; as we saw in Figure 28 and Figure 29, this difference is hardly noticeably in an eye diagram, although it is proportionally significant as an EOP value.

The rest of the simulations also support this assessed tendency (for 4 and 16 carriers).

Roll-off factor

As it was explained in the theoretical chapter, the conversion from an optical OFDM to an OTDM scheme with the multiplexing of several tributaries is accomplished through a pulse carver. The goal of this carver is to reduce the time duration of the pulses, so there is free space between them to allocate the pulses of the other tributaries. The ideal situation would be to obtain perfectly rectangular pulses after the carving process; however, this is not something to expect in a laboratory. A more realistic approach would be to expect the pulse shape being more similar to a raised-cosine.

This raised-cosine form has a parameter, the roll-off factor (α), which defines how close its shape is to a rectangular pulse. As this is the first parameter sweep concerning the shape of the pulses, we will allow ourselves to look for the most optimal shape. From here on, we need to remember the theoretical part of the raised-cosine pulse. In that section we saw how the spectrum of a raised cosine defined in the time domain evolves while changing its roll-off factor (α).

- When α is close to zero, the pulse shape is close to a rectangular one, so there is very little intertributary interference. However, the part of the carrier spectrum that coincides with the spectrum of other carriers has a relatively high power level, hence introducing intercarrier crosstalk. As each carrier has a different data pattern, this intercarrier crosstalk can be very different for each carrier, and so we will see very different EOP values.

- When α is close to one, the pulse shape is close to a Gaussian one, and is twice as broad as in the α=0 case; this essentially means that, if we want zero interference

between the different tributaries, the number of them that we can multiplex will be reduced by half. And if we want to keep the number of tributaries, then the pulses will interfere with each other. However, as the part of the spectrum that coincides with the spectrum of other carriers has a very low power level, there is very little intercarrier interference.

Following the line of thought of looking after the absolute worst case in our system, we will try to find the roll-off factor at which we find the highest EOP among all carriers. However, there is a factor that we need to take into account when choosing a roll-off factor for our system: the fact that in this simulation we are supposing a perfect multiplexing and demultiplexing process of the different tributaries. This implies that the shape of the pulse after demultiplexing (in the receiver) will be the same as after carving (in the transmitter). This assumption, while not being a key issue in the other simulations, can affect now our decision regarding the roll-off factor. From the two different cases stated above (α=0 and α=1), we will only be able to observe the first one; the latter will be distorted by the lack of multiplexing tributaries in the simulations.

We can see the results for this simulation in Figure 32:

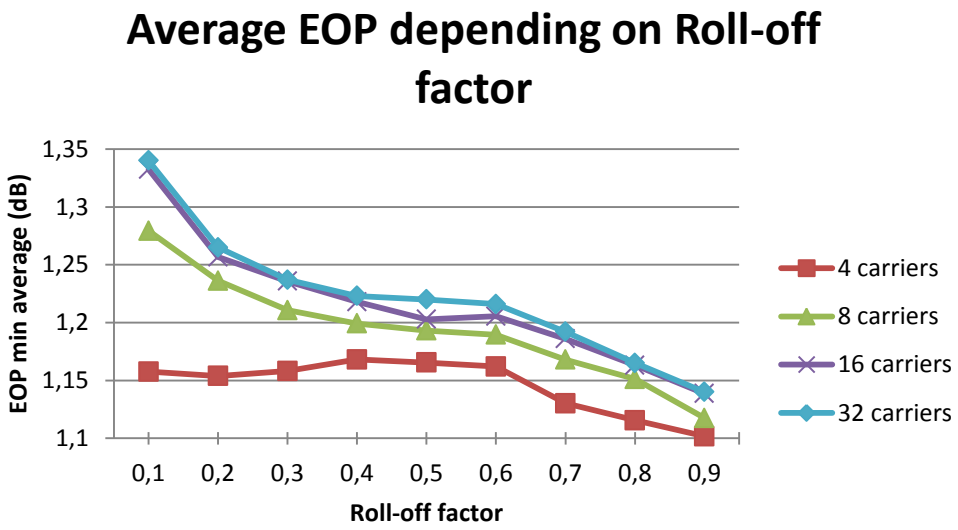

Figure 32 – Average EOP depending on Roll-off factor
Conditions: 50G DWDM; Laser relative phase = π; Number of symbols = 256; PRBS order = 8; OBPF BW = 23 GHz (4 carriers), OBPFW BW = 21 GHz (8 carriers), OBPF BW = 20 GHz (16 and 32 carriers); Data pattern = random; Number of simulation for the average = 15

Again, we can obtain some conclusions from these results. First of all, the general behaviour of the system is to have a better EOP when the roll-off factor increases. This tendency is very clear when there are 8, 16 or 32 carriers involved, while it is less realistic in the 4 carriers case. The roll-off factor where there is a larger difference between the

different situations is α=0,1; for the other α values, the EOP is quite similar in the 8, 16 and 32 carriers cases.

As we have already stated, in Figure 32 we cannot see the intertributary crosstalk that would happen for high values of α, because these simulations don't include the multiplexing of different tributaries. This is the reason why the EOP values keep decreasing when we increase the roll-off factor; a more realistic relationship (which included the tributaries multiplexing) would make the EOP increase again at some point, where the intertributary crosstalk became significant. This means that Figure 32 is useful to know how the spectrum shape of the raised cosine affects the performance of the system, without taking into account the pulse shape. It also means that in a real scenario it would be feasible to find an optimum roll-off factor value for which we had the lowest EOP, where the intertributary and the intercarrier crosstalk were equally significant.

As a reference, in the following eye diagrams we can observe the difference between the two extreme cases for 16 carriers: α=0,9 (Figure 34) and α=0,1 (Figure 33). While the eye diagrams are quite similar in the center of the diagram, it is easy to see that in the worst case (right) there is more power in the diagram, especially noticeable in the edges of the eye, and so worsening the EOP.

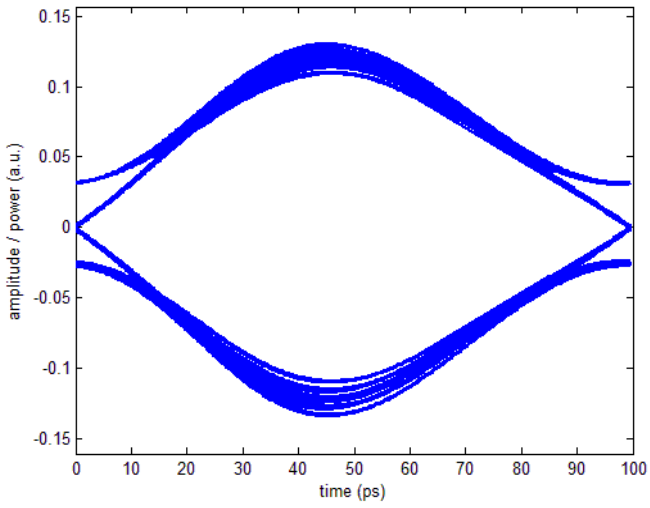

Figure 34 – Eye Diagram for lowest EOP Conditions: 16x50G DWDM; Laser relative phase = π; Number of symbols = 128; PRBS order = 7; OBPF BW = 20 GHz; Data pattern = random; Roll-off factor = 0,9

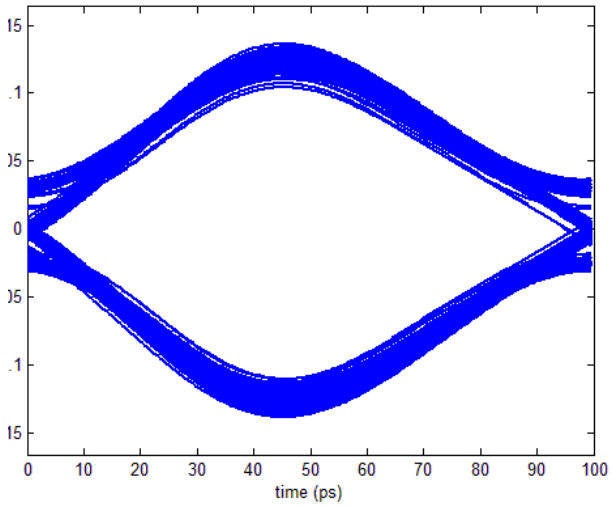

Figure 33 – Eye Diagram for highest EOP Conditions: 16x50G DWDM; Laser relative phase = π; Number of symbols = 128; PRBS order = 7; OBPF BW = 20 GHz; Data pattern = random; Roll-off factor = 0,1

For further simulations it is necessary to establish a criteria regarding the roll-off factor. As our goal is to find the worst possible scenario, it seems appropriate to choose α=0,1, as it has always the highest EOP.

In conclusion, even when the results show us that the highest the roll-off factor the lowest the EOP, we would need to reduce our system capacity by half in order to take a full advantage of that fact (to avoid intertributary interference). In addition, as we are not multiplexing tributaries in this thesis, we have no reliable results for high roll-off factor values. Our decision will be to use α=0,1 for all the simulations, as it is a feasible value in the laboratory, and it guarantees that the non-existing multiplexing/demultiplexing scheme in the simulations will not affect the final results.

Worst case

After finding the system parameters or conditions for the worst situations to happen, we need to put all those results together and find a final worst case scenario result. From the three previous sections we obtain that:

- Every carrier has an optimal OBPF BW, and we are taking the lowest one (which leads to the highest -*worst*- EOP value). The OBPF BW will be 23 GHz (4 carriers), 21 GHz (8 carriers), or 20 GHz (16 and 32 carriers);
- The phase difference between neighbour carriers will be π
- The roll-off factor will be α=0,1

In all the previous simulations, we obtained results as an average of 15 simulations, in order to find the convergence of the EOP values. That kind of result gives us information about the average performance of the system. However, it can also be useful to know the worst situation that we may face. This is the reason why we are now taking the one highest EOP value among all carriers and all the simulations (without average). With that purpose in mind, and applying the values for the other parameters stated above, we will get the absolute worst case of this setup. We can see the results in Figure 35:

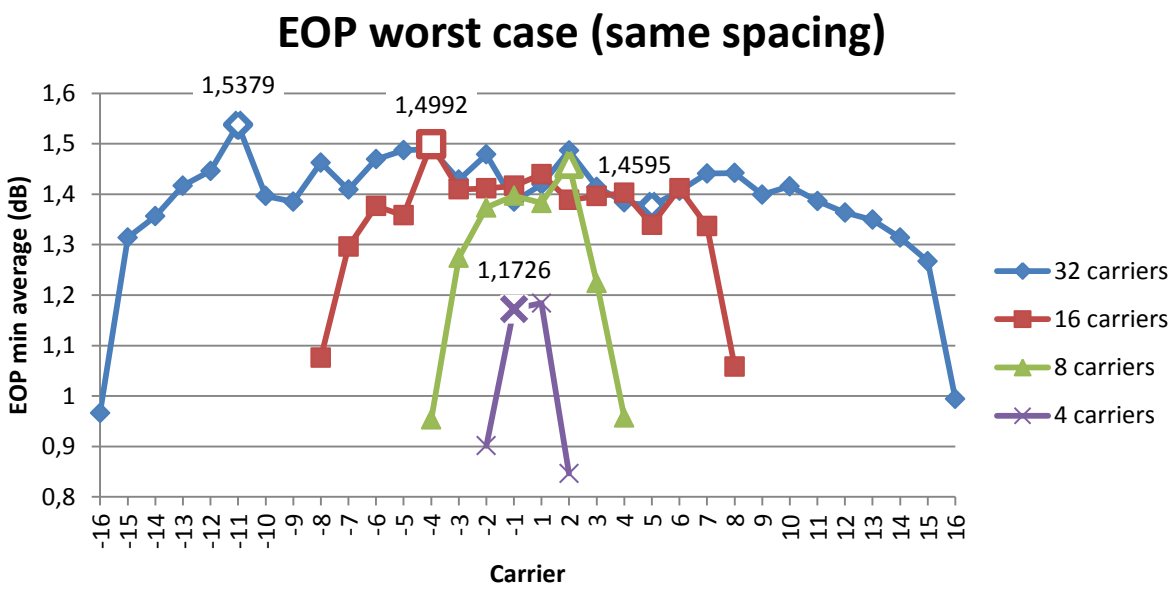

Figure 35 - EOP worst case (same spacing)
Conditions: 50G DWDM; Laser relative phase = π; Roll-off factor = 0,1; Number of symbols = 128; PRBS order = 7; OBPF BW = 23 GHz (4 carriers), OBPFW BW = 21 GHz (8 carriers), OBPF BW = 20 GHz (16 and 32 carriers); Data pattern = random; Number of simulations = 15 (NO AVERAGE)

What we notice in this graph, and comparing it to the one from OBPF BW sweep (Figure 25), is that there is a growth of 0,2 dB between the average EOP values and the highest possible ones. This is true except for the 4 carriers case, where there are so few carriers that the changes on the data patterns don't cause big EOP fluctuations (while they do with a larger number of carriers).

The conclusion is that there are some fluctuations in the EOP values that may cause the performance of the system to be worsened in a certain moment. These fluctuations move a 15% around the value of the average EOP; this means that proportionally they look significant, but as the average EOP value is low, they should not have a critical effect on the system.

4.2.3 Scenario 2

In our laboratory we have at our disposal a 50GHz DWDM source with 16 carriers, with a total spectrum width of 800 GHz. In this second scenario we will use pre-defined DWDM spacings (such as 25, 100 and 200 GHz) within that given bandwidth of 800 GHz.

The number of carriers to use in each case is:

$$Number\ of\ carriers\ (25\ GHz\ DWDM) = \frac{800\ GHz}{25\ GHz} = 32$$

$$Number\ of\ carriers\ (50\ GHz\ DWDM) = \frac{800\ GHz}{50\ GHz} = 16$$

$$Number\ of\ carriers\ (100\ GHz\ DWDM) = \frac{800\ GHz}{100\ GHz} = 8$$

$$Number\ of\ carriers\ (200\ GHz\ DWDM) = \frac{800\ GHz}{200\ GHz} = 4$$

The parameters that we will optimize are the OBPF BW, the relative phase between lasers and the roll-off factor; the same ones as in scenario 1. However, the goal now is to know how the distance to new added carriers affects the performance of the system.

Simulation parameters

Number of simulations

In the previous scenario we looked into how the number of simulations can affect the convergence of the results. However, at least two parameters change from the first scenario to the second one (carrier spacing and OBPF BW), so it is necessary to know the dependence of our results on the number of simulations for this new scenario. Our results are all based on EOP averages through 15 simulations, so we will show how this average value evolves when doing up to 50 simulations and compare it with the value at 15 simulations.

Figure 36 shows the EOP dependence on the number of simulations for the 25 GHz case. From simulation to simulation the main change happens in the data pattern of each carrier, which is randomized. The OBPF BW, the phase difference and the roll-off factor remain constant through all the simulations.

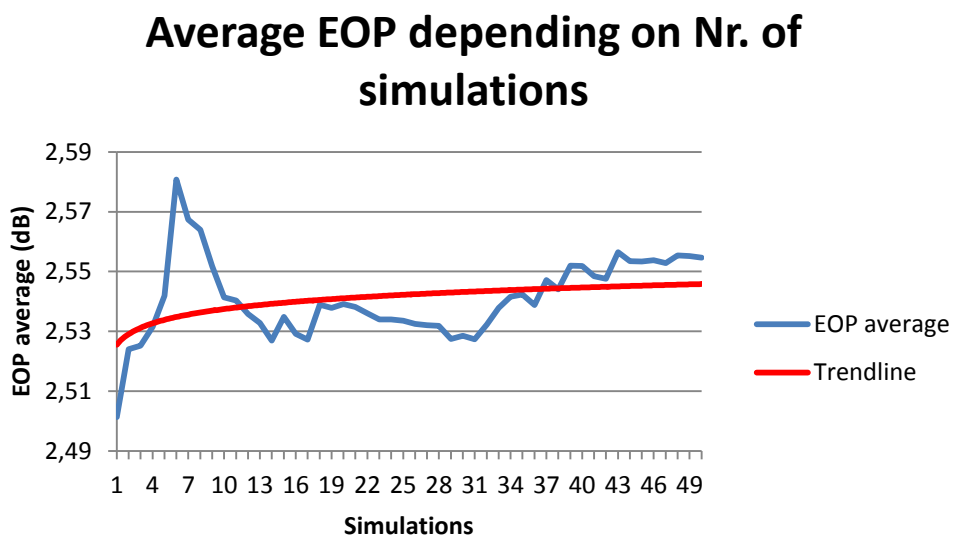

Figure 36 – Average EOP depending on the number of simulations
Conditions: 32x25G DWDM; OBPF BW = 16,5 GHz; Laser relative phase = π; Roll-off factor = 0,1; Number of symbols = 256; PRBS order = 8; Data pattern = random

As we can see, the average EOP value is still dependent on the particular data patterns used in a particular simulation. This is easy to see when looking at the variations of the average EOP value around the trend line. The trend line is automatically calculated as a logarithmic function by the graphics software (Microsoft Excel). The expression of this trend line is:

$$EOP = 0{,}0052 * \ln(x) + 2{,}5255$$

Where x is the number of simulations. The fact that it is possible to draw a trend line allows us to calculate the relative error when doing 15 simulations. For example, we can compare the average EOP value at 15 simulations (EOP_{15}) with the average EOP value at 50 simulations (EOP_{50}):

$$Error = \frac{|EOP_{15} - EOP_{50}|}{EOP_{50}} = 1{,}08\%$$

We can also compare the average EOP value at simulations (EOP_{15}) with the average EOP value in the trend line at 50 simulations ($EOP_{50}{}^{Trend}$)

$$Error = \frac{|EOP_{15} - EOP_{50}{}^{Trend}|}{EOP_{50}{}^{Trend}} = 0{,}43\%$$

These results show us that, on average, the values that we have obtained in this chapter are a 1% different from the possibly real ones, which is again acceptable.

We have chosen to show the 25 GHz case because it has the highest relative error among all of the possible spacings.

System parameters

OBPF BW

In the previous scenario, the optimal OBPF BW for each case was quite similar because the distance to the carriers was always the same. In this new scenario this distance changes, so it seems illogical to expect a similar result.

First of all we can see the dependence of the EOP on the OBPF BW for the 200 GHz spacing case, which is the most distant one to the reference case (50 GHz).

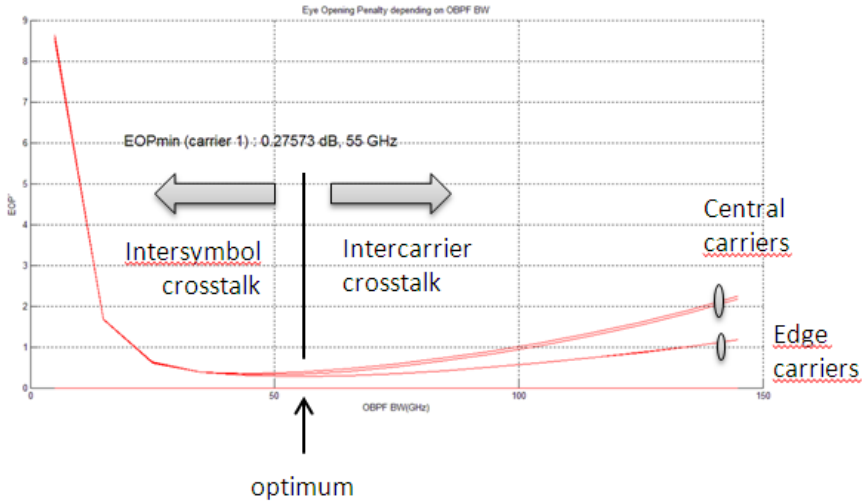

Figure 37 - EOP depending on OBPF BW
Conditions: 4x200G DWDM; Laser relative phase = π; Roll-off factor = 0,1; Data pattern = random; Number of simulations = 1 (NO AVERAGE); Number of symbols = 256. PRBS order = 8

At first sight we can see that the dependence is similar in the way it decreases so fast to its minimum and slowly raises afterwards. However, a quick checking at the same graph at the first scenario (Figure 23) will allow us to compare the EOP and OBPF BW values and see some important changes in them. In the same way that we did in the first scenario, we can calculate the optimal OBPF BW for each carrier and its corresponding EOP. We can do this while changing the frequency spacing, and calculating the average EOP in 15 iterations. An overview of all the results of this section is shown in Figure 38 and Figure 39.

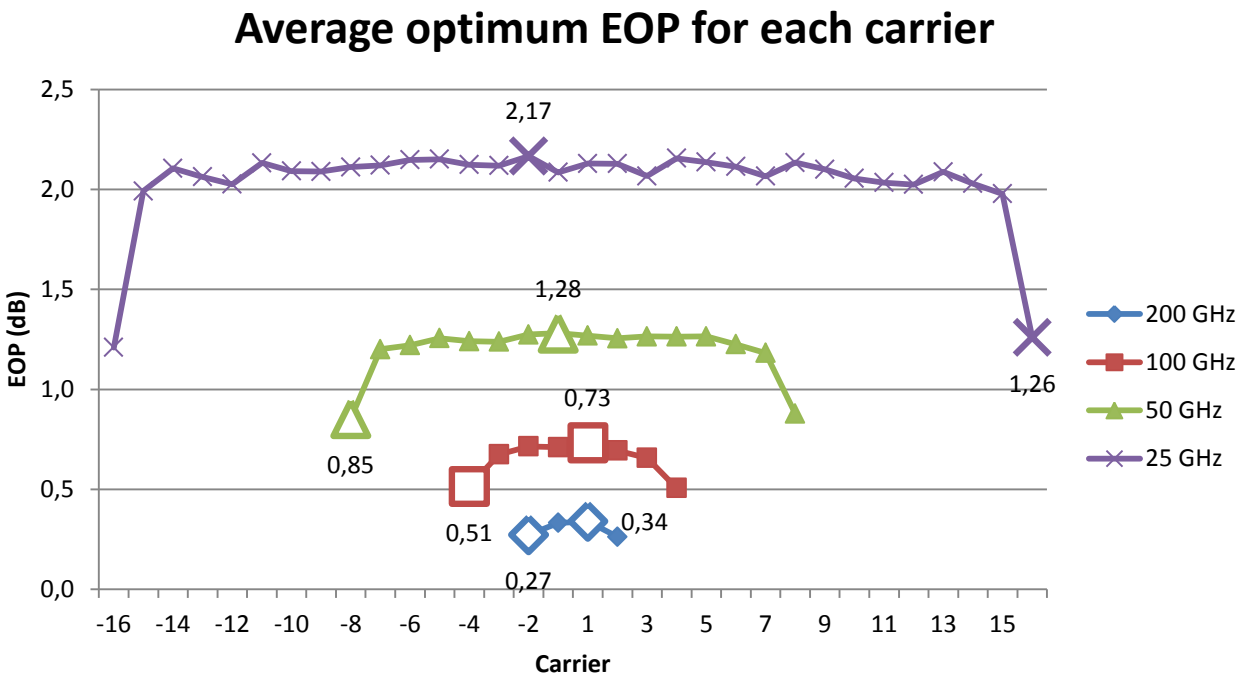

Figure 38 – Average optimum EOP for each carrier
Conditions: Laser relative phase = π; Roll-off factor = 0,1; Number of symbols = 256; PRBS order = 8; Data pattern = random; Number of simulations for the average = 15

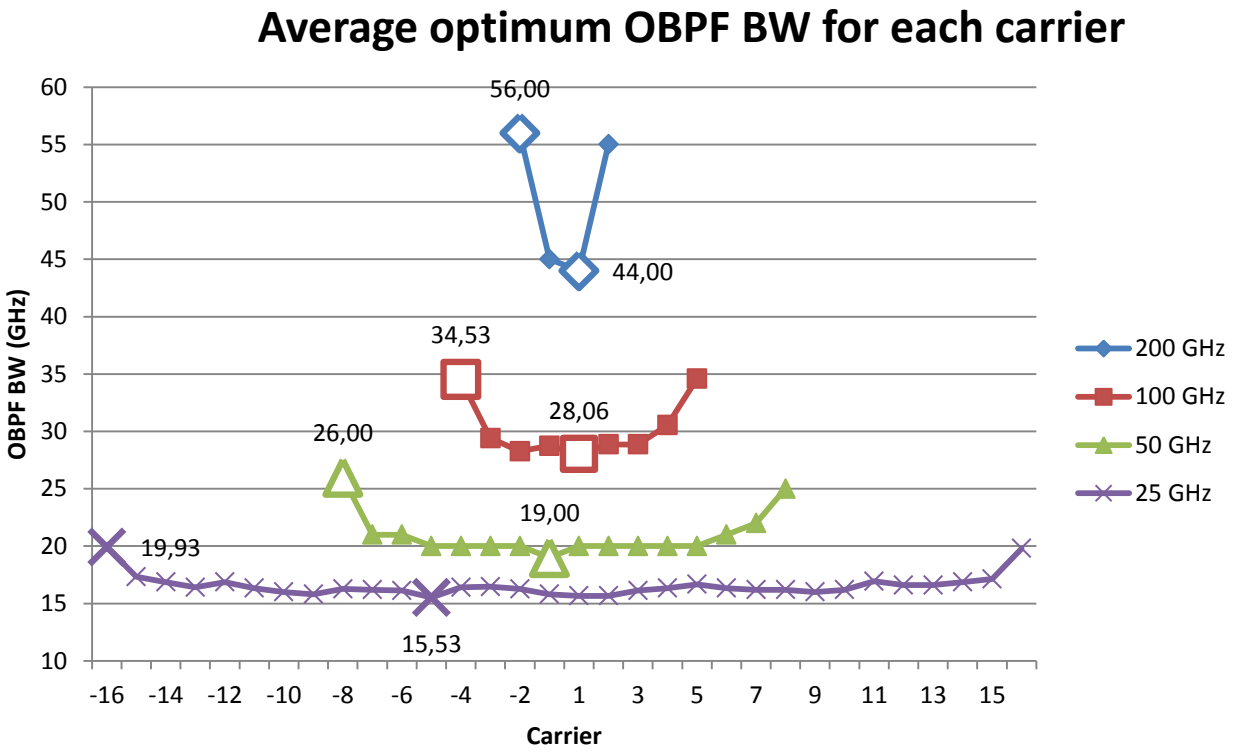

Figure 39 – Average optimum OBPF BW for each carrier
Conditions: Laser relative phase = π; Roll-off factor = 0,1; Number of symbols = 128; PRBS order = 7;Data pattern = random; Number of simulations for the average = 15

Back in the first scenario, we suggested two different criteria to choose the OBPF BW from then on:

- Worst case criteria: the lowest OBPF BW among all the carriers from Figure 39, which leads to the highest (worst) values of EOP. Interesting to look into the worst possible performance of the scheme.
- Best case criteria: the highest OBPF BW among all the carriers from Figure 39, which leads to the lowest (best) values of EOP.

In order to identify these two different criteria in this second scenario, we summarize the results from Figure 38 and Figure 39 into the following figures:

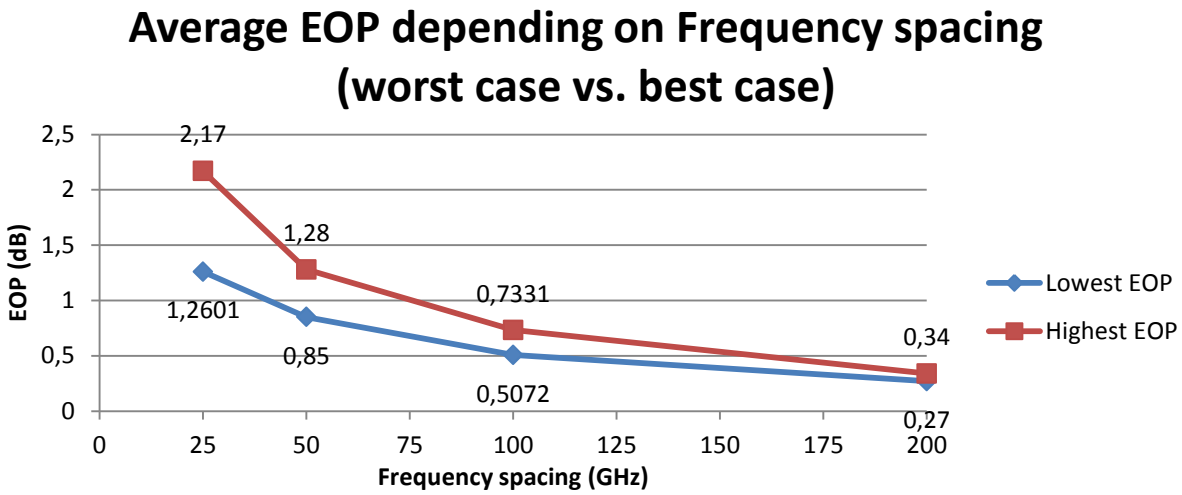

Figure 40 – Average EOP depending on Frequency spacing (worst case vs. best case)
Conditions: Laser relative phase = π; Roll-off factor = 0,1; Number of symbols = 256; PRBS order = 8; Data pattern = random; Number of simulations for the average = 15

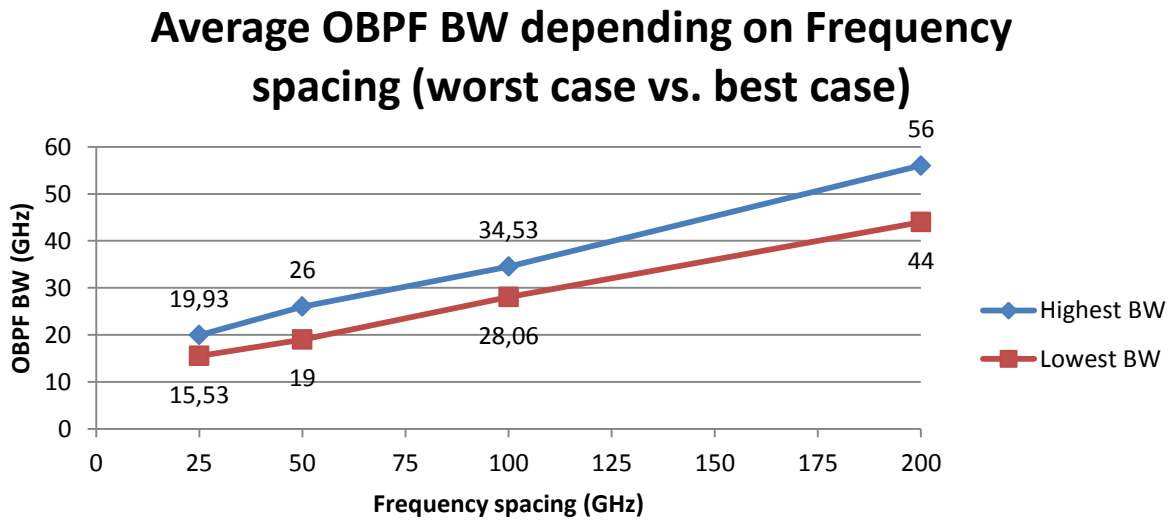

Figure 41 – Average OBPF BW depending on Number of carriers (worst case vs. best case)
Conditions: Laser relative phase = π; Roll-off factor = 0,1; Number of symbols = 256; PRBS order = 8; Data pattern = random; Number of simulations for the average = 15

At this point it becomes clear that this scenario is completely different from the one before. In this case there is a dependence of both the EOP and the OBPF BW on the frequency spacing. Now the optimal OBPF BW value is larger for larger spacing between carriers. The opposite can be said about the EOP, as for higher carrier spacings the level of interference between carriers after filtering decreases.

We can also notice that the highest and the lowest OBPF BW are very similar when the spacing is small (25 GHz), while the highest and lowest EOP are very different. This means that for short distances between carriers the smallest variance in the filter bandwidth implies a big change in the quality of the pulses. On the other hand, when the carrier spacing is very large (200 GHz), the best and the worst cases in terms of EOP are very similar. This result is important when doing an experimental setup, as the OBPF BW becomes a very critical point when working with small carrier spacings, hence needs to be accurately fixed.

Regarding the concrete EOP values from Figure 40, the most distant ones can be found in the worst case for 25 GHz (2,17 dB) and the best case for 200 GHz (0,27 dB), as they are very different from the values obtained in the first scenario (Figure 26). In order to visualize this difference we have the following eye diagrams:

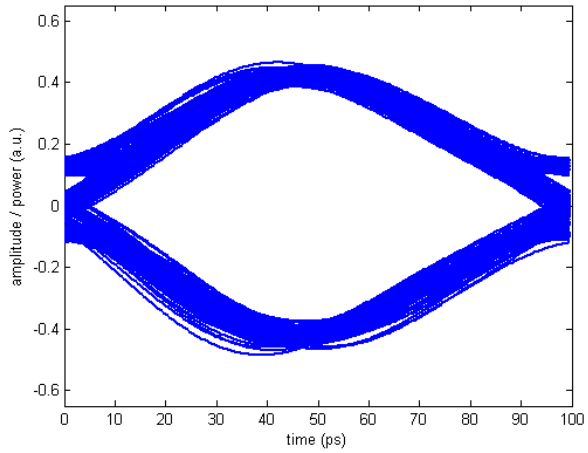

Figure 43– Eye Diagram without neighbours Conditions: 32x25G DWDM; Laser relative phase = π; Number of symbols = 256; PRBS order = 8; OBPF BW = 16,5 GHz; Data pattern = random; Roll-off factor = 0,1

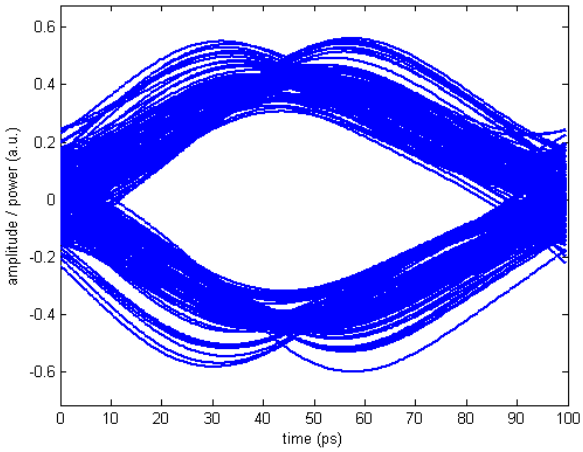

Figure 42 – Eye Diagram for highest EOP Conditions: 32x25G DWDM; Laser relative phase = π; Number of symbols = 256; PRBS order = 8; OBPF BW = 16,5 GHz; Data pattern = random; Roll-off factor = 0,1

In Figure 42 we can see the eye diagram in the worst case for 25 GHz spacing, while in Figure 43 we can see the eye diagram for the same case but without the two neighbour carriers. It is clear that those carriers highly worsen the eye diagram and the EOP; there is even a mismatch in the sampling instant between the different carriers that appear in the left diagram.

The explanation for this phenomenon is that, when the OBPF BW (16,5 GHz) is very close to the frequency spacing (25 GHz), a lot of power from the neighbour carriers survives the filter and interferes with the main carrier.

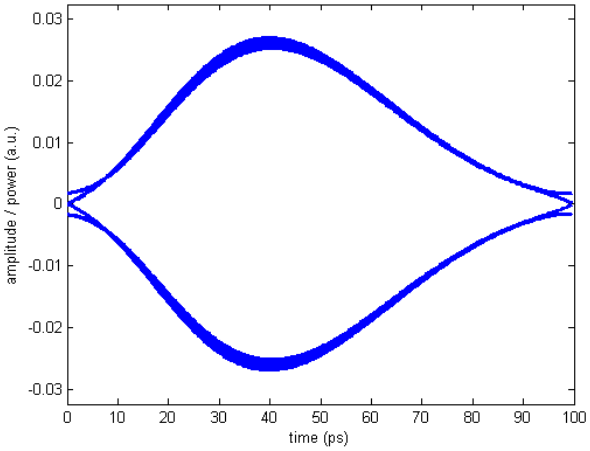

Figure 44 – Eye Diagram for lowest EOP
Conditions: 4x200G DWDM; Laser relative phase = π;
Number of symbols = 256; PRBS order = 8; OBPF BW = 44 GHz;
Data pattern = random; Roll-off factor = 0,1

Figure 44 represents the eye diagram for the best case with 200 GHz spacing. The eye is much more well-defined than before, as it has an EOP of only 0,27 dB. In this case there is a long distance between neighbour carriers (200 GHz) and a proportionally small (56 GHz) width of the optical filter. With these conditions, very little power from the neighbours survives the filter, and so the performance of the system is almost unaffected.

LASER RELATIVE PHASE

Once we have found the optimal OBPF BW for each carrier distance, we need to know if the system performance is affected by the phase difference between carriers. We have already confirmed that adding distant carriers without changing the spacing affects very little the EOP values, and in that situation we always obtain a worst case performance when the relative phase is π. However, we don't have any information about the dependence of the EOP on the lasers relative phase when changing the carrier spacing.

In the current scenario we are going to test the EOP values, again, over three cases: π phase difference, same phase, or random phase. We will show the results for the two extreme cases, 25 GHz spacing and 200 GHz spacing, as they are representative of what is happening; the 200 GHz spacing case is representative of the 50 GHz case and the 100 GHz case, as the behaviour of the system is very similar in all of them; on the other hand, the 25 GHz spacing case need to be analysed alone.

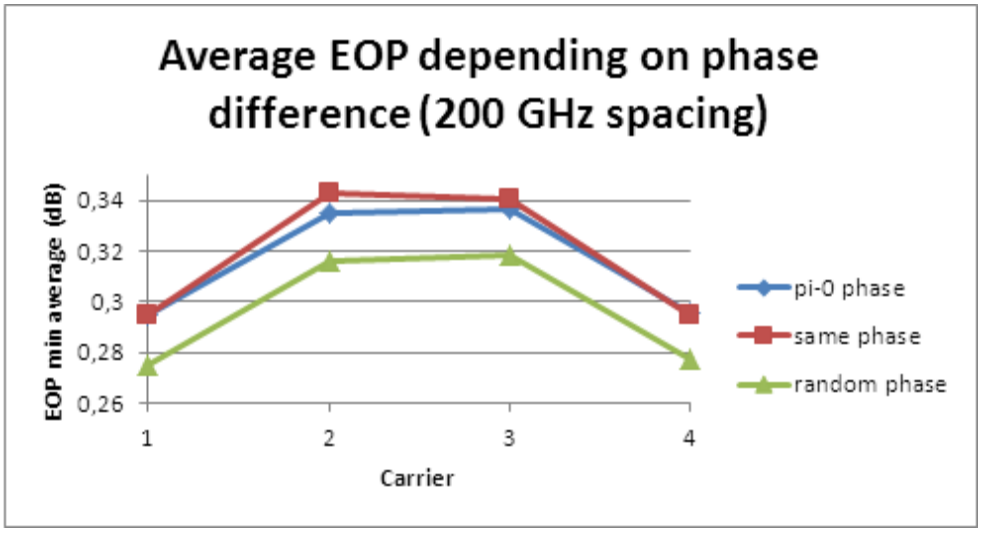

Figure 45 – Average EOP depending on phase difference (200 GHz spacing) Conditions: 4x200G DWDM; OBPF BW = 44 GHz; Roll-off factor = 0,1; Number of svmbols = 256:

As we can see, the results here are very similar to the results obtained in scenario 1. The π phase difference and the identical phase are the worst cases, while the random phase is always below. The order of magnitude of the values is in agreement with the results for the OBPF BW sweep (Figure 38), where the EOP for the 200 GHz case is always the lowest one among all cases (the values of EOP move around 0,3 dB). We can also notice that difference in the EOP between a random phase or a π phase difference is very small (≈0,03 dB). We have seen that this difference increases to ≈0,05 dB with a 100 GHz spacing and to ≈0,15 dB with a 50 GHz spacing. This confirms that, if one parameter can affect the phase of the fields (and hence the EOP), the influence will be higher for lower values of frequency spacing.

The dependence on the phase difference in this scenario is similar to the previous one. The phase difference dependence for the 50 GHz and 100 GHz cases is the same as in this case. However, when we look into the 25 GHz case we find the following:

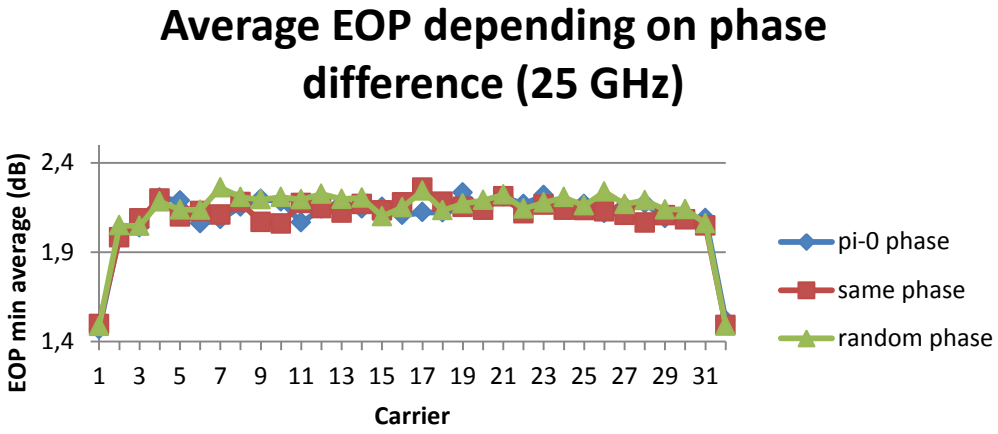

Conditions: 32x25G DWDM; OBPF BW = 16,5 GHz; Roll-off factor = 0,1; Number of symbols = 256; PRBS order = 8; Data pattern = random; Number of simulations for the average = 15

In this case there is no dependence between the EOP values and the phase difference between carriers: all the phase options give similar results. The order of magnitude of the results in Figure 46 (around 2,2 dB) also agrees with the results in the OBPF BW sweep section.

It is important to have this information because in a commercial setup it is usually not possible to control the lasers phase, as different DFB lasers are incoherent. When working with 50 GHz or higher spacing DWDM schemes, the best results are obtained for a random relative phase between carriers, which means that the lasers incoherence can be beneficial. On the other hand this is a parameter that can be ignored when working with 25 GHz DWDM schemes, because there is no longer dependence with the phase difference.

ROLL-OFF FACTOR

The third parameter that we can sweep in this scenario is the roll-off factor of the raised cosine. While it is true that regardless of the results in this section we will use a roll-off factor of α=0,1 (in order to avoid intertributary interference), it is still interesting to know what is the behaviour of the system in this new scenario.

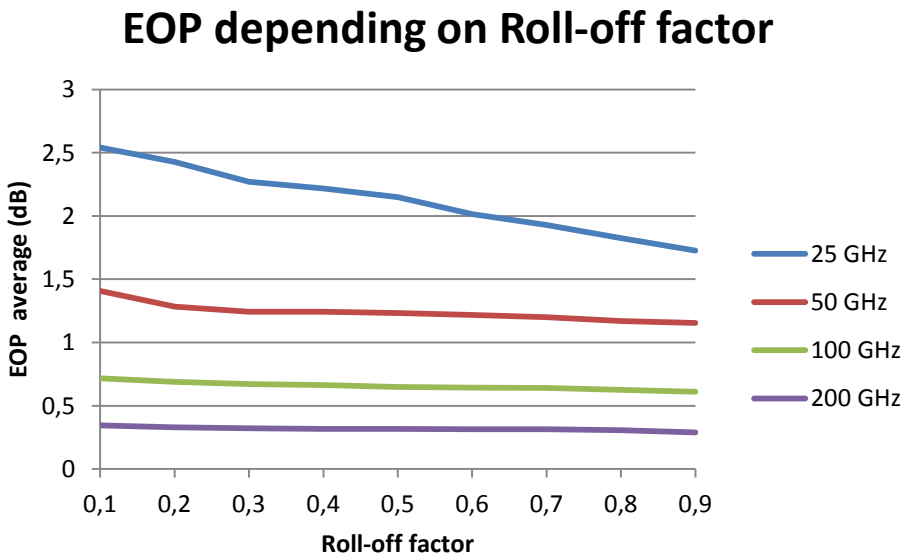

Figure 47 - Average EOP depending on Roll-off factor
Conditions: DWDM; Laser relative phase = π; Number of symbols = 256; PRBS order = 8; OBPF BW = 16,5 GHz (25 GHz), OBPFW BW = 20 GHz (50 GHz), OBPF BW = 28 GHz (100 GHz), OBPF BW = 45 GHz (200 GHz); Data pattern = random; Number of simulation for the average = 15

In the figure above we can observe that the EOP dependence on the roll-off factor is the expected: higher roll-off factor, better EOP. The variation is very narrow, though; it is only clearly noticeable in the 25 GHz case, while the other cases follow an almost flat line dependence. This agrees with the general results in scenario 1, where the variations in the EOP values where always smaller than 0,2dB (Figure 32). The explanation to this decreasing

dependence between the EOP and the roll-off factor can be found in scenario 1 (roll-off factor section), and is again related to the different spectrum form for each roll-off value. Depending on the roll-off factor applied, the part of the spectrum of a carrier that interferes with the other carriers can have more or less power, hence affecting more or less their EOP.

The reason why the roll-off factor has a larger impact for smaller carrier spacings can be found in Figure 41. In that figure we can observe that the relation between the carrier spacing and the filter bandwidth is 3 times larger for the 200 GHz case than for the 25 GHz case. On other words: for a spacing of 25 GHz the filter bandwidth is 16,5 GHz, while for a spacing of 200 GHz the filter bandwidth is 45 GHz. In the latter case, and compared to the former one, there is less power from the neighbour carriers inside the filter bandwidth. This fact, together with the theoretical explanation given in the previous paragraph, explains why the curve in Figure 47 for the 25 GHz case has a much larger slope than the other cases.

Worst case

After the three previous sections we are now able to give the parameters in order to get the worst possible results in this scenario. We will call these results the *worst case*, as it is the worst situation that we can find. In this section we are not calculating an average EOP value; we are interested in the absolutely worst single EOP value that can be obtained. The conditions are the following:

- Every carrier has an optimal OBPF BW, and we are taking the lowest one (which leads to the highest -*worst*- EOP value). The OBPF BW will be 16,5 GHz for 25G, 20 GHz for 50G, 28 GHz for 100G, and 45 GHz for 200G
- Laser phase difference: π (it could be as well the same phase, or even random phase for 25G)
- Roll-off factor: α=0.1

When we apply these parameters to our simulations, we obtain the following results:

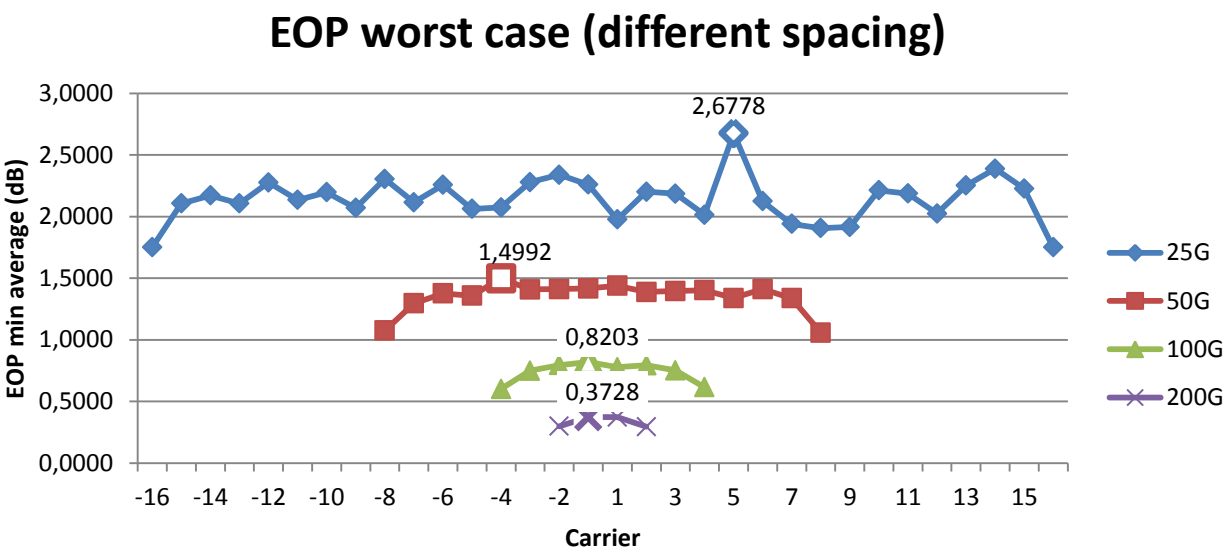

Figure 48 – EOP worst case (different spacing)
Conditions: DWDM; Laser relative phase = π; Roll-off factor = 0,1; Number of symbols = 256; PRBS order = 8; OBPF BW = 16,5 GHz (25 GHz), OBPFW BW = 20 GHz (50 GHz), OBPF BW = 28 GHz (100 GHz), OBPF BW = 45 GHz (200 GHz); Data pattern = random; Number of simulations = 15 (NO AVERAGE)

As expected in this scenario the EOP values for each carrier spacing strongly differ. If we compare these values to the average results from Figure 40 and Figure 41 we can see that the worst case value is not always so different to the average one. In the following chart we can see those values compared:

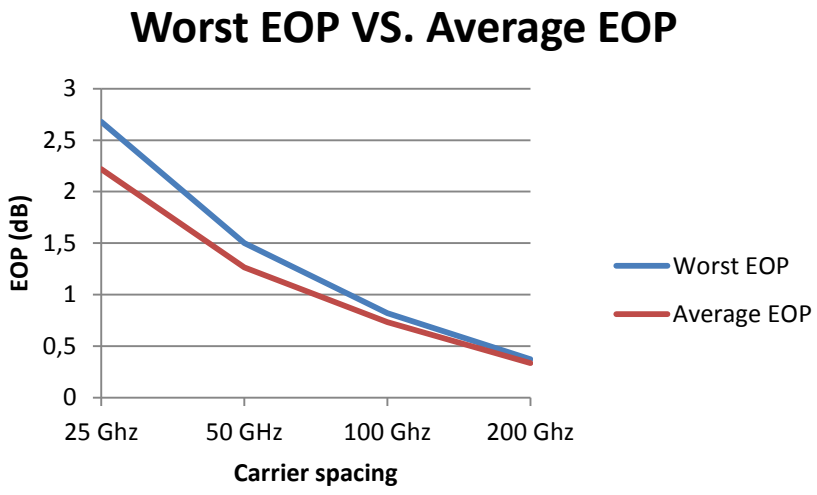

Figure 49 - Worst EOP vs. Average EOP
Conditions: DWDM; Laser relative phase = π; Roll-off factor = 0,1; Number of symbols = 256; PRBS order = 8; OBPF BW = 16,5 GHz (25 GHz), OBPFW BW = 20 GHz (50 GHz), OBPF BW = 28 GHz (100 GHz), OBPF BW = 45 GHz (200 GHz); Data pattern = random; Number of simulations = 15

The difference between the worst EOP and the average EOP, as seen in Figure 49, shows the dependence of the EOP on the data pattern for a single simulation. While in the 200 GHz spacing this dependence is almost non-existent (same value for the average and the worst case), in the 25 GHz spacing the worst situations can have an EOP 0,5 dB above the average. Again this happens because of the relation between the carrier spacing and the filter bandwidth: if a higher proportion of the neighbour carriers falls inside the filter bandwidth, the EOP on the given carrier will depend more on the data patterns of those neighbour carriers. Another important fact is that in the 25 GHz spacing there are 32 carriers, while in the 200 GHz spacing there are only 4, so in the former case the EOP in a particular carrier depends on more neighbours than in the latter case; however, the most critical neighbours are the two closer ones, so the main explanation for this phenomena is the one stated above regarding the filter bandwidth.

Chapter 5

Experiment

5.1 Experiment setup

In order to verify the principle explored in this thesis, we perform an experimental demonstration of a 640Gbit/s OTDM+OFDM signal encoded with DPSK to a 50GHz DWDM grid. This signal is built from an OTDM combination of 4 tributaries, with an emulated 160Gbit/s rate each. Each of those tributaries consists of an OFDM signal with 16 subcarriers, with a base rate per subcarrier of 10Gbit/s. Figure 50 shows the experimental setup, with some key power references under the EDFAs. This setup has been used before in 10,08 Tb/s all-optical OFDM signal transmission.

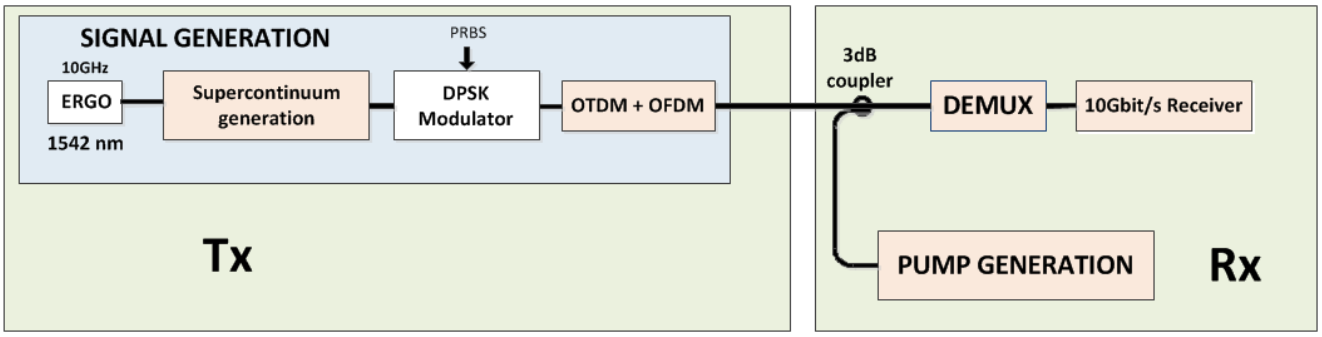

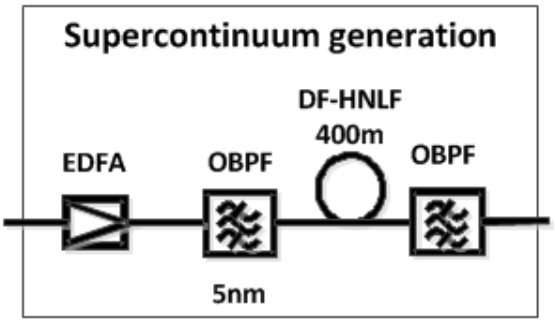

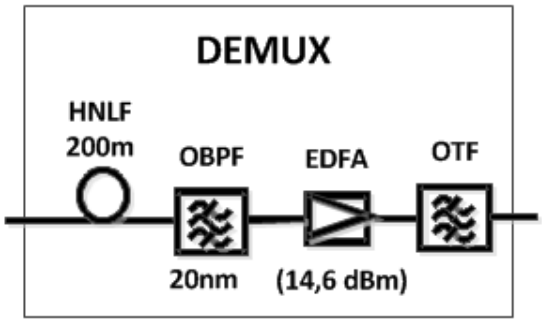

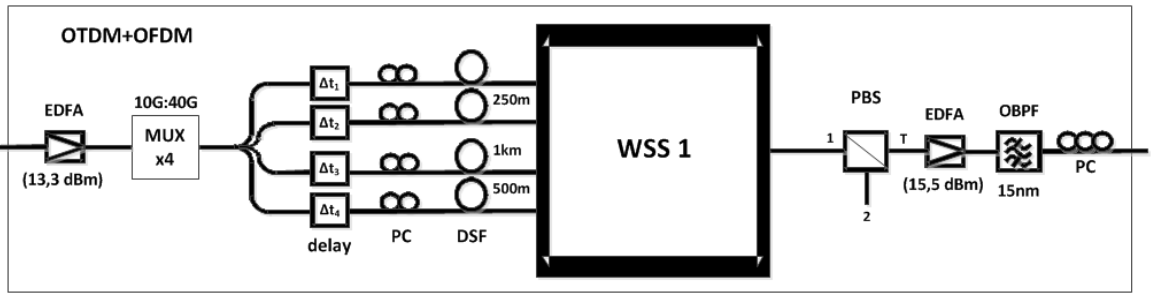

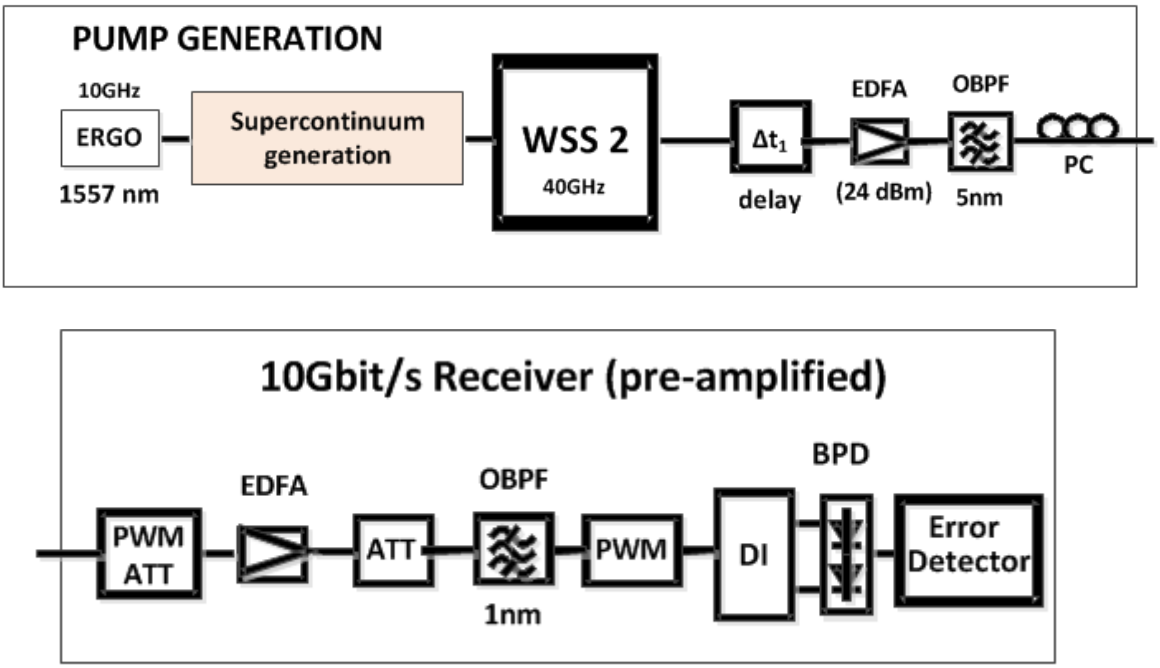

Figure 50 – Experimental setup modules

Transmitter

OTDM mux

The output of a 10 GHz Erbium-glass oscillator pulse generating laser source (ERGO-PGL) at 1542 nm provides us with a frequency comb signal of 1,5ps pulses, with a line spacing of 10GHz.This signal goes through a dispersion-flattened highly nonlinear fiber (DF-HNLF), where its spectrum is broadened by means of self-phase modulation, hence creating a supercontinuum. At the DF-HNLF output an optical band-pass filter (OBPF) with a 9 nm bandwidth allows us to limit the bandwidth of the generated continua. After that, the signal is DPSK modulated with an I/Q modulator with only one active arm (we would use both of them in case of encoding with DQPSK). This modulator is electrically driven by a 10Gbit/s data pattern created in a PRBS generator (with length 2^{15}-1). The result of this phase modulation is that the comb-line spectrum has been converted to a white spectrum with a 9 nm bandwidth. The data-modulated pulses are then multiplexed from 10Gbit/s to 40Gbit/s OTDM using two passive fiber-based delay-line multiplexer (MUX) stages.

OFDM mux

This OTDM signal is splitted into four paths, where we will be able to control their relative delay and polarization. Three of the paths will also include a dispersion-shifted fiber

(DSF), but with a different length in each case (250m, 500m and 1km), so the carriers in the four paths become decorrelated. Each of these paths go into a different port of a wavelength selective switch (WSS), that will generate a part of the desired OFDM spectrum out of them. The WSS is based on a programmable liquid crystal on silicon array that can control both the amplitude and phase of an input waveform as a function of frequency. Each port of the WSS will have then an OFDM signal with 4 carriers, spaced 200 GHz from each other. However, each port is frequency shifted 50GHz from the previous one, so when the four paths are coupled together, the full OFDM spectrum with 16 carriers and a 50GHz spacing is obtained. It is critical to synchronize the four ports with the delays before the WSS. After the WSS, a polarizing beam splitter (PBS) is set to guarantee that the different components of the signal (from the different ports) are copolarized. a polarization-controller (PC) is used to optimize the latter interaction with the control signal.

Receiver

OTDM demux

In order to perform OTDM demultiplexing we need to generate a control signal (pump), which is created similarly to the main signal. A supercontinuum is generated from the output of a 10GHz ERGO-PGL at 1557nm (again with 1,5ps pulses), filtered with a 16nm bandwidth OBPF, and then sent into a WSS that will carve the desired shape into it; in this case, a 40GHz *sinc* shape, which corresponds to a 25ps pulse. After that, a delay line will allow us to synchronize the pump with one of the OTDM tributaries. We will also be able to control the relative polarization state between the pump and the signal with polarization controllers (PCs), in order to optimize their latter interaction. The pump and the main signal are coupled together and sent into an HNLF, where by means of four-wave mixing (FWM) an idler is generated; it is a replica of the tributary synchronized with the pump, but at a new wavelength, hence achieving OTDM demultiplexing. Then, we filter the idler's bandwidth to remove the signal and the pump. The details of the HNLF are as follows: length 200 m, nonlinear coefficient $\gamma \approx 10\ W^{-1}km^{-1}$, zero-dispersion wavelength ≈1552,06 nm and dispersion slope 0,018 $ps/(nm^2 \cdot km)$.

OFDM demux

We perform the OFDM demultiplexing with an optical tunable filter (OTF), just before the pre-amplified receiver. An attenuator (PWM ATT) will let us check the power at the receiver's input, as it will be the reference point for the power dependence of the system. An OBPF with a narrow bandwidth of 1nm removes the ASE noise from the pre-amplifier. Finally, classic DPSK detection is performed through a delay interferometer (DI) and a balanced photo-detector (BPD). After detection we will be able to measure the BER with an error detector.

5.2 Laboratory Results

The results shown in this chapter belong to the experimental demonstration of the novel principle explored in this thesis. We will divide these results into two separate scenarios, depending on the setup used:

- Setup without multiplexing/demultiplexing of tributaries: this setup is similar to the one simulated in the previous results chapter. There will be no intertributary interference, and so the conditions will be similar to the ones in the simulation, which will allow us to make an approximately direct comparison between numerical and experimental results.
- Setup with multiplexing/demultiplexing of tributaries: this setup performs the full principle, which will allow us to observe the real performance of the system with all the possible interference in it, and hence to obtain some conclusions about the feasibility of the principle.

5.2.1 Setup without multiplexing/demultiplexing

Parameters

The scenario where no OTDM multiplexing/demultiplexing is performed acts as a connection between the simulation results and the full principle experimental results. This is why we will specify for this experimental setup the different parameters that were declared in the simulation results chapter:

- **Carrier spacing and number of carriers**: regarding these two parameters, we are restricted by the flexibility of the equipment. The original idea was to adapt this principle to a DWDM source, but our experimental setup creates the OFDM signal in a different way. Therefore, we will stick to the carrier spacing and number of carriers combinations defined in the second scenario in the numerical results section:

Channel spacing (GHz)	Number of carriers
25	32
50	16
100	8
200	4

- **Roll-off factor**: regarding the shape of the pulses after the pulse carver, we did all of our simulations for a roll-off factor of 0,1 for the raised cosine, and we will keep using this value. This parameter provides us with near flat-top pulses, which

increases intercarrier interference but also reduces intertributary interference after demultiplexing (as seen in the theoretical part).

- **Laser relative phase**: while in our simulations each carrier was generated with a random and independent initial phase, in the laboratory setup the method that we follow for generating the OFDM signal allows us to decorrelate only four groups of carriers. As we can see in Figure 51 if we divide all the carriers into groups of four consecutive ones, each one of those four carriers will belong to a different port from the waveshaper. The same figure will allow us to understand where the intercarrier interference comes from for a given carrier. Focusing on the central carrier (which in this example comes from port 1 of the waveshaper), we can see that its closer neighbour carriers come from port 4 and 2 respectively, so they will be decorrelated, both between them and with the carrier from port 1. As we saw in our simulations, a random relative phase between carriers is the best scenario, as the interference raises for fixed relative phases of 0 or π. However, if we look further, we can see that the second neighbour carrier, for lower and higher wavelengths, comes from port 3. They will be still decorrelated with the carrier from port 1, but not between them, i.e., they will cause the same interference in the carrier from port 1. This means that the overall intercarrier interference in a given carrier is not an addition of independent noises. This case has not been simulated, and it would be interesting to see, in some future work, the performance of the system given these circumstances, so we could compare it to the results that we obtained in the experiment.

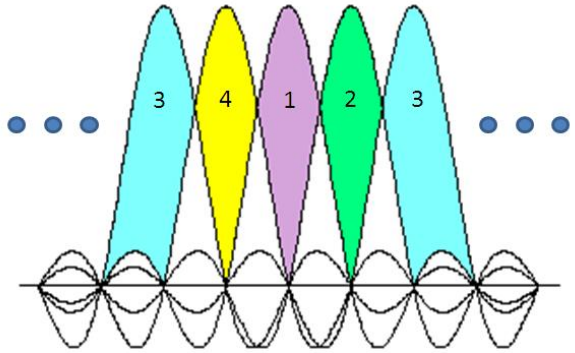

Figure 51 –Carriers depending on port number

- **OBPF BW:** Optimizing this parameter will be our main concern in this first scenario, as it is critical to the performance of the system.

Other parameters:

- **Filter transfer function:** In the simulations the filter had a Gaussian transfer function, but the usual tunable filter in the laboratory has a rectangular one. We will try both and see which one provides the best result.

- **Modulation:** In the simulations we used a DPSK modulation. In the laboratory experiment we will start using DPSK, but we will also test the performance of the system with DQPSK.

Quality of the pulses

One of our main concerns in the laboratory was to know the exact shape of the pulses transmitted, because it can have an important effect on the interference after detection and hence in the performance of the system. The following images illustrate the shape of the pulses as seen in the oscilloscope used in the laboratory. However, the oscilloscope's bandwidth doesn't allow us to see the real shape of the pulse, so we also use an autocorrelator to analyse the shape of the pulses. Figure 52, Figure 53, Figure 54 and Figure 55 show the OFDM symbol and its autocorrelation for different carrier spacings:

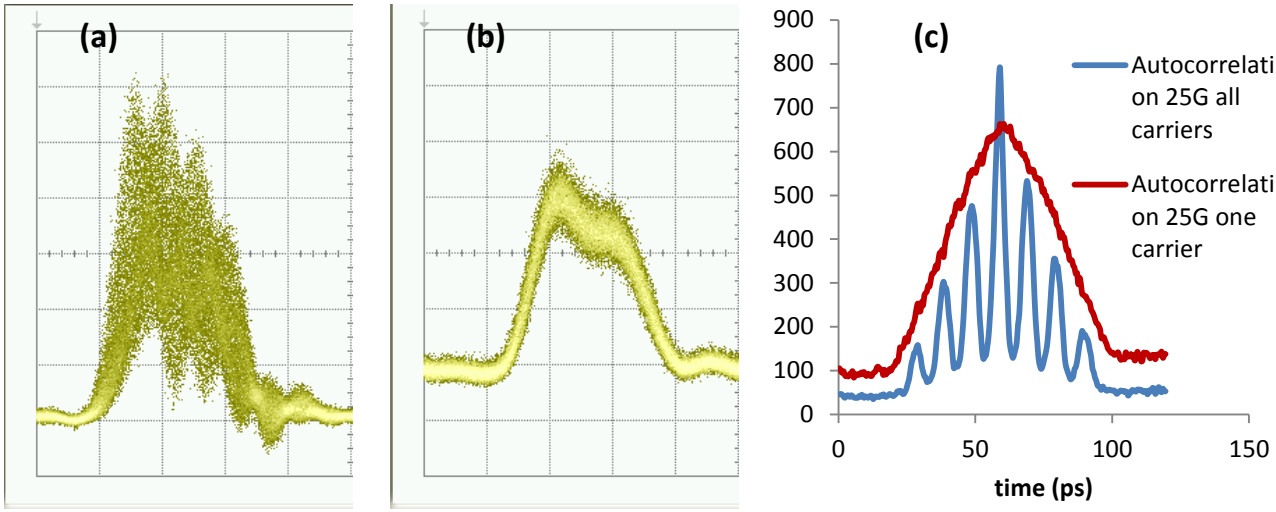

Figure 52 – Quality of the 25G OFDM pulse
(a) OFDM symbol with all carriers, (b) OFDM symbol with one carrier, (c) Autocorrelation of the OFDM symbol with one and all carriers. Conditions: 32x25GHz OFDM, 10mV/div, 20ps/div (oscilloscope)

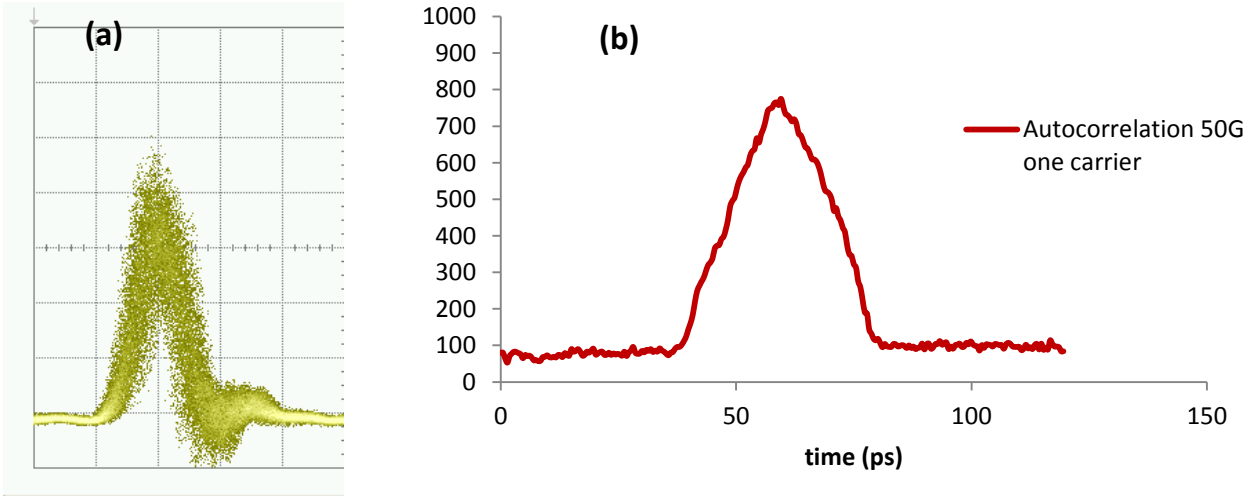

Figure 53 – Quality of the 50G OFDM pulse
(a) OFDM symbol with all carriers, (b) Autocorrelation of the OFDM symbol with one and all carriers. Conditions: 16x50GHz OFDM, 10mV/div, 20ps/div (oscilloscope)

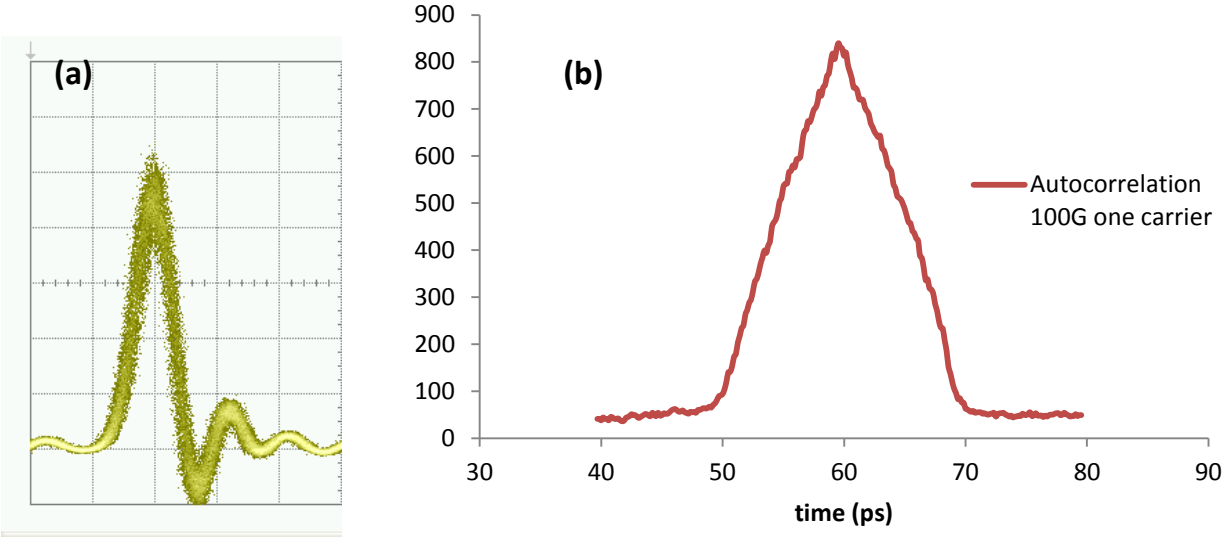

Figure 54– Quality of the 100G OFDM pulse
(a) OFDM symbol with all carriers, (b) Autocorrelation of the OFDM symbol with one and all carriers.
Conditions: 8x100GHz OFDM, 10mV/div, 20ps/div (oscilloscope)

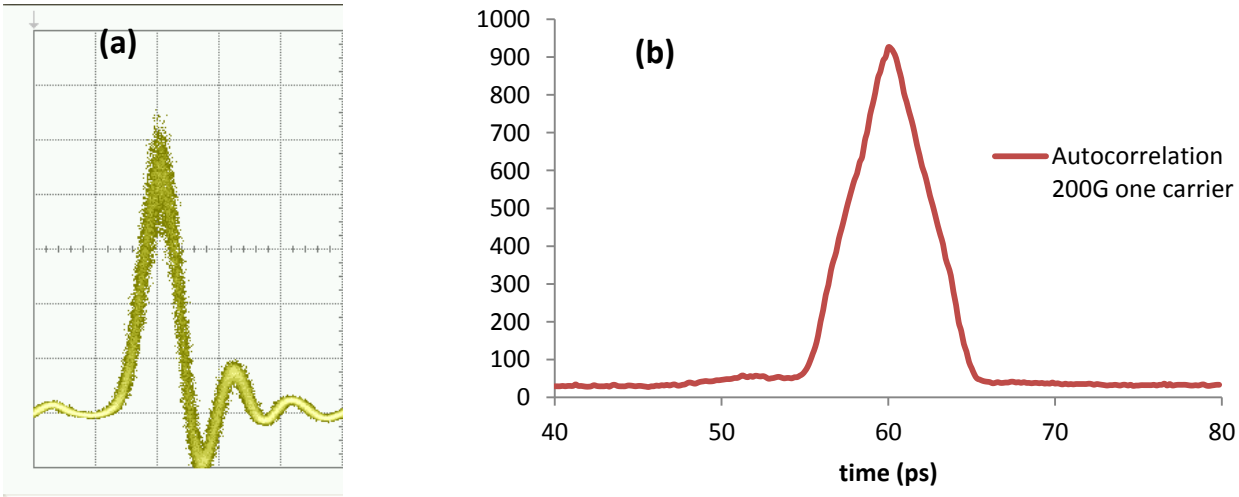

Figure 55– Quality of the 200G OFDM pulse
(a) OFDM symbol with all carriers, (b) Autocorrelation of the OFDM symbol with one and all carriers.
Conditions: 4x200GHz OFDM, 10mV/div, 20ps/div (oscilloscope)

Channel spacing (GHz)	Expected width (ps)	Autocorrelation FWHM (ps)	Guard band (ps)
25	40	45	10
50	20	21	5
100	10	11	2,5
200	5	5	1,25

Table 1 – Experimental FWHM in the autocorrelator

We can see that only one pulse is broad enough as to observe its flatness, and it is the 25G one with only one carrier (Figure 52.b), where we can see that it is far from being flat-top (using the oscilloscope). This may be caused by the limited resolution of the WSS, which could provide a non-ideal *sinc* shape. We will be able to see that in the spectrum diagrams.

If we look at the autocorrelation shapes for the different spacings and only one carrier (which is the only one that gives us information on a single pulse), we can see that they are overall near-triangular, which indicates that the pulse is near-rectangular. Considering that we are generating these pulses with a raised-cosine shape and a roll-off factor of 0,1 (which looks near-rectangular), the autocorrelation shape makes sense. The autocorrelation with all the carriers is only shown in the 25GHz as an example. When there are several carriers involved, the time-domain pulse is formed by a train of pulses whose envelope follows the pulse shape (as we can see in Figure 52.c). The autocorrelation of this pulse doesn't help us when trying to know what the shape of the pulse is.

Finally, and regarding the pulse width, we can see in Table 1 that the FWHM values obtained for the autocorrelation are a bit larger than the expected pulse widths. However, in all the cases the difference between the ideal and the real pulse widths is smaller than the guard band left between tributaries, so it should not cause intertributary interference after time-demultiplexing.

Spectrum

Another of our main concerns in the experimental setup is to obtain a good OFDM signal in terms of orthogonality of the carriers, which is crucial for reducing the intercarrier interference to the minimum. In order to analyse this orthogonality, we will show, for each carrier spacing, the spectrum with all four ports connected (full OFDM signal) and the spectrum with only one port connected (one group of carriers). Figure 56, Figure 57 Figure 58 and Figure 59 show these spectrums:

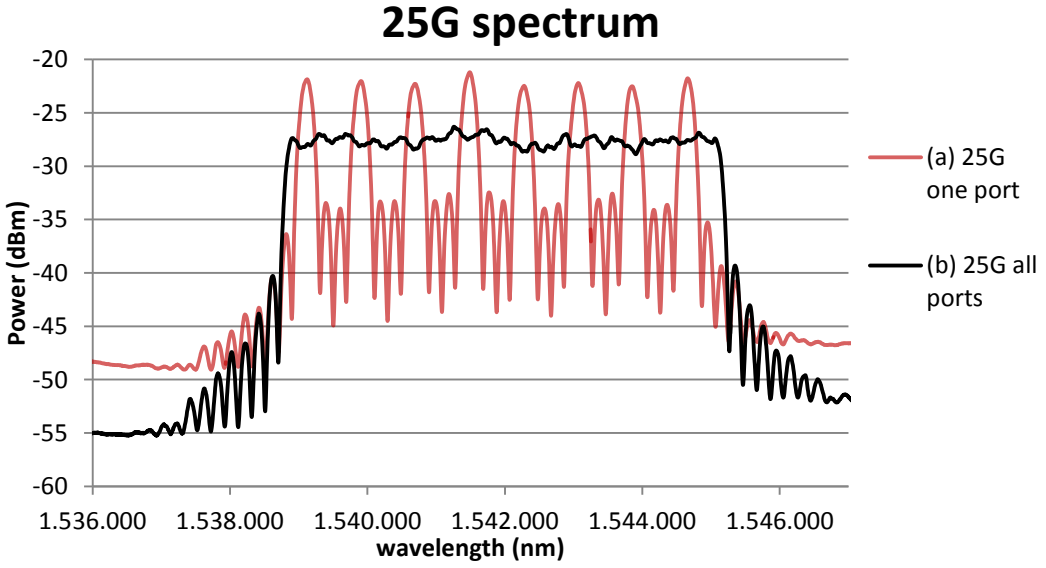

Figure 56 – Spectrum. 25G signal NO MUX
Conditions: 32x25GHz OFDM, OSA resolution = 0.02 nm.

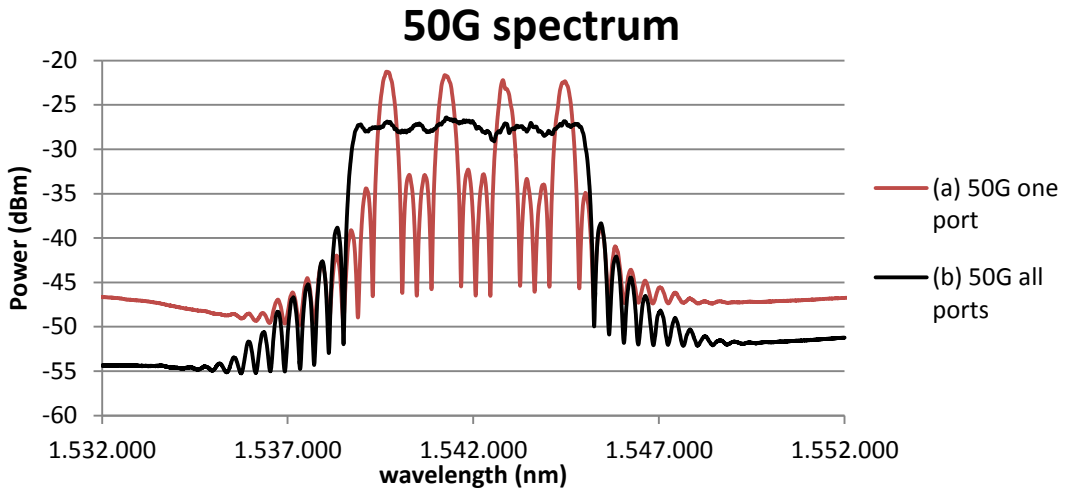

Figure 57– Spectrum. 50G signal NO MUX
Conditions: 16x50GHz OFDM, OSA resolution = 0.02 nm.

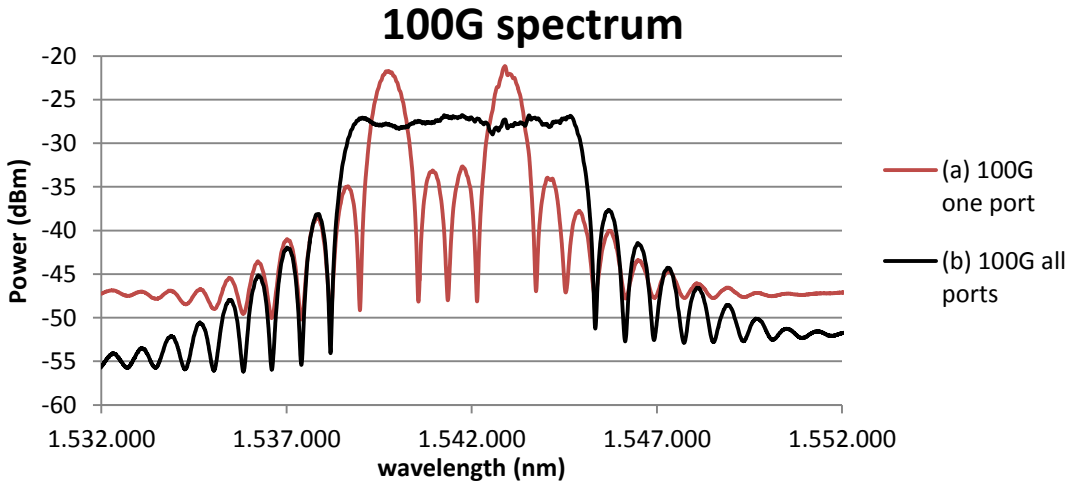

Figure 58– Spectrum. 100G signal NO MUX
Conditions: 8x100GHz OFDM, OSA resolution = 0.02 nm.

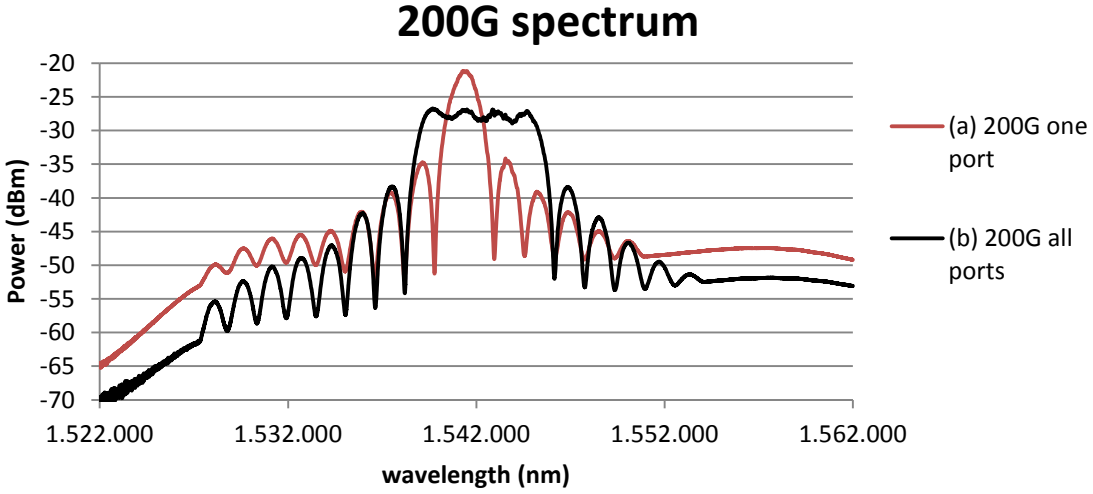

Figure 59– Spectrum. 200G signal NO MUX
Conditions: 4x200GHz OFDM, OSA resolution = 0.02 nm.

There are different ways to inspect these spectrum diagrams. First of all, as we said, we should look into the orthogonality of the carriers. This can be done by looking at the side lobes of the spectrum; we can see that the lobes when only one port is connected have their zeros at the same wavelengths as the lobes when all ports are connected, which is expected since the same WSS generates all the ports. These zeros are marked in Figure 60 and we can check the orthogonality between carriers. The same can be observed for the other carrier spacings, which means that we always achieve orthogonality for the OFDM signal. We can also see in Figure 60 that the *sinc* shape is not symmetrical, which can be caused by the WSS resolution problems when working with very low bandwidth signals. This non-perfect *sinc* shape could be the cause of the non-flatness of the pulses that we observed in the previous section.

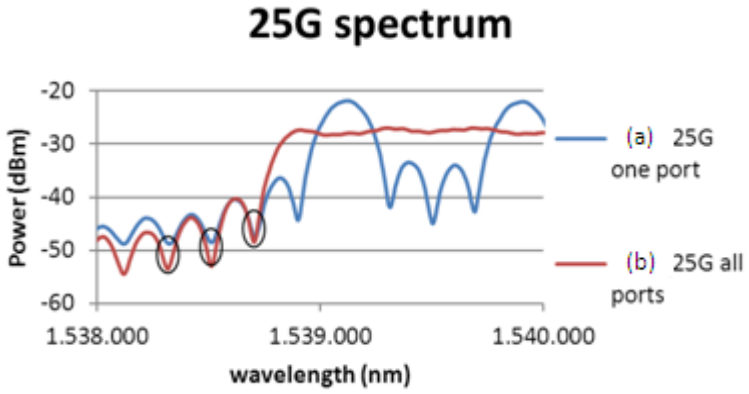

Figure 60 – Spectrum. Carrier orthogonality
Conditions: 32x25GHz OFDM, OSA resolution = 0.02 nm. (a) Peak level = -21,2 dBm, Peak wavelength = 1541,49 nm (b) Peak level = -26,31 dBm, Peak wavelength = 1541,26 nm

Another way to inspect the spectrum diagrams is to look at the flatness of the OFDM spectrum. Even just looking at the spectrum with only one port connected, we can already see that each carrier has a different power. The addition of all the ports (and so, of all the carriers) creates an OFDM spectrum with a lot of irregularities in the top zone, which will make the performance of each channel different from one to another. These irregularities can be controlled to a certain point with polarization controllers, in order to make the spectrum look as flat as possible, but it is difficult to achieve perfect flatness.

Filter transfer function

The OBPF BW sweeping has been performed for two different filter transfer functions: rectangular and Gaussian. The results in this chapter will be obtained using a Gaussian filter generated with a WSS, because this way we can be consistent with the simulations (which also were done with a Gaussian filter). However, as in the setup it is easy to change between the two different transfer functions, we decided to test the flat-top one as well. The rectangular transfer function is generated with an OTF (Santec OTF-350 tunable filter) and is perfectly rectangular for high BW values, while for low BW values (close to 10 GHz) the response will not be a perfect rectangle, but a more rounded (bell-shaped) transfer function.

The first step when trying to characterize the system is to choose the power at the receiver's input (P_{rec}), which needs to be low enough to have a measurable BER at the receiver. We choose a P_{rec} of -43 dBm for the DPSK case, and a P_{rec} of -37 dBm for the DQPSK case (which will be explored later), as it requires a higher power in order to achieve a similar BER. We will always use those power levels when looking for the OBPF BW, in order to give reliability to the results and their comparison. The results are found in Figure 61:

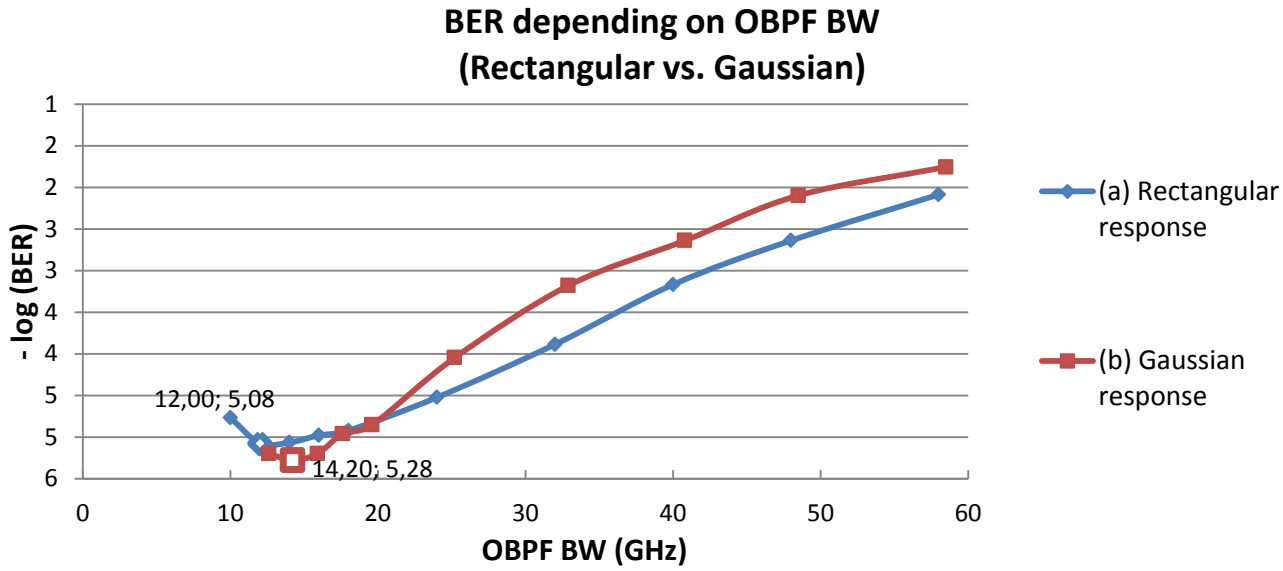

Figure 61 – BER. Comparison Rectangular filter vs. Gaussian filter
Conditions: 16x50GHz OFDM, central carrier, -43 dBm at receiver's input, DPSK
(a) Rectangular filter (b) Gaussian filter.

As we can see, for large values of OBPF BW the rectangular filter offers a better performance. On the other hand, for low values of OBPF BW (where the optimum is found) the Gaussian filter offers the best BER, so we will use the Gaussian response for obtaining the experimental results in this section. In Figure 62 we can observe the eye diagram of the detected signal with the rectangular filter (left) and the Gaussian one (right), both for their optimum OBPF BW value (12 GHz for rectangular, 14,6 GHz for Gaussian). The difference in the measured BER can be observed in the higher eye opening for the Gaussian filter. The rectangular filter has a *sinc* shape in the time-domain, which spreads further than the signal pulse, while the Gaussian filter has a Gaussian shape in the time-domain, which is more adjusted to the duration of the signal pulse, hence allowing a higher power through it, which could explain the differences in the measured BER.

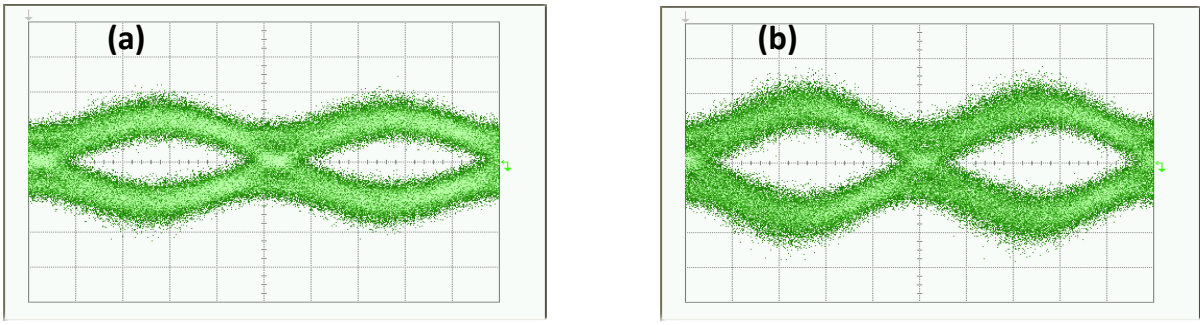

Figure 62 – Eye diagram. Comparison Rectangular filter vs. Gaussian filter
Conditions: 16x50GHz OFDM, central carrier, -43 dBm at receiver's input, DPSK, 10mV/div, 20ps/div (oscilloscope).

Center carrier vs. Edge carrier

In the simulations we could observe, as expected, that the performance of the system (in terms of EOP) was better in the edge channels compared to the middle ones. Furthermore, the optimal OBPF BW was larger for those edge channels. In this experiment we are mainly focused on the middle channels, as they are the ones with the highest interference and hence where we want to achieve the error-free state. However, it can also be interesting to confirm what we saw in the simulations.

In the following figures we can see the BER in both an edge subcarrier (1st) and a central subcarrier (8th) for the 16 channels-50 GHz case, with DPSK modulation. In Figure 63 we can see the BER for a power at the receiver's input (P_{rec}) of -43 dBm, and in Figure 64 we can see the BER for a power of -40 dBm at the same point. This latter power value is the power for which error-free (BER=10^{9}) performance is achieved (using the optimal OBPF BW), what we will call *sensitivity*. In Figure 64 we can also see the EOP curves obtained in a single simulation (for random data patterns and laser phases) in both an edge carrier and a central carrier.

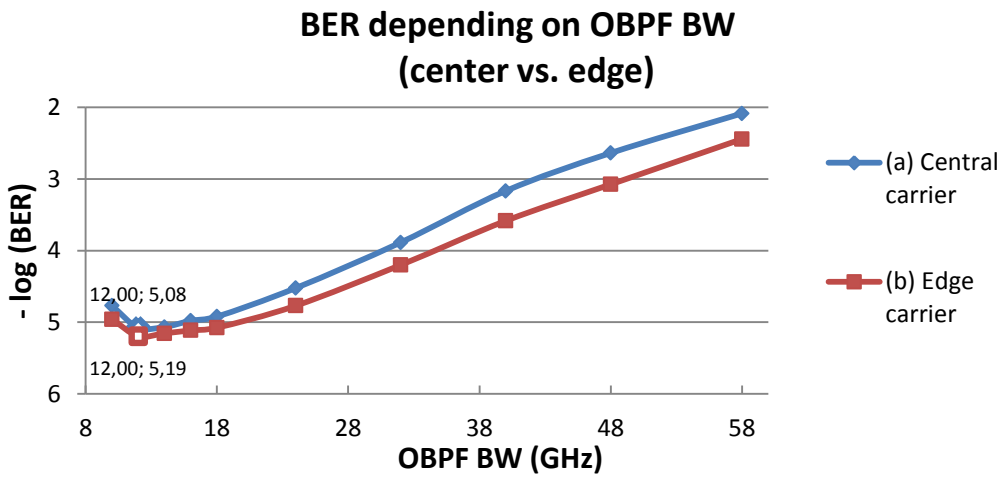

Figure 63 – BER. Comparison Center carrier vs. Edge carrier
Conditions: 16x50GHz OFDM, rectangular filter, -43 dBm at receiver's input, DPSK.
(a)8th carrier (b) 1st carrier

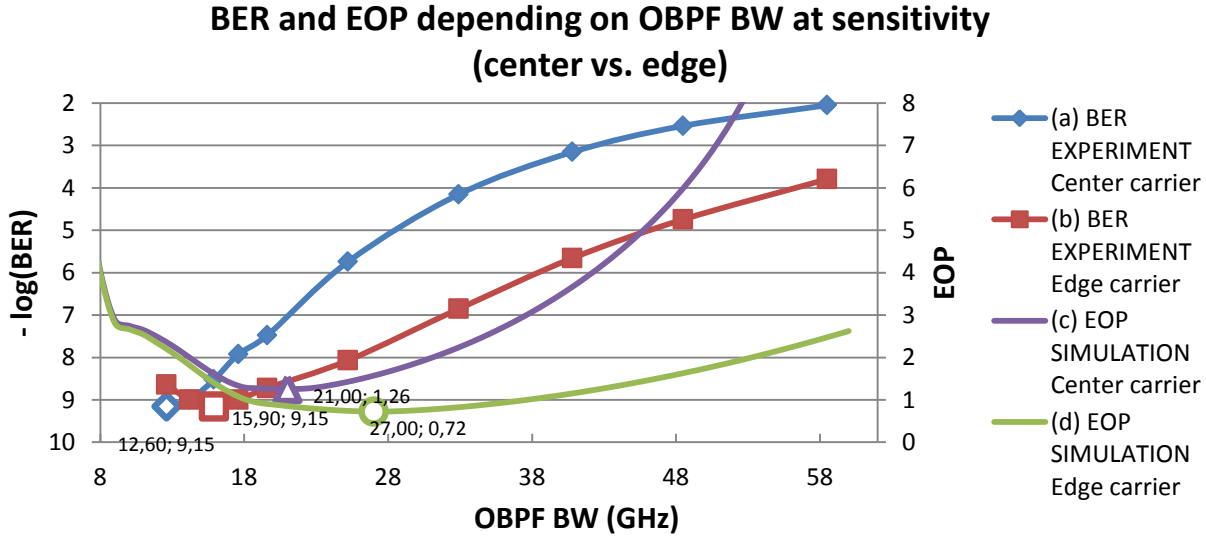

Figure 64 – BER, EOP. Comparison Center carrier vs. Edge carrier
Conditions: 15x50GHz OFDM, rectangular filter (BER), Gaussian filter (EOP), -40.5 dBm at receiver's input, DPSK. (a) BER, 1st carrier. (b) BER, 8th carrier. (c) EOP, 1st carrier. (d) EOP, 8th carrier.

We can observe that for high levels of noise or low levels of signal power (like P_{rec}= -43 dBm) the difference between the edge and central channels is very small in terms of BER, and the optimal OBPF BW is the same. On the other hand, when there is enough power to reach the error-free condition (like P_{rec}= -40.5 dBm), the BER performance of the edge channels greatly improves for large values of OBPF BW, and the optimal OBPF BW is also larger compared to the central channel. In conclusion, broadening the filter response will only affect positively the system performance in the edge channels and only if the channel power level is high enough. We could observe something similar in our simulations: the optimal OBPF BW value for the edge carrier is larger than for the central carrier, even when the difference between these two values changes from simulations (BW=27 GHz vs. BW =21 GHz) to the laboratory (BW= 15,9 GHz vs. BW=12,6 GHz). The reason behind this is that in the laboratory we obtained our results in the form of BER, while in the simulations we used EOP. These are both valid ways to evaluate the performance of the system, but they are calculated with different methods. We did a verification in the simulations and saw that, under the same conditions, the value for the optimal OBPF BW depending on the BER was always lower than depending on the EOP, which agrees with the results obtained in the laboratory. We must also note that the simulations where independent of P_{rec}, so a direct comparison involving all the parameters is not possible.

OBPF BW optimization

We have swept the OBPF BW over different values, for a carrier spacing of 50 GHz and 16 carriers. The BER values have been measured in the 8th carrier, which is a central carrier. The result for this experiment is in Figure 65, where we can also see the EOP curve depending on the OBPF BW obtained in the simulations:

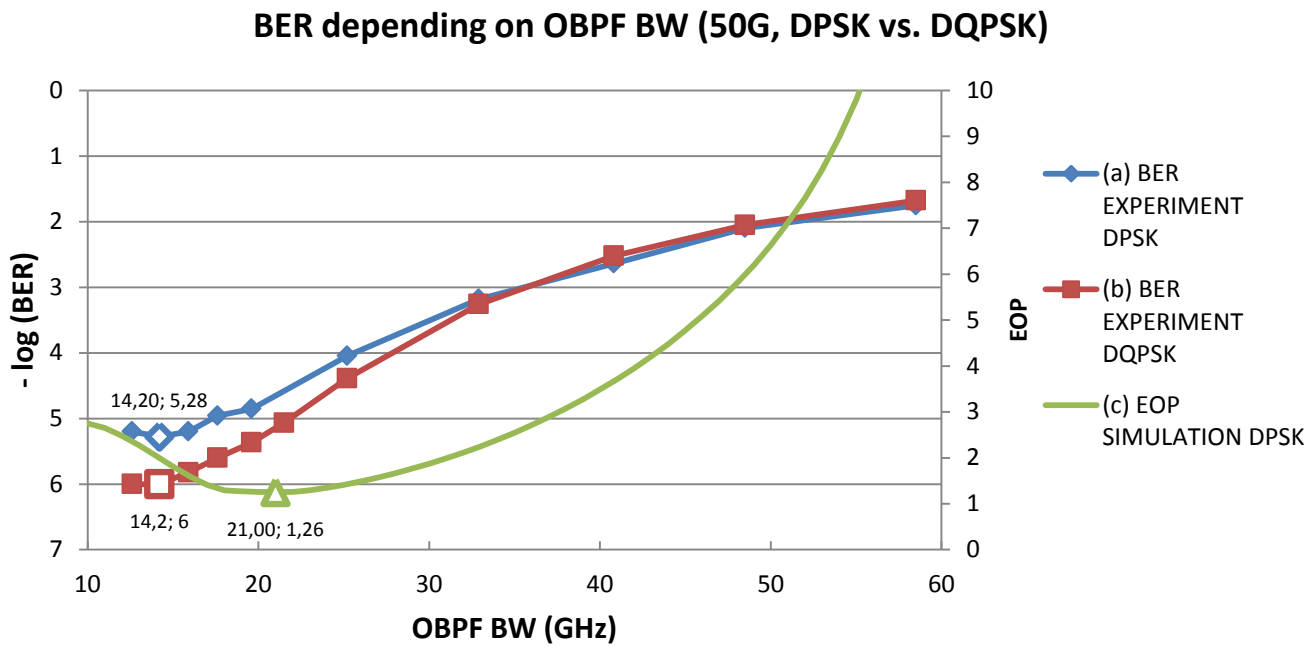

Figure 65 - BER. Comparison DPSK vs. DQPSK.
(a) BER, DPSK, -43 dBm at receiver's input. (b) BER, DQPSK, -37 dBm at receiver's input. (c) EOP, DPSK. Conditions: 16x50GHz OFDM, central carrier, Gaussian filter.

We can observe that the evolution of the BER in dependence of the OBPF BW is similar to the evolution of the EOP in dependence of the OBPF BW in the simulations. As we have said, BER and EOP are calculated in a different way, hence offering different results; the optimum value for a 50 GHz spacing and 16 carriers is 21 GHz for the given simulation, while it is 14,2 GHz in the laboratory. We can also observe that the optimum value doesn't change with the modulation: it is the same for DPSK and DQPSK.

The same experiment has been performed using 25 GHz spacing with 32 carriers, obtaining again the same results for DPSK and DQPSK (regarding the OBPF BW optimum value). Following this trend, for the remaining carrier spacings (100 GHz and 200 GHz) we have only measured the optimum OBPF BW value for DQPSK. In Figure 66 we can see a summary of those results:

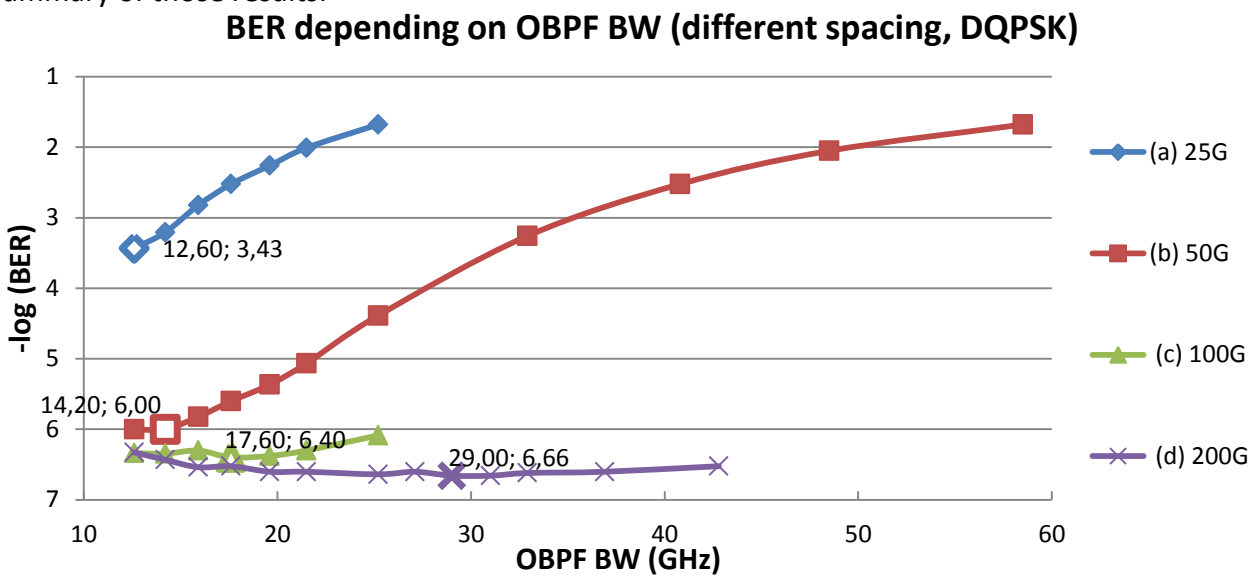

Figure 66 – BER. OBPF BW optimization
(a) 32x25GHz OFDM. (b) 16x50GHz OFDM. (c) 8x100GHz OFDM. (d) 4x200GHz OFDM.
Conditions: central carrier, Gaussian filter, DQPSK, -37 dBm at receiver's input.

As expected, we can see that the optimal OBPF BW changes with the carrier spacing, as does the measured BER. In terms of performance, we can see that the cases of 50G, 100G and 200G offer a similar BER value in their optimal OBPF BW, while the 25G case is much worse We already explained in the simulation results chapter why this happens, and everything is related to having less intercarrier interference (and so, better performance) when the optimal OBPF BW is small compared to the carrier spacing.. The optimal OBFP BW values for each carrier spacing, showed in Figure 66, are summarized in Table 2:

Channel spacing (GHz)	Optimal OBPF BW
25	12,6
50	14,2
100	17,6
200	29

Table 2– Optimal OBFP BW values for different spacings

BER curves

Once the optimal OBPF BW has been found, the main measurement can be done: we need to know the dependence of the BER on the power at the receiver's input (P_{rec}). If possible, we also want to know the sensitivity, i.e. to find the power for which the system reaches error-free performance.

Using these values we have obtained the BER curves depending on P_{rec}, for all the different channel spacings and for DPSK and DQPSK (always at a central carrier). In Figure 67 we can see the results using DPSK:

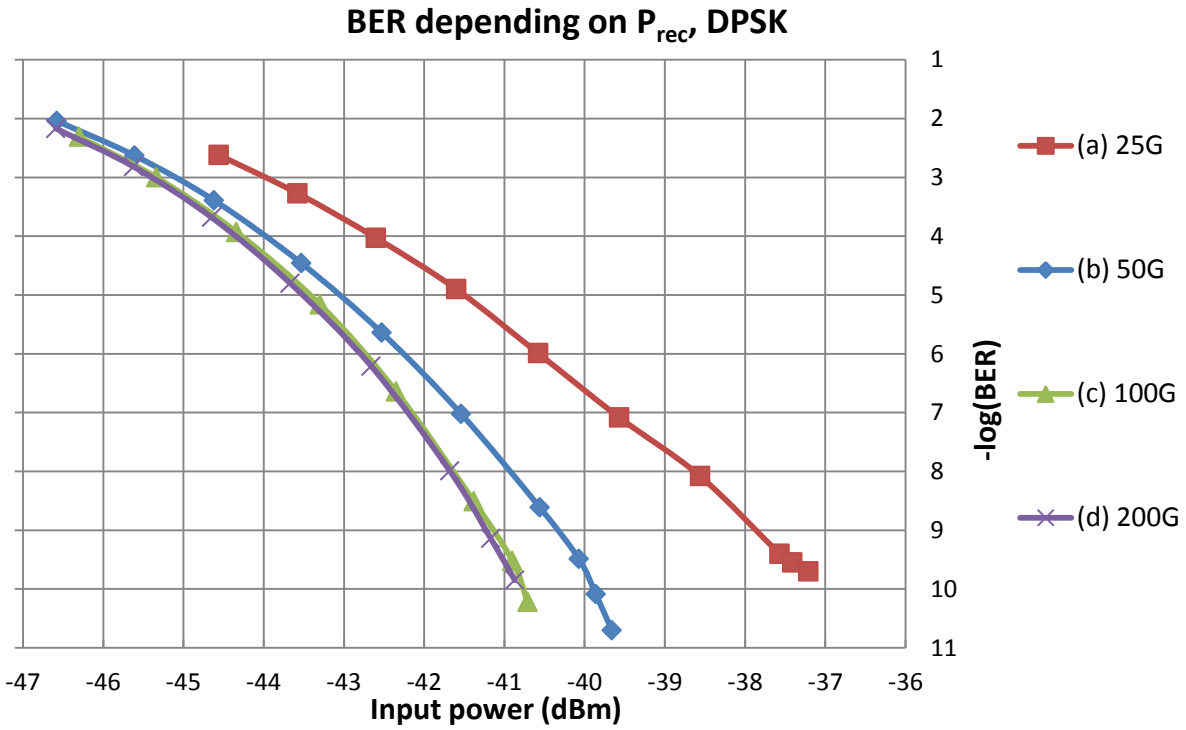

Figure 67 – BER. Dependance on P_{rec} for DPSK
(a) 32x25GHz OFDM. (b) 16x50GHz OFDM. (c) 8x100GHz OFDM. (d) 4x200GHz OFDM.
Conditions: DPSK, Gaussian filter, central carrier.

When we optimized the OBPF BW in Figure 66 we already could see that, for a given input power, the BER was better for larger carrier spacings. Now that we sweep the input power, we can see the same behaviour. The difference between curves increases for larger input powers; for an input power of -44 dBm, the difference between 25G and 200G is a factor ≈ 25, while for an input power of -41 dBm and the same spacings the difference is a factor 10^4 (always regarding the BER). In the same way, the sensitivity (BER=10^{-9}) for the 25G is at -38 dBm, while for 200G it is at-41,2 dBm. This is can be understood very easily by comparing the optimal OBPF BW and the carrier spacings: for a 25 GHz spacing the OBPF BW is 12,6 GHz (≈ factor 1/2), while for a 50 GHz spacing the OBPF BW is 14,2 GHz (≈ factor 1/3); there is, proportionally, much more power from the neighbour carriers in the 25 GHz case after demultiplexing, which will induce a higher intercarrier interference.

Despite the different input power requirements when changing the carrier spacing, it is important to note that we achieve error-free performance (BER=10^{-9}) for all of them. This is the first necessary step before attempting the full system (with time multiplexing/demultiplexing).

In Figure 68 we can see the results for both quadratures in a DQPSK modulation, and again for all the different channel spacings:

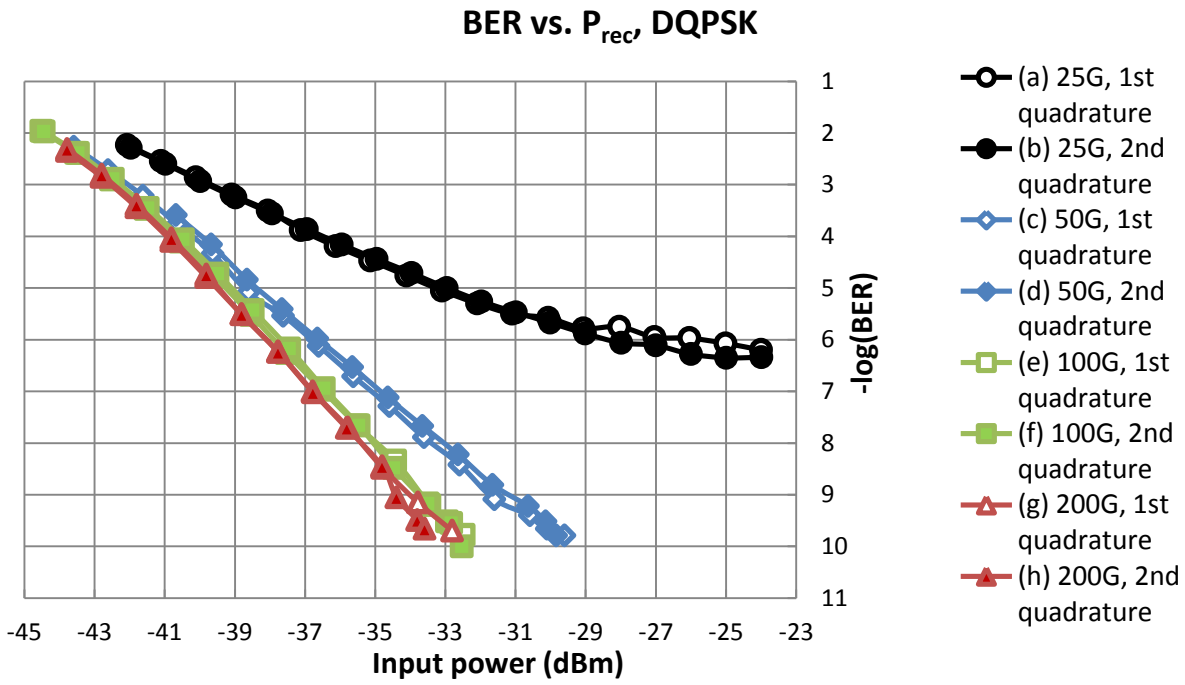

Figure 68 – BER. Dependance on P_{rec} for DQPSK
(a, b) 32x25GHz OFDM. (c, d)16x50GHz OFDM. (e, f) 8x100GHz OFDM. (g, h) 4x200GHz OFDM.
Conditions: DQPSK, Gaussian filter, central carrier.

As we can see, for each carrier spacing the two quadratures have a rather identical performance. One of the differences with the BER curves for DPSK is that the input power levels that we are using now are much higher than before; this is expected, as DQPSK requires a higher power compared to DPSK to offer a similar performance. However, the main difference can be observed in the 25G curves, as they never reach error-free transmission, independently of how high the applied input power is. Until this point we have seen many times that the performance of the system for 25G spacing is always worsened by the higher crosstalk that this case has compared to higher spacings; now, these limitations have become critical, making it unfeasible.

We expect the full system (with mux/demux) to introduce a penalty on the performance, which will have to be countered with a higher P_{rec}. We also know, from the results in this chapter, that DQPSK has higher power requirements than DPSK in order to perform similarly. It seems like the use of DQPSK in the full system may require a very high P_{rec}, which could make the system incapable of reaching free-error performance.

5.2.2 Setup with multiplexing/demultiplexing

In this setup we will be able to test the feasibility of the full principle explored in this thesis. The starting point will be the setup used in the previous section, with the addition of the necessary components to perform an OTDM multiplexing and demultiplexing process through FWM. The OFDM signal will be generated in the same way, so there will be the same limitations regarding intercarrier interference. We will do our experiment for 50G spacing and DPSK; if that experiment is successful, then DQPSK can be tested. A new variable appears in this section: the flatness of the control pulse. If this pulse is not flat enough, it can introduce even larger irregularities in the pulse of the demultiplexed tributary, hence worsening the performance of the system. This will lead us to inspect the quality of the control pulse.

Pulse quality

In the previous section we inspected how the OFDM symbols look, and we came to the conclusion that we cannot be sure about their exact shape(regarding flatness) and they were a bit broader than expected (for the 50G spacing case, 21 ps instead of 20 ps), which can be due to the resolution of the WSS.

As we have said, the key aspect is the pump pulse shape. The intensity in a given instant of the pump pulse will interact with the OFDM pulse intensity at the same instant, generating the idler; if the intensity in the pump pulse changes from one instant to another (i.e. it is not flat-top), the FWM conditions change in those instants, and hence the idler generation changes too. In the theoretical chapter we saw that the idler field is proportional to the square of the pump field. As we want our idler to be identical to our signal, we need a flat-top control pulse; any other shape that the control pulse has will affect the idler to the square. In Figure 69 we can see the pump pulse in the time-domain:

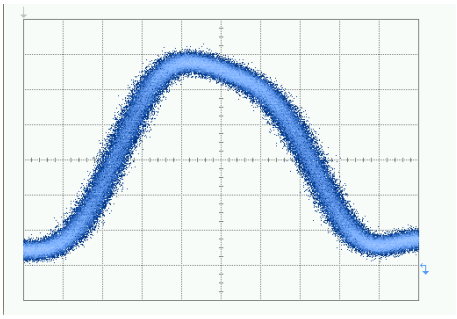

Figure 69 – Pump pulse
Conditions: 568 µW/div, 5 ps/div (oscilloscope)

We can observe that the pump pulse is far from being flat-top, even when it has been the result of an optimization process over its spectrum generation and its polarization state. As said, this will affect the time-demultiplexing process and can be a crucial aspect in the performance of the system.

Another time-domain representation is the time-multiplexed signal. In Figure 70.a we can see the signal at the data modulator output, before going through the multiplexer. In Figure 70(b) we can see the same signal at the multiplexer output, after going through two multiplexing stages (in order to have 4 copies of the input signal, progressively delayed and coupled together). Both figures have the same vertical scale (20mV/div).

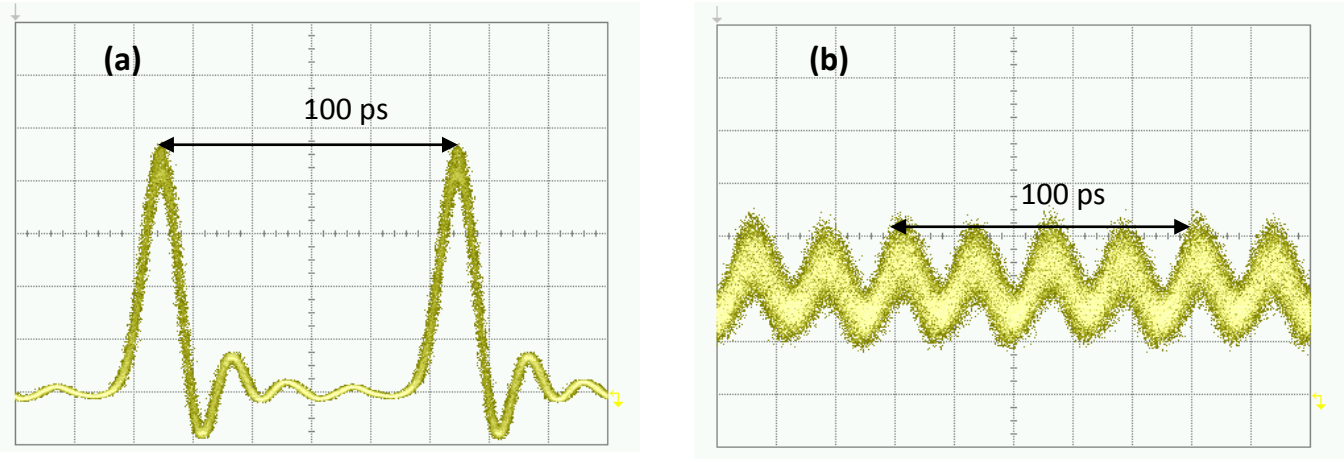

Figure 70 – Multiplexed signal
(a) Signal before multiplexing. (b) Signal after multiplexing. Conditions: 20 mV/div, 20 ps/div (oscilloscope)

Spectrum

As explained in the laboratory setup section, the switching method used is FWM. This means that the *idler* is generated mirror-like in relation to the pump. It is also interesting to check how the spectrum of the combination of signal, pump and idler looks, both before and after the HNLF where the FWM process takes place. We can see it in Figure 71:

:

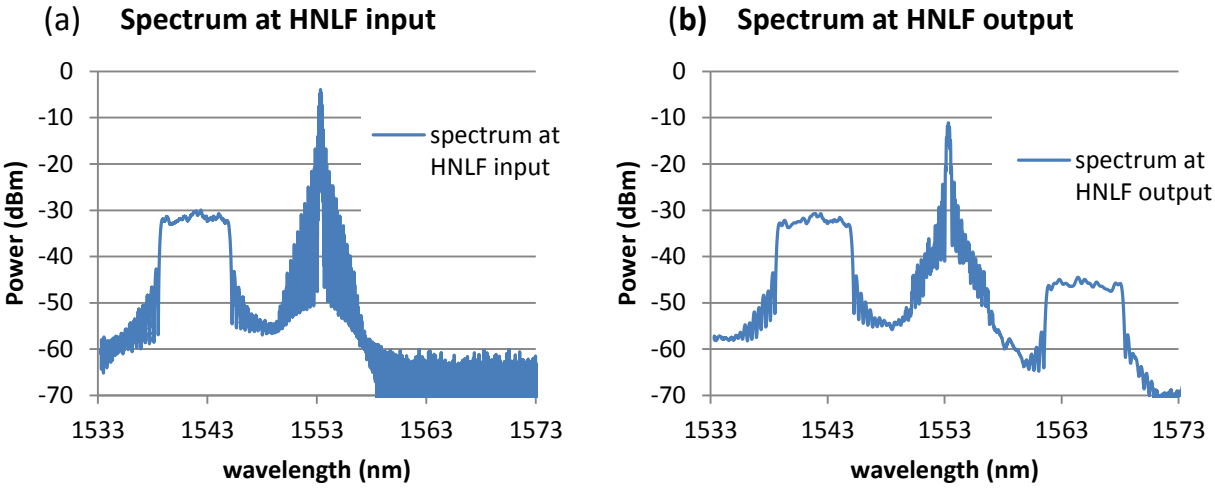

Figure 71 – Spectrum. Data + pump + idler
Conditions: 16x50GHz OFDM (data), 40GHz (pump). (a) Full spectrum at HNLF input, only data and pump. Resolution = 0,02nm. (b) Full spectrum at HNLF ouput, with data, pump and idler. Resolution = 0,1nm.

Here we can see the effects of the FWM process: the apparition of the idler as a copy of the multiplexed tributary. Note that the difference in the pump between the two figures is due to the different resolution of the OSA. We can also see that the idler has a low power compared to the signal; this is partially because there is only one tributary, and also because it depends on the pump power and conversion efficiency of the FWM process.

Figure 72 we can see the signal spectrum put on top of the idler inverted spectrum (as it is generated mirror-like). We can see that the spectrum shape is similar with very slight variations, which could be attributed to the non-flatness of the pump pulse. There is also some spectral broadening, but that is because the idler is found in different wavelengths than the signal, so the same spectral width looks broader.

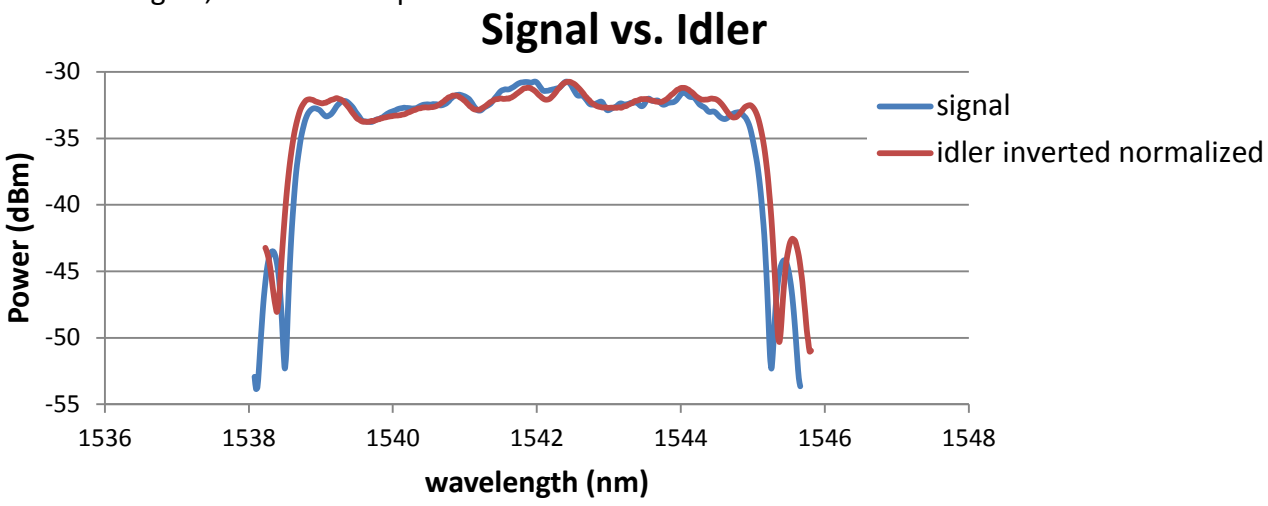

Figure 72 – Spectrum. Signal vs. Idler
Conditions: 16x50GHz OFDM. Resolution = 0,1nm.

In Figure 73 we can see the pump spectrum before the HNLF and in Figure 74 we can see the pump spectrum after the HNLF:

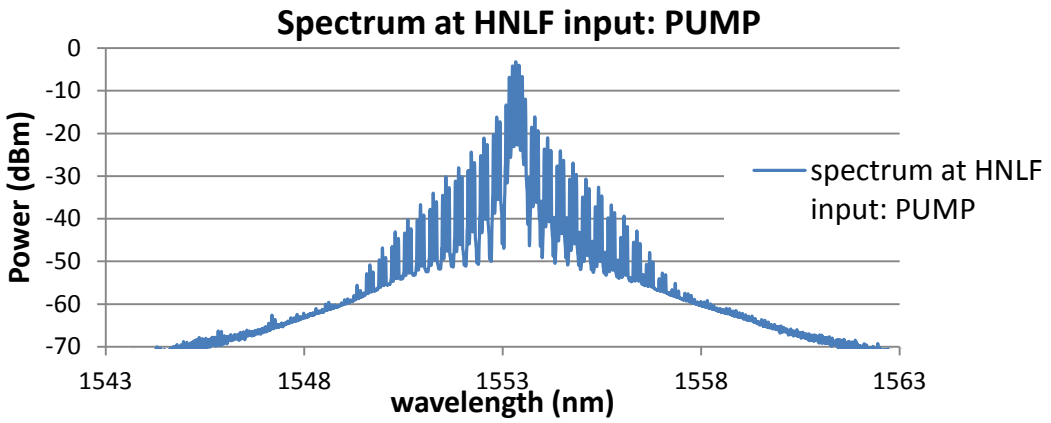

Figure 73 – Spectrum. Pump at HNLF input
Conditions: 40Ghz pump. Resolution=0,02 nm

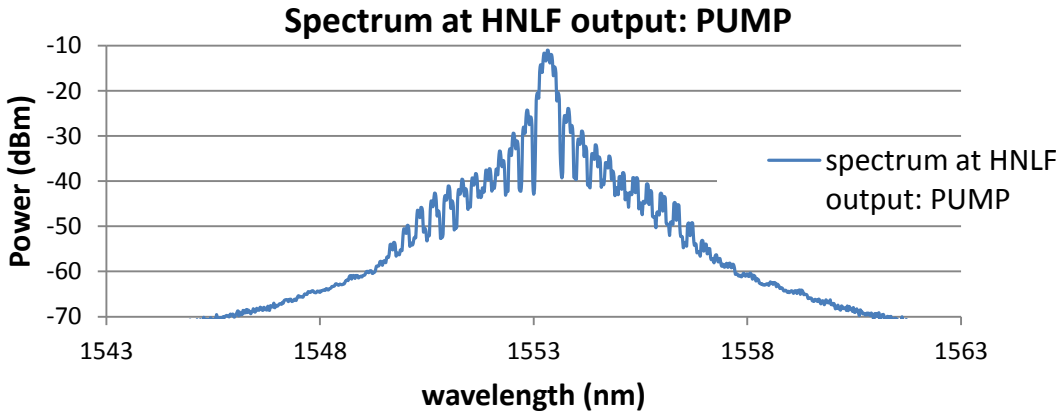

Figure 74– Spectrum. Pump at HNLF output
Conditions: 40Ghz pump. Resolution=0,1 nm

It is clear that the pump spectrum has a *sinc* shape, because it is a rectangular pulse in the time domain. The pulse width has been chosen as 25ps in order to be broader than the OFDM pulse width (which is 21 ps). The main difference between the two diagrams is that at the HNLF output we can observe a higher level in the side lobes (compared to the main lobe), consequence of the XPM in the fiber.

BER measurements

Now we are evaluating the full system based on the principle explored in this thesis, in a particular case with 4 time-multiplexed tributaries and 16 frequency-multiplexed carriers for each tributary. We have collected the different sensitivities for all those channels. These results are shown in Figure 75:

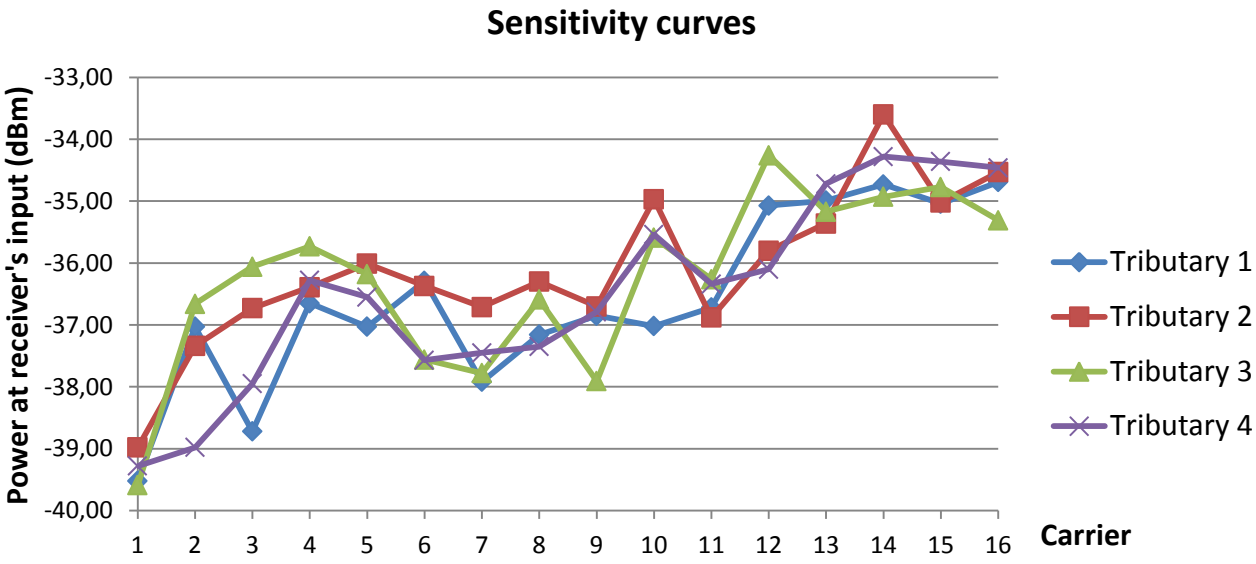

Figure 75 – Sensitivity curves

Conditions: 16x50GHz. All tributaries, All subcarriers. OBPF BW =14,2 GHz, Gaussian filter, DPSK

First of all, we must note that there are 64 data points in the graph, which means that error-free was fully achieved for the whole system, for 50 GHz spacing and DPSK modulation. In the previous section, when we tested the system without performing OTDM multiplexing/demultiplexing, the sensitivity for a central channel (8th), DPSK and 50G spacing was -40,5 dBm (as seen in Figure 67). With the full system implemented the sensitivity for the same channel increases until -37 dBm. In general the sensitivities are found in a range from -33,6 dBm to -39,3 dBm, with the average around -36 or -37 dBm, which means a 3dB worsening due to OTDM mux/demux.

We can see that both the best and worse situation happen close to the edge: the best one is at carrier 1, and the worst one at carrier 14, with carriers 15 and 16 also being worse than the average. This is completely different from what we saw in the simulations. In Figure 57 we saw that the OFDM spectrum had many irregularities and was far from flat-top, which means that each carrier had a different power. The performance of the system for a given carrier is sensitive on its neighbour carriers, which leads to each subcarrier having a different sensitivity. However, we can see that they don't only have different sensitivities, but they follow some kind of trend, where the carriers closer to the 1st have better performance than the ones closer to the 16th. We have later seen that adjusting the polarization of the different signals involved in the setup we can improve the performance on some carriers with high sensitivity. The origin of this strange behaviour could also be found on the super-continuum generation.

In this experiment there are some key aspects that have not been fully optimized and can have a negative effect on the performance of the system, mainly the pump shape. If the pump shape cannot be improved, it may be interesting to change the switching method to one that is less dependent on the pulse shape (like the Kerr-shutter). Even without optimizing these aspects we have managed to reach error-free performance, to the point of only having a 3dB worsening compared to the system without mux/demux (on average).

Chapter 6

Conclusions

6.1 Simulation conclusions

In the simulations of the principle, we find two groups of results. The first group characterizes the performance of the system for a 50GHz carrier spacing and a variable number of carriers. The second group of results characterizes the performance of the system given a fixed spectral bandwidth, variable carrier spacings and inversely proportional number of carriers.

For the first group of results, we have found that the performance of the system depends on some parameters (OBPF BW, roll-off factor, laser's relative phase, number of carriers), but this performance stops changing once we reach 8 or more carriers. This conclusion can be approached in different ways:

- The optimal OBPF BW is almost the same for 8 or more carriers.
- For a given OBPF BW, the EOP stabilizes for 8 or more carriers.
- The general behaviour of the back-to-back system (with no OTDM multiplexing) is to have a better performance when the roll-off factor increases, as the intercarrier interference decreases. Again, this trend is very clear for 8 or more carriers. However, we cannot rely on this result when considering the full system (with OTDM multiplexing), where intertributary interference could happen.

Other conclusions that we obtain from this first group of simulations are:

- The highest EOP happens always when the carriers have the same phase or a π difference.
- The optimal OBPF BW is always larger in the edge carriers than in the central ones. Similarly, the EOP is lower. This is caused by the lack of neighbour carriers in the edge carriers (in one of their sides)
- Considering the worst possible conditions, the performance of the system fluctuates up to a 15% around the average performance (in terms of EOP). This is caused by the momentary phase conditions of each carrier, which depend on the data pattern they transmit and their initial phase.

For the second group of simulations, we have seen that a key parameter is the OBPF BW and its relation with the carrier spacing. We can obtain the following conclusions:

- The optimal OBPF BW value is larger for larger spacing between carriers. Also, the EOP is lower for larger carrier spacings. This is related to the fact that the OBPF BW cannot be reduced proportionally to the carrier spacing, as intersymbol interference would happen. Instead, the optimal OBPF BW for low carrier spacings is comparatively larger, allowing higher intercarrier interference and worsening the performance.
- The quality of the pulses is very sensitive to the filter bandwidth for low carrier spacings. In this case, the OBFP BW becomes a critical parameter, and needs to be accurately fixed.
- A low roll-off factor increases intercarrier interference, and this effect is larger for low carrier spacings.
- The fluctuations in the performance around the average EOP are higher for lower spacings.

6.2 Experimental conclusions

- The performance depends on the response of the demultiplexing filter. A Gaussian response filter offers a better performance than a Rectangular response filter at low OBPF BW values.
- It is confirmed that the optimal OBPF BW is larger for larger spacings, and the BER is lower. The optimal OBPF BW is lower than in the simulations, which can be attributed to the fact that it is calculated on the BER, not the EOP. However, the dependence of the performance of the system on the OBPF BW is similar. The optimal OBPF BW is the same for both DPSK and DQPSK.
- The optimal OBPF BW in the edge carriers is larger than in the central ones but only for a high enough power at the receiver's input.
- For a given input power at the receiver, a larger spacing will have a better BER. For a larger input power, the difference in BER between spacings increases.

6.2.1 Achievements in the non-multiplexing/demultiplexing experimental scheme

- We have reached error-free performance (BER=10^{9}) using DPSK in a central carrier for 25G, 50G, 100G and 200G spacings. For the 50GHz, the penalty compared to the back-to-back measurement (with only one port connected) is 0,6 dB.

- We have achieved error-free performance using DQPSK in a central carrier for 50G, 100G and 200G spacings. The penalty in the sensitivity for using DQPSK, comparing to DPSK, is 7dB. The penalty compared to the back-to-back measurement is 3,2 dB.

6.2.2 Achievements in the full experimental scheme

- We have reached error-free performance using DPSK for 50GHz spacing, for all tributaries and all subcarriers. Total data rate achieved of 640Gbits/s. We can observe a dependency of the sensitivity on the wavelength. The penalty in the sensitivity, compared to the system without mux/demux, is 3dB on average.

6.3 Future work

The results obtained in this work encourage future research on the direction of this thesis, in order to optimize the different parameters involved and to improve the data rate:

- Other relative phase relations could be investigated (like the one that happens in the WSS-generated OFDM).
- Limited resolution in WSS causes a non-perfect *sinc* spectrum and a non-flat pulse. This is an important aspect in the pump pulse generation. It could be investigated how the pump pulse shape affects the performance, and how the raised-cosine shape is transmitted to the idler.
- In a different setup, all-optical pulse carving should be performed and hence investigated in order to apply to a WDM transmitter.
- Different frequency responses for the demultiplexing filter could also be investigated.
- It is also interesting what the performance of the principle is using DQPSK. This experiment has been carried out (and has yet to be published) after changing the demultiplexing method to a Kerr-shutter variant in order to reduce the performance dependence on the pump pulse shape. Free-error performance has been reached but only for some carriers, so the setup needs to be further investigated.
- Another future area of research could be the use of OFT (e.g. spectral magnification) to improve the frequency-demultiplexing process.

References

[1] S. Chandrasekhar and X. Liu,. “OFDM Based Superchannel Transmission Technology”, *Journal of Lightwave Technology*, vol. 30, no. 24, pp.3816-3823, Dec. 2012

[2] Sano et al., “No-guard interval coherent optical OFDM for 100-Gb/s long-haul WDM transmission”, *Journal of Lightwave Technology*, vol. 27, no. 6, pp. 3705-3713, 2009.

[3] D. Hillerkuss et al., “26 Tbit s^{-1} line-rate super-channel transmission utilizing all-optical fast Fourier transform processing”, *Nature Photonics*, vol. 5, no. 6, pp. 364-371, 2011

[4] L. B. Du et al., “Flexible All-Optical OFDM using WSSs”, *OFC’13*, Paper PDP5B.9, 2013.

[5] P. J.Winzer, G. Raybon, C. R. Doerr, M. Duelk, and C. Dorrer, “107 Gb/s optical signal generation using electronic time-division multiplexing,” *Journal of Lightwwave Technology*, vol. 24, pp.3107–3113, 2006.

[6] C. Schubert, R. H. Derksen, M. Möller, R. Ludwig, C.-J. Weiske, J. Lutz, S. Ferber and C. Schmidt-Langhorst, “107 Gbit/s Transmission Using An Integrated ETDM Receiver”, *European Conference on Optical Communication*, paper Tu1.5.5 , Sep.2006,

[7] H. C. Hansen Mulvad, L. K. Oxenløwe, M. Galili, A. T. Clausen, L. Grüner-Nielsen, and P. Jeppesen,“1.28 Tbit/s single-polarisation serial OOK optical data generation and demultiplexing,” *Electronic Letters*, vol. 45, no. 5, pp. 280–281, 2009

[8] T. Richter, E. Palushani, C. Schmidt-Langhorst, M. Nölle, R. Ludwig, and C. Schubert, "Single Wavelength Channel 10.2 Tb/s TDM-Data Capacity using 16-QAM and coherent detection," in *Optical Fiber Communication Conference*, OSA Technical Digest (CD) (Optical Society of America, 2011), paperPDPA9.

[9] R. Freund et al., “Single- and Multi-Carrier Techniques to Build up Tb/s per Channel Transmission Systems”, *International Conference on Transparent Optical Networks*, Paper Tu.D1.4, July 2010

[10] M.A. Foster, R. Salem, and A. L. Gaeta**, “**Ultrahigh-Speed Optical Processing Using Space-Time Duality”, *Optics and Photonics News*, Vol. 22, Issue 5, pp. 29-35 (2011)

[11] T.T. Ng, F. Parmigiani, M. Ibsen, Z. Zhang, P. Petropoulos, and D.J. Richardson, “Compensation of linear distortions by using XPM with parabolic pulses as a time lens”. *IEEE Photonics Technology Letters*, vol. 20, no. 13, pp. 1097-1099, 2008

[12] E. Palushani, H. C. Hansen Mulvad, D. Kong, P. Guan, M. Galili, and L.K. Oxenløwe, “All-optical OFDM demultiplexing by spectral magnification and band-pass filtering”, *Optics Express,* Vol. 22, Issue 1, pp. 136-144 (2014)

[13] G. P. Agrawal. *Nonlinear Fiber Optics*. Academic Press, Third edition, 2001. ISBN 0-12-045143-3.

[14] K. Blow, N. Doran, B. Nayar, and B. Nelson. “Two-wavelength operation of the nonlinear fiber loop mirror", Optics Letters, vol. 15, no. 4, pp. 248-50, 1990.

[15] T. Yamamoto, E. Yoshida, and M. Nakazawa. “Ultrafast nonlinear optical loop mirror for demultiplexing 640 Gbit/s TDM signals", Electronics Letters, vol. 34, no. 10, pp. 1013-1014, 1998.

[16] T. Morioka and M. Saruwatari. “Ultrafast all-optical switching utilizing

the optical kerr effect in polarization-maintaining single-mode fibers", IEEE Journal on Selected Areas in Communications, vol. 6, no. 7, pp. 1186-1198, 1988.

[17] S. Watanabe, R. Okabe, F. Futami, R. Hainberger, C. Schmidt-Langhorst, C. Schubert, and H. Weber. “Novel fiber Kerr-switch with parametric gain: Demonstration of optical demultiplexing and sampling up to 640 Gb/s", in Proceedings European Conference on Optical Communication, ECOC'04, Stockholm, Sweden, Paper Th4.1.6 (postdeadline), September 2004.

[18] J. Hansryd, P.A. Andrekson, M. Westlund, J. Li, and P. Hedekvist, “Fiber-Based Optical Parametric Amplifiers and Their Applications”, Jorunal of selected topics in quantum electronics, vol. 8, no. 3, May/June 2002

[19] M. Nakazawa, T. Hirooka, P. Ruan, and P. Guan, “Ultrahigh-speed “orthogonal” TDM transmission with an optical Nyquist pulse train”, Optics Express, vol. 20, no. 2, pp.1129-1140, Jan. 2012

[20] J. G. Proakis, Digital Communications, 5th ed. (McGraw Hill, 2007).

[21] H. Gnauck and P. J. Winzer, “Optical Phase-Shift-Keyed Transmission”, Journal of Lightwave Technology, vol. 23, no. 1, pp. 115-130, Jan. 2005

[22] H.C. Hansen Mulvad, “All-Optical Signal Processing for 640 Gbit/s Applications”, PhD at DTU Fotonik, 2008